INFORMATION TO USERS

This material was produced from a microfilm copy of the original document. While the most advanced technological means to photograph and reproduce this document have been used, the quality is heavily dependent upon the quality of the original submitted.

The following explanation of techniques is provided to help you understand markings or patterns which may appear on this reproduction.

1. The sign or "target" for pages apparently lacking from the document photographed is "Missing Page(s)". If it was possible to obtain the missing page(s) or section, they are spliced into the film along with adjacent pages. This may have necessitated cutting thru an image and duplicating adjacent pages to insure you complete continuity.

2. When an image on the film is obliterated with a large round black mark, it is an indication that the photographer suspected that the copy may have moved during exposure and thus cause a blurred image. You will find a good image of the page in the adjacent frame.

3. When a map, drawing or chart, etc., was part of the material being photographed the photographer followed a definite method in "sectioning" the material. It is customary to begin photoing at the upper left hand corner of a large sheet and to continue photoing from left to right in equal sections with a small overlap. If necessary, sectioning is continued again — beginning below the first row and continuing on until complete.

4. The majority of users indicate that the textual content is of greatest value, however, a somewhat higher quality reproduction could be made from "photographs" if essential to the understanding of the dissertation. Silver prints of "photographs" may be ordered at additional charge by writing the Order Department, giving the catalog number, title, author and specific pages you wish reproduced.

5. PLEASE NOTE: Some pages may have indistinct print. Filmed as received.

Xerox University Microfilms
300 North Zeeb Road
Ann Arbor, Michigan 48106

76-27,606

TUCKER, William Allen, 1948-
THERMAL STRUCTURE OF LAKES.

The University of Michigan, Ph.D., 1976
Physical Oceanography

Xerox University Microfilms, Ann Arbor, Michigan 48106

THERMAL STRUCTURE OF LAKES

by
William Allen Tucker

A dissertation submitted in partial fulfillment
of the requirements for the degree of
Doctor of Philosophy
(Oceanic Science)
in The University of Michigan
1976

Doctoral Committee:

Assistant Professor Albert W. Green, Jr., Chairman
Professor William P. Graebel
Professor Stanley J. Jacobs
Assistant Professor Philip A. Meyers
Lecturer Edward C. Monahan, University College,
Galway, Ireland

ACKNOWLEDGEMENTS

I would like to note my special appreciation to Dr. Albert W. Green who suggested the problem and supported and encouraged my work at the University of Michigan since my first days in Ann Arbor. Without his stimulating and constructive criticism, this dissertation would be much less than it is. Thanks also go to Dr. Stanley J. Jacobs for many stimulating discussions which broadened the scope of this work. Dr. Philip A. Meyers' encouragement and assistance in matters of chemical and biological applications of this study is sincerely appreciated. Dr. Edward C. Monahan's suggestions, encouragement, and prompt responses to all my inquiries were most helpful to me. Thanks also to Dr. William P. Graebel for his comments throughout the course of this research and his careful editing of the first manuscript.

Dr. Robert L. Pickett and Mr. Frank Rodante of NOAA, Great Lakes Environmental Research Lab, provided much of the IFYGL data used in the dissertation with a promptness that went beyond the requirements of their jobs, and were attentive to any problems I encountered in the utilization of the data archive.

Mr. Edward Ryznar was most helpful in sharing his library and knowledge of air-sea transfer and the atmospheric boundary layer. Mr. Paul Liu deserves a note of

thanks for many discussions about wind-wave generation and fetch-limited waves. The assistance provided by Mr. James Sterken during many frustrating debugging sessions with MTS was priceless. To fellow travelers, Dr. James Allender and Mr. Larry Danek, thanks for the competition.

I thank my father and mother, Fred and Betty Tucker, for everything that a father and mother can provide, because they gave me nothing but their best.

Finally, more than just thanks goes to my wife Judi without whose solace and comfort this work would not have been completed, and in particular for her especially skillful typing of the many drafts of this dissertation.

TABLE OF CONTENTS

		Page
ACKNOWLEDGEMENTS		ii
LIST OF TABLES		v
LIST OF FIGURES		vi
LIST OF SYMBOLS		viii
CHAPTER		
I.	INTRODUCTION	1
II.	THE GOVERNING EQUATIONS: A SCALE ANALYSIS	17
III.	RECENT THEORETICAL STUDIES OF THE SEASONAL THERMOCLINE	30
IV.	A LAKE THERMOCLINE MODEL a. Derivation of model equations b. Representation of the forcing functions	50
V.	METHOD OF SOLUTION	87
VI.	MODEL VERIFICATION	91
VII.	MODEL SENSITIVITY STUDIES	132
VIII.	APPLICATIONS	146
IX.	CONCLUSIONS	152
REFERENCES		155

LIST OF TABLES

Table		Page
1	Albedo Coefficients.	62
2	Variation of the Coefficient m.	65
3	Parameter Values.	86
4	PDCS Sensor Heights, IFYGL.	95
5	Statistics on Llyn Cwellyn Verification Run	129

LIST OF FIGURES

Figure		Page
1	Annual cycles of insolation and lake surface temperature of Lake Mendota, Lake Cayuga, and Lake Ontario.	4
2	Map of Lake Ontario showing the stations of the IFYGL Physical Data Collection System.	93
3	Surface conditions, Lake Ontario, July and August, 1972.	101
4	Lake Ontario, July-August, 1972, mean surface temperature.	103
5(a-l)	Lake Ontario, July-August, 1972, mean temperature profiles at 5 day intervals.	104
6	Lake Ontario, July-August, 1972. Isotherm depths vs. time as predicted by the model.	111
7	Lake Ontario, July-August, 1972. Isotherm depths vs. time as observed by PDCS.	112
8(a-d)	Lake Ontario, July-August, 1972, model predicted T vs. t at four depths.	113
9	Surface conditions, Lake Ontario, October, 1972.	118
10	Lake Ontario, October, 1972, mean surface temperature.	120
11(a-c)	Lake Ontario, October, 1972, mean temperature profiles at 10 day intervals.	121
12	Tilted model profile, Lake Ontario, October 16, 1972.	123
13	Tilted model profile, Lake Ontario, October 31, 1972.	123
14	Lake Ontario, October, 1972, model predicted T vs. t at four depths.	125
15	Map of Llyn Cwellyn, Wales.	127

LIST OF FIGURES (continued)

Figure		Page
16	Enthalpy change per cm^2 in Llyn Cwellyn, June 1, 1966.	128
17	Llyn Cwellyn temperature profiles, June 1, 1966.	130
18	Model sensitivity to perturbation of β.	136
19	Model sensitivity to perturbation of B.	136
20	Model sensitivity to changes in lake surface area.	139
21	Model sensitivity to perturbation of the dissipation rate.	139
22	Model sensitivity to perturbation of the ratio of wave mixed layer depth to significant wave height, a.	142
23	Model sensitivity to perturbation of $\frac{\tau_w}{\tau_o}$.	142
24	Model sensitivity to changes in the wind speed at 3 m.	145
25	Lake Ontario, July-August, 1972, results of simulation of dissolved oxygen depletion.	148

LIST OF SYMBOLS

a	ratio of wave mixed layer depth to the significant wave height
a^*, b^*	empirical coefficients used in albedo computation
c	phase speed of surface gravity waves
c_k	empirical coefficient in diffusivity formula (Kullenberg, 1971)
c_p	specific heat at constant pressure
d	mean depth of lake
d_z	transfer coefficient, latent heat
e_a	atmospheric water vapor pressure
f, f_o	Coriolis parameter, its approximate magnitude
g	acceleration due to earth's gravity
h	depth of mixed layer
h_o	linear approximation to h
h_c	depth of convective region
h_{wm}	wave mixed layer depth
h_z	transfer coefficient, sensible heat
k	molecular thermal conductivity
k'	empirical coefficient for cloud effects on incident short wave radiation
k_v	von Karman constant
ℓ	turbulent eddy length scale (large eddies)
ℓ_b, ℓ_r	maximum turbulent length in stably stratified or rotating fluid, respectively
m	coefficient relating surface kinetic energy production rate to the rate of increase of potential energy of a fluid column

LIST OF SYMBOLS (continued)

m_o	optical air mass
n	cloud cover, $0<n<1$
p, p_o, p'	pressure, its approximate magnitude, and fluctuating component
q	$\sqrt{u^2+v^2+w^2}$, square root of turbulent intensity
q_*	specific humidity fluctuation scale
q_s	saturation specific humidity at temperature, T_s
q_z	specific humidity at height, z
r	ratio of scattered to direct solar radiation at lake surface
r_s, r_c	empirical coefficients in dissipation formula for shear and convectively produced turbulence, respectively
s	slope of the lake surface
t, t_o	time, scale of time
t_{max}, t_{end}	span of simulation
u, u_o	horizontal velocity fluctuation, its approximate magnitude
u_s', u_c'	characteristic velocity scales for turbulence generated by shear and convection
u_*	atmospheric surface friction velocity
v, v_o	analogous to u, u_o
w, w_o	vertical velocity fluctuation, its approximate magnitude
w_{sfc}	surface velocity scale
w_*	water surface friction velocity
x, y	horizontal coordinates
z	vertical coordinate

LIST OF SYMBOLS (continued)

z_b	distance to nearest boundary
z_o	boundary roughness length
A	area of a horizontal plane extending to lake boundaries at a given depth
A_r	albedo
A_z	turbulent viscosity
B*	net transfer of heat from air to lake by infrared radiation, sensible and latent heat exchange
B	$B^*/\rho_o c_p$
C	empirical coefficient for κ_b (Lumley, 1964)
C_L	empirical coefficient for effect of clouds on long wave radiation
C_z	drag coefficient
D*	rate of turbulent energy dissipation in the mixed layer
D	$D^*/g\alpha\rho_o$
D_s^*, D_c^*, D_w^*	mixed layer dissipation rate for turbulence generated by the shear flow, convection, and wave-breaking, respectively
E	relative error in heat conservation during model simulation
$\dot{E}_s$	interface energy flux to the shear flow
$\dot{E}_w$	interface energy flux to the wave field
F	fetch distance
F_o	gF/U^2_{10}, dimensionless fetch parameter
F_s	flux of dissolved oxygen to the sediments
G*	production rate of turbulent energy associated with wind forcing

LIST OF SYMBOLS (continued)

G	$G^*/g\alpha\rho_o$
G_s^*, G_w^*	contributions to G* from shear instability and wave-breaking, respectively
H	depth at which annual cycle of water temperature is negligible
$H_i(t)$	enthalpy change exhibited by model predicted temperature profiles
$H_{1/3}$	significant wave height
I_o	incident solar radiation
I_d	direct solar radiation incident on lake surface
I_s	scattered solar radiation incident on lake surface
$I(z,\lambda)$	radiant intensity vs. z and wavelength, λ
K	turbulent exchange coefficient
K_e	surface heat exchange coefficient
K_m	minimum allowable hypolimnion diffusion coefficient
K_z	vertical turbulent heat diffusivity
L	length scale of horizontal variations in water properties
L_e	latent heat of evaporation, water
N	Brunt-Vaisala frequency
O_2	concentration of dissolved oxygen (mg/l)
P	atmospheric transmission coefficient, solar radiation
Q	internal sources or sinks of heat
$Q_i(t)$	time intergral of surface heat flux, computed in the model

Q_s, Q_ℓ	turbulent flux of heat from air to lake by sensible and latent heat
R_e	$\frac{\rho_o U_o L}{\mu}$, Reynolds number
R_i	$\frac{g}{\rho}\frac{\partial \rho}{\partial z}\Big/\left(\frac{\partial U}{\partial z}\right)^2$, gradient Richardson number
R_{ib}	$\frac{gz}{T_z}\frac{T_z - T_s}{(U_z)^2}$, bulk Richardson number
R_{is}	a bulk Richardson number used by Sundaram and Rehm (1971)
R_{icr}	critical Richardson number, a stability criterion for stably stratified shear flow
R_ℓ	net long wave radiation transfer from air to lake ($R_\ell < 0$)
R_o	$\frac{U_o}{f_o L}$, Rossby number
S^*	penetrating component of solar radiation
S	$S^*/\rho_o c_p$
T, T_o	temperature (ensemble average), its approximate magnitude
T_a	air temperature
T_c	equilibrium temperature
T_h	temperature just below mixed layer, $\lim_{\delta \to 0} T(-h-\delta)$
T_s, T_ℓ	lake surface temperature
T_z	atmospheric temperature at height, z
T_{oh}	magnitude of horizontal temperature variations
U, U_o	horizontal velocity component (ensemble average), its approximate magnitude

LIST OF SYMBOLS (continued)

U_s	surface current speed
U_z	wind speed at elevation, z
V, V_o	analogous to U, U_o
W, W_o	vertical velocity component (ensemble average) and its approximate magnitude
W^*, W	rate of conversion of kinetic energy to potential energy, $W^*/g\alpha\rho_o$
α	$\frac{1}{\rho_o}\frac{\partial\rho}{\partial T}$, thermal expansion coefficient
β	attenuation coefficient for solar radiation
δ	interface thickness at z=-h
δ_e	turbulent Ekman layer depth
$\delta(z)$	Dirac delta function
ϵ	turbulent energy dissipation rate
ζ	error bound in numerical integration
θ, θ_o	turbulent temperature fluctuation, its approximate magnitude
θ_*	atmospheric temperature fluctuation scale, analagous to u_*
θ_z	sun's zenith angle
κ	turbulence wave number
κ_b	boundary of buoyancy-inertial subrange in turbulent spectrum
κ_{wb}	wave number associated with turbulence generated by wave-breaking
λ	wave length, solar radiation

LIST OF SYMBOLS (continued)

λ_c	region of gravitational instability in initially homogeneous water, heated by solar radiation and cooled at the surface
μ	molecular viscosity
ν	kinematic viscosity
$\bar{\rho}, \rho_o$	density of water (ensemble average) and its approximate magnitude
ρ', ρ_f	density fluctuations and their approximate magnitude
ρ_a	density of air
σ_1, σ_2	coefficients in mixing length approximation for a stably stratified fluid
τ	diffusive time scale
τ_o	surface stress
τ_s	air-sea interface momentum flux to the shear flow
τ_w	air-sea interface momentum to the wave field
ϕ	latitude
X, χ	ensemble average and fluctuating component of a scalar property
Λ	Heaviside step function
$\psi_1\|_z$	correction to dimensionless wind shear due to atmospheric stability at height, z
$\psi_2\|_z$	correction to dimensionless partial derivative of temperature and specific humidity due to atmospheric stability at height, z
Ω	earth's rotation frequency

CHAPTER I

INTRODUCTION

The typical thermal cycle of temperate lakes is well known and is discussed in detail by Hutchinson (1957). Some of its features and the physical processes most important in effecting temperature changes will be discussed qualitatively below.

Most temperate lakes exhibit a spring mixing period in which the temperature is nearly uniform and near 4°C, the temperature of maximum density. Solar heating warms the lake surface waters, and wind mixing carries this heat away from the surface. During spring and early summer, the solar heating generally adds more heat (and buoyancy) to the upper waters than can be efficiently removed from the surface by turbulence in the water, and the surface becomes much warmer than the deep waters. Separating the warm surface waters from the denser bottom waters is a region in which temperature changes rapidly with depth, the thermocline. The upper (epilimnion) and lower (hypolimnion) layers have much lower vertical temperature gradients than the thermocline region.

As insolation diminishes in late summer, air temperatures also fall, and the surface is cooled by turbulent exchange of heat to the atmosphere. Winds are generally stronger in autumn than in mid summer, and thermal

convection provides an additional source of turbulent energy in the epilimnion. Turbulence at the top of the thermocline entrains the lower water into the epilimnion and the thermocline deepens. Cooling and convection continue until the whole lake is once again isothermal.

This is a typical cycle which is repeated in moderate to large lakes year after year. In very deep lakes the bottom temperature never exceeds 4°C. Hutchinson (1957) classifies these as first class lakes. In lakes of moderate depth, the bottom temperature will exceed 4°C, but a well defined thermocline is present (second-class lake, Hutchinson, 1957). In shallow lakes no thermocline develops, the whole lake remaining nearly isothermal throughout the summer (third class lake according to Hutchinson).

Whether a lake is "very deep", "moderately deep", or "shallow" in this sense depends not only on its depth, but also on the mixing characteristics of the lake and the climatic regime.

This typical seasonal cycle may vary in many details (such as surface temperature, epilimnion depth, etc.) from lake to lake. Basin morphometry, optical properties of the lake water, variations in incoming solar radiation and atmospheric conditions are responsible for most of these variations. As the different thermal cycles of large and small lakes is one of the subjects investigated in this

work, it is instructive to consider the annual variation of one readily available thermal property, surface temperature, in three lakes of different size subjected to nearly the same thermal forcing. Figure 1 shows the annual trends of insolation, I_o, air temperature, T_a, and lake surface temperature, T_s, for Lake Cayuga, New York (42°45'N, 76°47'W), Lake Ontario (43°40'N, 78°W), and Lake Mendota, Wisconsin (43°7'N, 88°25'W). The vertical bars encompass the typical diurnal range of air temperature. All of the temperature curves represent climatological means. These lakes are within 1° of latitude and subjected to very similar atmospheric forcing. Cayuga and Ontario are first-class lakes, while Mendota is a second class lake (bottom temperature 12°C during summer stratified season). The smaller lakes warm more rapidly than the larger lake in the period April 15 to June 30.

Blanton (1973) showed that the rate of deepening of the thermocline is greater in larger lakes. One possible source of energy for the more vigorous mixing in large lakes is the correspondingly greater energy in the surface wave field.

The occurrence of the thermocline is an important event in the annual cycle of a lake. The considerable density difference across the thermocline suppresses turbulent exchange of dissolved and suspended constituents, heat, and momentum. The ecology of the lake is so

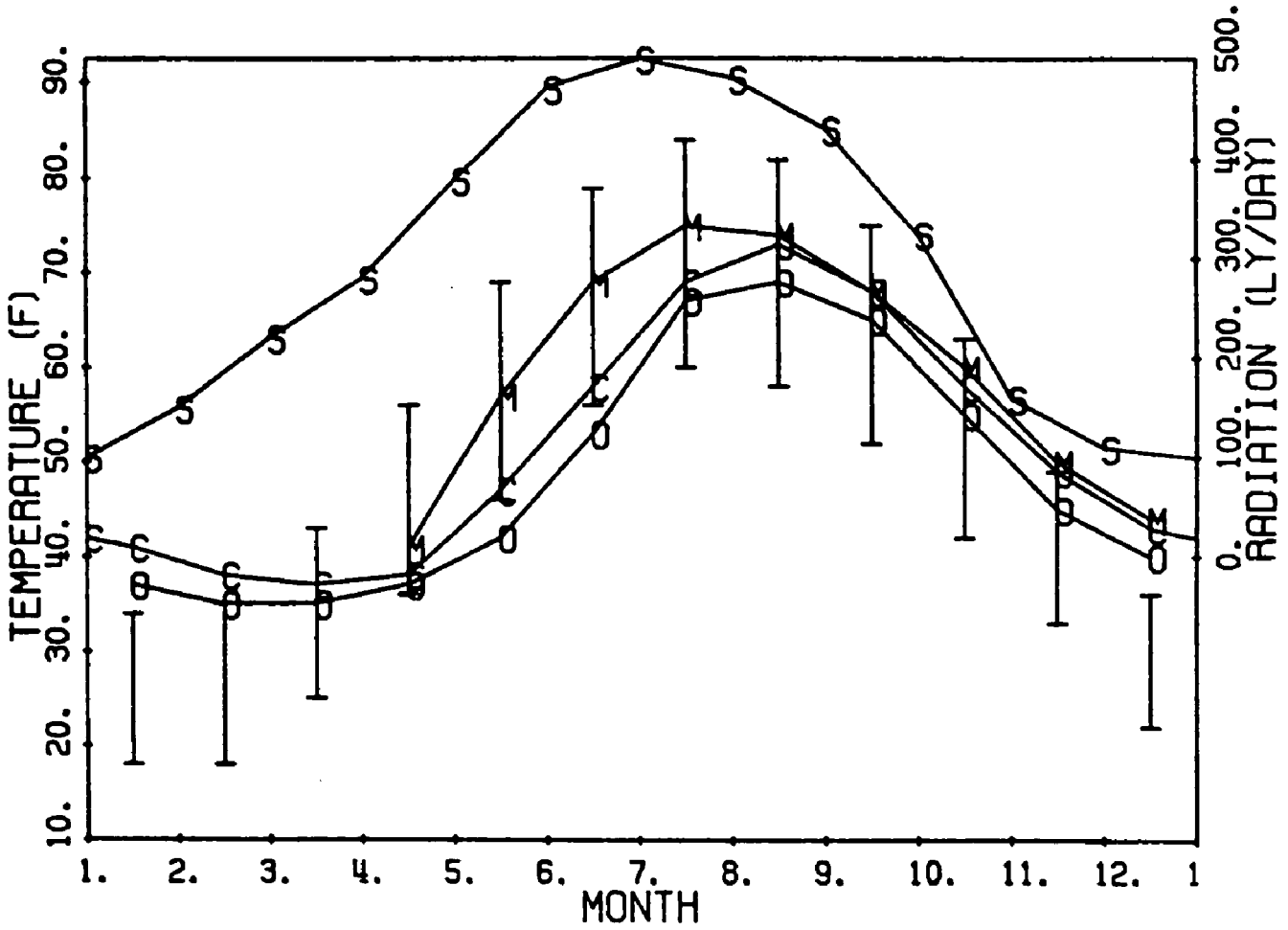


Fig. 1. Annual cycles of insolation (S) and lake surface temperature of Lake Mendota (M), Lake Cayuga (C), and Lake Ontario (O). The typical diurnal range of air temperature is indicated by the vertical bars. Lake Ontario is much larger than the other two lakes.

strongly dependent on the density stratification that prediction of the thermal structure must be considered as the first step in any attempt to model a lake's ecology. One of the goals of this research has been to develop an economical, physically sensible model to serve this purpose.

The following section of this introduction is a qualitative discussion of the physical processes believed to be important in effecting temperature changes throughout the lake. Then the annual cycle will be reviewed and interpreted in light of these physical mechanisms.

Solar radiation. The surface flux of solar radiation exhibits strong annual and diurnal variations, which are responsible for the significant diurnal and annual cycles of the water temperature. Most of the energy which passes through the atmosphere is in the visible portion of the spectrum. This also corresponds to the spectral range in which lake water is most transparent. Infrared radiation is absorbed in the first few centimeters. Ultraviolet attenuation varies widely among natural water bodies, but with a maximum scale length, β^{-1}, of 2m (Hutchinson, 1957).

The radiant intensity decays exponentially at any given wavelength. Thus,

$$I(z) = \int I(z,\lambda)d\lambda = \int I_o(\lambda)e^{\beta(\lambda)z}d\lambda \qquad (1)$$

For pure water the dependence of β on λ is known. In lakes various dissolved and suspended contaminants,

primarily of biological origin, alter the optical characteristics of the water, changing not only the magnitude of β, but also its wavelength dependence. Determination of $\beta(\lambda)$ is not a simple matter, and the integral (1) cannot generally be evaluated. Subsequently, the approximation $I(z) = S^{*}e^{\beta z}$, is generally used and found to be of sufficient precision for considerations of the distribution of solar heating with depth. Lakes exhibit considerable variations in optical properties. Deep, unproductive lakes fed by clear streams are most transparent. In the clearest lakes $\beta = .001\ cm^{-1}$, in which 99% of the penetrating component of surface radiation is attenuated by a depth of 46m. Values of $\beta = .05\ cm^{-1}$ are not uncommon in shallow coastal regions, or in extremely productive lakes. In that case nearly all the incoming radiation is absorbed in, and used to heat, the upper meter of water.

Surface heat exchange with the atmosphere. Heat is transferred between the air and water at their interface by three mechanisms, (a) transfer of sensible heat due to air-sea temperature differences, (b) transfer of latent heat by evaporation or condensation, depending on the saturation of the lower atmosphere with respect to the water surface; and (3) transfer of infrared radiation. Both the atmosphere and the water surface radiate in the

infrared, but the flux is invariably from water to air due to the higher emissivity of the water.

Likewise, evaporation occurs more frequently and at greater rates than condensation so this flux is also generally directed upward. The air-sea temperature difference, and subsequent sensible heat flux, change sign and magnitude with annual and diurnal cycles.

Latent and sensible heat transferred at the air-sea interface must first pass through a laminar boundary layer at rates controlled by molecular properties of the two media and the imposed temperature difference across the sublayers. In the context of this work, these molecular properties may be considered invariant. After passing these sublayers, turbulent exchange dominates. The intensity of turbulent exchange affects the transfer at the boundary by changing the thickness and gradients of the sub-layers. The turbulent exchange processes are highly variable on all time scales of interest.

Nearly all lakes, regardless of their size, are surrounded by much greater expanses of land. The land surface, of course, has quite different thermal and mechanical properties than the lake. The surface air, which has been interacting with the land surface, may be far from equilibrium with the lake surface. When the lake surface temperature is warmer than the air, convective motions are likely to increase heat transfer in both fluids and

through the interface. When the air is warmer, both fluids tend to be gravitationally stable, and turbulent exchange is suppressed. These variations exhibit a seasonal cycle, primarily because the land surface temperature responds more rapidly than the lake to seasonal changes in insolation. From Fig. 1, peak air temperatures lag peak insolation by only 15 days. The lakes respond more slowly, their surface temperatures peaking ≈45 days after maximum insolation.

The lower atmosphere is generally warmer than the lake surface during the spring, and the transfer of sensible heat is downward at the interface. This transfer tends to stabilize both fluids and diminish further turbulent exchange. In the fall, the lake surface is warmer than the atmosphere, and convection will amplify turbulent exchange of heat and water vapor. The author limits use of the term, convection, to motions caused by an unstable density stratification.

The air-lake temperature difference also exhibits diurnal fluctuations, with convective transfer more likely to occur at night.

Wind forcing (mechanical). Wind blowing over the lake surface transfers momentum and kinetic energy to the water in two modes, by normal pressure fluctuation and tangential stress. The pressure fluctuations build the wave field, and the stress initiates a shear flow in the

water. Recent observations (Dobson, 1971; Hasselmann, et al, 1973) and theoretical treatments (Hasselmann, 1974) indicate that the transfer to the wave field accounts for most of the transfer of energy and momentum at the surface.

The wave motion is not primarily turbulent and is not capable of producing mixing. However, as the waves grow and become more steep, they become unstable and break. Waves steepen and break in shallow water, and this process accounts for a large part of the dissipation of the wave field, but steep waves also break in deep water. When they do, a portion of the considerable kinetic energy of the waves becomes available for mixing. The energy loss from the wave-field by wave-breaking is postulated by Hasselmann (1974) to increase linearly with the wave energy, which increases with the fetch or distance over which the wind acts on the water. The model to be presented in Chapter 5 is based on the supposition that wave breaking is a significant fetch-dependent source of turbulent energy for the epilimnion. That some fetch-dependent mixing mechanism must exist can be inferred from the work of Blanton (1973), who showed that the rate of deepening of the thermocline is positively correlated with lake size.

Observations of the temporal change of turbulence spectra near the surface of Lake Ontario by Lemmin, et al

(1974) provide evidence that wave generated turbulence is a significant mechanism for mixing the near surface waters of a large lake.

The energy transferred tangentially at the surface may be much less than the energy fed to the waves, but it is by no means unimportant in effecting temperature change. While wave-breaking produces turbulence only at or near the surface, the shear flow may be unstable in the interior of the fluid. Wave-breaking may be most important in keeping the epilimnion mixed, while shear instability at the thermocline and the boundary layer type turbulence associated with the shear flow may be of greater importance in deepening the mixed layer.

Of course, the momentum transferred at the surface by these processes generates a horizontal mean current which can transport heat laterally by advection. This current is often unstable to large scale (order of the epilimnion depth) cellular motions, called Langmuir cells, which are undoubtedly of great importance in mixing the epilimnion.

At the onset of strong winds, energy is passed quickly into inertial currents, largely confined to the epilimnion. This causes a considerable shear across the thermocline which can cause vertical mixing through the Kelvin-Helmholtz instability.

Interaction of turbulence with stratification. The gravitational field of the earth is strong enough that even the very small density variations occurring in lakes produce buoyancy forces which have significant dynamical consequences. The stable density gradient across the thermocline is of the greatest importance in suppressing turbulent motions which might otherwise reduce the gradient. Any turbulent eddy which mixes heat downward does so at the expense of its own kinetic energy. In mixing light water downward, and dense water up, the center of mass of the mixed water has been raised, increasing its potential energy. The source of this potential energy is the kinetic energy of the turbulence. The general technique of the model presented in this work is to account for all other sources and sinks of kinetic energy. The remaining portion is assumed to be used to increase the potential energy of the lake by vertical mixing.

Conversely, an unstable stratification contributes to the turbulent kinetic energy by causing convective motion. As the surface is generally the locus of heat losses from the lake, convection generally proceeds from the surface down to a depth, z, where $T(z) = T_s$. Kraus and Rooth (1961) suggested that since the solar heating is penetrative, while the cooling processes are limited to the top

millimeter or so, convection could occur within a shallow region, even if the sun is shining. This phenomenon was first observed by Woodcock (1941).

Convection is unarguably of great importance in autumn deepening of the mixed layer, but there is some debate concerning the role of nocturnal convection in mixing the epilimnion during spring and early summer. Latent heat flux and infrared radiation combine almost invariably to cause a cooling of the lake surface. If sensible heat flux is also directed upward at night then convection must occur. Again we refer to Fig. 1 to indicate the diurnal variation in T_a. If nocturnal air temperatures are less than the lake surface temperature, convection should mix the surface waters. As can be seen, this is more likely to occur in small lakes than in large ones in the same climatic regime. Consequently, spring-time nocturnal convection probably plays a greater role in small lakes than large ones.

Dissipation of turbulent energy. A large part of the turbulent energy generated by the aforementioned processes is not converted to potential energy, but to heat through viscous dissipation. As the heat capacity of water and the mechanical equivalent of heat are both large, this is an insignificant source in the heat budget, but a significant sink in the mechanical energy budget. Small scale motions, e.g., those associated with wave-breaking, are

rapidly dissipated because of the intense local velocity gradients. Large-scale organized motions like Langmuir rolls and convective cells have a lower dissipation rate. For this reason, wave-generated turbulence must decrease in intensity rapidly with depth, while motions associated with Langmuir cells and convection can be significant at the base of the epilimnion.

Perhaps at this time a clarification of the scales of motion designated as turbulence is in order. Essentially, all motions with scales of the order of the epilimnion thickness, or less, are considered turbulence in the context of this work. Variations on a larger scale are constrained by the stratification to two-dimensionality, and are therefore not of much use in accomplishing vertical mixing except in the event of shear instability at the thermocline. The largest modes of turbulent motion in this sense are convective cells and Langmuir cells.

Generation of internal waves. Internal waves are apparently ubiquitous at the thermocline, especially when the epilimnion kinetic energy is large. Two mechanisms for generation of internal waves have been shown to be important in their effects on vertical mixing. The epilimnion is generally fully turbulent, and the turbulent pressure fluctuations at the top of the thermocline can generate internal waves in an analogous manner to the Phillips (1957) mechanism for the generation of gravity

waves at the sea surface. The turbulent energy is then transferred to the internal waves which may radiate this energy horizontally and vertically without causing any local mixing.

Another source of energy for internal waves is the vertical shear of the horizontal current. If $Ri = -\frac{g}{\rho}\frac{\partial \rho}{\partial z} / \left|\frac{dU}{\partial z}\right|^2 \leq \frac{1}{4}$, the thermocline or some internal density interface associated with it, will be unstable, and internal waves will grow. If the shear is maintained, they break and mix a limited layer of water. This should increase Ri, the Richardson number, and tend to restore stability. In this case, energy associated with the larger scale horizontal current, which may be considered unavailable for vertical mixing, is, through a two step process, converted into potential energy and heat (through viscous dissipation).

The magnitude and relative importance of these two energy exchange processes in various environments is not well known. However, Kaye (1974) has shown shear instability to be effective in lakes, and Linden (1975) constructed a laboratory experiment in which turbulent pressure fluctuations generate internal waves.

Additional comments on thermal cycles of lakes. The thermal cycle of lakes is recapped in light of the mechanisms discussed above. After spring overturn the air-lake

temperature difference is generally positive, and the stable stratification suppresses vertical exchange of heat, water vapor, and kinetic energy on both sides of the air-lake interface. Insolation is the dominant thermal input, and convection and wind mixing are generally too sluggish to distribute the solar heating to deeper parts of the lake. The temperature profile tends toward an exponential shape, characteristic of the distribution of solar heating. If nighttime air temperatures fall below the temperature of the lake surface, convection will occur. Wave action may keep a shallow layer mixed at the surface. In mid-summer, air and lake temperatures equalize, so little sensible heat is exchanged, although evaporation rates may be quite high. Nocturnal convection and occasional storms gradually deepen the mixed layer, while its temperature remains fairly uniform. Solar radiation continues to be the largest term in the heat budget. In fall, insolation diminishes, while the air-lake temperature difference becomes negative. Convective motions facilitate large fluxes of heat from the lake to the air. Convection and wind mixing drive the weakening thermocline toward the lake bottom.

This concludes a qualitative discussion of the major physical processes responsible for the observed thermal cycle of lakes. Although a similar annual sequence of events occurs in many lakes, the particulars of the

cycle, such as surface temperature, mixed layer depth, and bottom temperature, vary substantially with basin morphometry, optical characteristics, and climatic regime.

CHAPTER II

THE GOVERNING EQUATIONS: A SCALE ANALYSIS

To determine the relative magnitudes of terms in the momentum, heat, and turbulent kinetic energy conservation equations, a scaling analysis is in order. The thermocline is the result of mixing processes which are predominantly turbulent in lakes. In order to examine the interactions which occur, consider the classical separation of velocities and scalar properties into mean and fluctuating parts:

$$p = \bar{p} + p', \quad \rho = \bar{\rho} + \rho', \quad T = \bar{T} + \theta, \quad v_1 = U + u,$$

$$v_2 = 0, \quad v_3 = W + w$$

where p is pressure, ρ is density, T is temperature, v_i is the ith component of the velocity vector, and the bar denotes an average over an ensemble of observations during which the external conditions are unchanged. For geophysical observations it is generally impossible to determine the ensemble average, which is generally approximated as an average over a finite interval of time, long compared to the turbulent fluctuation time scale. This is sensible, if not rigorous, since the goal of the analysis is to distinguish rapid fluctuations from slowly varying quantities. However, the ensemble average and the finite time average are not identical, and this approximation should not be overlooked in the analysis of observations.

The equations of motion will be initially considered in only two dimensions, $v_2 = 0$, to avoid unnecessary complication in the scaling analysis. Scaling analysis for the x-component is identical to that of the y-component. After the equations have been somewhat simplified, the y-component will be introduced, especially to consider the effects of rotation.

With the partitioning of mean and fluctuating components the Navier-Stokes equations become

$$\frac{\partial}{\partial t}(\bar{\rho}U + \overline{\rho' u}) + \frac{\partial}{\partial x}(\bar{\rho}U^2) + \frac{\partial}{\partial z}(\bar{\rho}UW) = -\frac{\partial \bar{p}}{\partial x} + \left[\mu(+2\frac{\partial^2 U}{\partial x^2} + \frac{\partial^2 W}{\partial x \partial z} + \frac{\partial^2 U}{\partial z^2}\right] - \frac{\partial}{\partial x}(\overline{\rho u^2}) - 2\frac{\partial}{\partial x}(U\overline{\rho' u}) - \frac{\partial}{\partial z}(\overline{\rho u w}) - \frac{\partial}{\partial z}(W\overline{\rho' u}) \quad (2)$$

$$- \frac{\partial}{\partial z}(U\overline{\rho' w});$$

and

$$\frac{\partial}{\partial t}(\overline{\rho' w}) = -\frac{\partial \bar{p}}{\partial z} + \mu(2\frac{\partial^2 W}{\partial z^2} + \frac{\partial^2 W}{\partial x^2} + \frac{\partial^2 U}{\partial x \partial z}) - \frac{\partial}{\partial x}(\overline{\rho u w}) - \frac{\partial}{\partial z}(U\overline{\rho' w})$$

$$- \frac{\partial}{\partial z}(\overline{\rho w^2}) - \bar{\rho} g; \quad (3)$$

and the continuity equation is

$$\frac{\partial \bar{\rho}}{\partial t} + \frac{\partial}{\partial x}(\bar{\rho}U + \overline{\rho' u}) + \frac{\partial}{\partial z}(\bar{\rho}W + \overline{\rho' w}) = 0. \quad (4)$$

The thermal energy conservation equation for constant specific heat, conductivity, and viscosity is

$$\frac{\partial}{\partial t}(\rho\overline{T}) + \frac{\partial}{\partial x}(\overline{\rho T}U) + \frac{\partial}{\partial z}(\overline{\rho T}W) + \frac{\partial}{\partial t}(\overline{\rho'\theta}) + \frac{\partial}{\partial x}(\overline{\rho'\theta}U) + \frac{\partial}{\partial x}(\overline{\rho'\theta}U)$$

$$+ \frac{\partial}{\partial z}(\overline{\rho'\theta}W) = \frac{\partial}{\partial x}(\overline{\rho\theta u}) + \frac{\partial}{\partial z}(\overline{\rho\theta w}) - \frac{\partial}{\partial x}(\overline{\rho' uT}) - \frac{\partial}{\partial z}(\overline{\rho' wT}) \quad (5)$$

$$+ \frac{k}{c_p}\frac{\partial^2\overline{T}}{\partial z^2} + \frac{Q}{c_p},$$

where Q is the sum of all sources and sinks.

The density is assumed to depend on temperature only, with the equation of state, $\rho = f(T)$, implying

$$\overline{\rho} = f(\overline{T}),\ \rho' = f(\overline{T} + \theta) - f(\overline{T}),\ \frac{\partial\overline{\rho}}{\partial t} = f'\frac{\partial\overline{T}}{\partial t}$$

Let $\overline{p} = p^{atm} - \rho gz + \tilde{p}(x,z,t)$, where p^{atm} is the atmospheric pressure, assumed constant, the second term is the hydrostatic pressure field, and the third term results primarily from the slope of the lake surface.

To convert these equations to dimensionless form, let $\overline{\rho} = \rho_o\rho_s$, $U = U_oU_s$, $u = u_ou_s$, $w = w_ow_s$, $\theta = \theta_o\theta_s$, $\overline{T} = T_o\overline{T}_s$, $\rho' = \rho_f\rho_s$, $z = hz_s$, $x = Lx_s$, $p' = \rho_o u^2{}_o p'_s$, $t = t_o t_s$,

$$\frac{\partial\overline{p}}{\partial z} = [-\rho_o g + \frac{\tilde{p}_o}{h}]\frac{\partial\overline{p}_s}{\partial z_s},\ \frac{\partial\overline{p}}{\partial x} = [\frac{\tilde{p}_o}{L}]\frac{\partial\tilde{p}_s}{\partial x_s},$$

where a subscript s denotes a dimensionless quantity whose magnitude is nearly one.

For convenience, the "s" subscripts are dropped. All variables in the equation to follow are non-dimensional.

The continuity equation becomes

$$[f'T_o]\frac{\partial \bar{T}}{\partial t} + [\frac{\rho_o W_o}{h}]\frac{\partial}{\partial z}(\bar{\rho}\bar{W}) + [\frac{\rho_f w_o}{h}]\frac{\partial}{\partial z}(\overline{\rho' w}) + [\frac{\rho_o U_o}{L}]\frac{\partial}{\partial x}(\bar{\rho}U) + [\frac{\rho_f u_o}{L}]\frac{\partial}{\partial x}(\overline{\rho' u}) = 0 . \quad (6)$$

Since $f' << 1$, $\rho_f << \rho_o$, $w_o < W_o$, $u_o < U_o$, to first order,

$$[\frac{U_o}{L}]\frac{\partial U}{\partial x} + [\frac{W_o}{h}]\frac{\partial W}{\partial z} = 0, \quad (7)$$

which implies

$$W_o = \frac{U_o h}{L} .$$

After converting to dimensionless form and rearranging the coefficients, the z-momentum equation becomes

$$\left[\frac{\rho_f w_o}{\rho_o g t_o}\right]\frac{\partial}{\partial t}(\overline{\rho' w}) = \left[-1 + \frac{\tilde{p}_o}{\rho_o g h}\right]\frac{\partial \bar{p}}{\partial z} + \left[\frac{2\mu U_o}{\rho_o g h L}\right]\frac{\partial^2 W}{\partial z^2} + \left[\frac{\mu U_o h}{\rho_o g L^3}\right]\frac{\partial^2 W}{\partial x^2} + \left[\frac{\mu U_o}{\rho_o g h L}\right]\frac{\partial^2 U}{\partial x \partial z} - \left[\frac{u_o w_o}{gL}\right]\frac{\partial}{\partial x}(\overline{\rho u w}) \quad (8)$$
$$- \left[\frac{U_o \rho_f w_o}{\rho_o g L}\right]\frac{\partial}{\partial x}(U\overline{\rho' w}) - \left[\frac{w_o^2}{gh}\right]\frac{\partial}{\partial z}(\overline{\rho w^2}) - 1,$$

where $R_e = \frac{\rho_o U_o L}{\mu}$, is the Reynolds number.

To examine the magnitudes of the various terms, one must specify the scale of the problem in question. For instance, consider daily changes of the epilimnion of a moderate to large lake:

$t_o = 10^5 s$, $L = 2 \times 10^6 cm$, $\rho_o = 1 \frac{gm}{cm^3}$, $\mu = 10^{-2} \frac{gm}{cm\ s}$, $h = 10^3 cm$,

$\rho_f = 3 \times 10^{-4} \frac{gm}{cm^3}$, $U_o = 20 \frac{cm}{s}$, $u_o = 10 \frac{cm}{s}$, $g = 10^3 \frac{cm}{s^2}$,

$\tilde{p}_o = \rho_o g s L = 2 \times 10^4$,

where $s(\approx 10^{-5})$ is the magnitude of the surface slope. It is assumed that the turbulence is isotropic, so that $u_o = w_o$.

The magnitudes of the various terms in the z-momentum equation (8) are

$$\frac{\rho_f w_o}{\rho_o g t_o} = 3\times10^{-11},\quad \frac{\tilde{p}_o}{\rho_o g h} = 2\times10^{-2},\quad \frac{2\mu U_o}{\rho_o g h L} = 4\times10^{-13},\quad \frac{\mu U_o h}{\rho_o g h L} = 2\times10^{-13},$$

$$\frac{\mu U_o h}{\rho_o g L^3} = 2\times10^{-19},\quad \frac{u_o w_o}{gL} = 1\times10^{-7},\quad \frac{U_o \rho_f w_o}{\rho_o g L} = 6\times10^{-11},\quad \frac{w_o^2}{gh} = 10^{-4},$$

which illustrates that, to first order, the vertical pressure gradient balances the force of gravity.

The x-momentum equation in dimensionless form is

$$\left[\frac{L^2\rho_o}{t_o\mu}\right]\frac{\partial}{\partial t}(\bar{\rho}U) + \left[\frac{\rho_f u_o L^2}{t_o U_o \mu}\right]\frac{\partial}{\partial t}(\overline{\rho' u}) + R_e\frac{\partial}{\partial x}(\bar{\rho}U^2)$$
$$+ R_e\frac{\partial}{\partial z}(\bar{\rho}UW) = -\left[\frac{\rho_o g s L^2}{U_o\mu}\right]\frac{\partial \bar{p}}{\partial x} + 2\frac{\partial^2 U}{\partial x^2} + \frac{\partial^2 W}{\partial x\partial z} + \left[\frac{L^2}{h^2}\right]\frac{\partial^2 U}{\partial z^2}$$
$$- \left[\frac{\rho_o u_o^2 L}{U_o\mu}\right]\frac{\partial}{\partial x}(\overline{\rho u^2}) - \left[\frac{2\rho_f L u_o}{\mu}\right]\frac{\partial}{\partial x}(U\overline{\rho' u}) \qquad (9)$$
$$- \left[\frac{\rho_o u_o w_o L^2}{U_o\mu h}\right]\frac{\partial}{\partial z}(\overline{\rho u w}) - \left[\frac{\rho_f u_o L}{\mu}\right]\frac{\partial}{\partial z}(W\overline{\rho' u})$$
$$- \left[\frac{L^2\rho_f w_o}{\mu h}\right]\frac{\partial}{\partial z}(U\overline{\rho' w});$$

$$\mathrm{Re} = 4\times10^9,\quad \frac{L^2\rho_o}{t_o\mu} = 4\times10^9,\quad \frac{\rho_f u_o L^2}{t_o\mu U_o} = 6\times10^5,\quad \frac{\rho_o g s L^2}{U_o\mu} = 2\times10^{11},$$

$\frac{L^2}{h^2}=4x10^6$, $\frac{\rho_o u_o{}^2 L}{U_o \mu}=10^9$, $\frac{2\rho_f L u_o}{\mu}=1.2x10^6$, $\frac{\rho_o u_o w_o L^2}{U_o \mu h}=2x10^{12}$, $\frac{\rho_f u_o L}{\mu}=6x10^5$, $\frac{L^2 \rho_f w_o}{\mu h}=1.2x10^9$. To lowest order, retaining all terms whose magnitude is $>10^{11}$,

$$\left[\frac{\rho_o g s L^2}{U_o \mu}\right] \frac{\partial \bar{p}}{\partial x} + \left[\frac{\rho_o u_o{}^2 L^2}{U_o \mu h}\right] \frac{\partial}{\partial z}(\rho \overline{uw}) = 0.$$

Retaining all terms whose magnitude are of order $4x10^9$ or greater, yields

$$\left[\frac{L^2 \rho_o}{t_o \mu}\right] \frac{\partial}{\partial t}(\bar{\rho} U) + Re \left[\frac{\partial}{\partial x}\bar{\rho} U^2 + \frac{\partial}{\partial z}\overline{\rho u w}\right] = - \left[\frac{\rho_o g s L^2}{U_o \mu}\right] \frac{\partial \bar{p}}{\partial x} - \left[\frac{\rho_o u_o{}^2 L^2}{U_o \mu h}\right] \frac{\partial}{\partial z}(\overline{\rho u w}). \quad (10)$$

Thus in any problem in which the local accelerations are important, non-linear terms must be retained.

The thermal energy equation in dimensionless form is

$$\left[\frac{h T_o}{\theta u_o t_o}\right] \frac{\partial}{\partial t}(\overline{\rho T}) + \left[\frac{h T_o U_o}{L \theta_o u_o}\right] \left\{\frac{\partial}{\partial x}(\overline{\rho T U}) + \frac{\partial}{\partial z}(\overline{\rho T W})\right\}$$

$$+ \left[\frac{\rho_f h}{\rho_o u_o t_o}\right] \frac{\partial}{\partial t}(\overline{\rho' \theta}) + \left[\frac{\rho_f U_o h}{\rho_o u_o L}\right] \left\{\frac{\partial}{\partial x}(\overline{\rho' \theta U}) + \frac{\partial}{\partial z}(\overline{\rho' \theta W})\right\} =$$

$$- \left[\frac{h}{L}\right] \frac{\partial}{\partial x}(\overline{\rho \theta u}) - \left[\frac{\rho_f T_o h}{L \rho_o \theta_o}\right] \frac{\partial}{\partial x}(\overline{\rho' u T}) + \left[\frac{k T_o h}{c_p \rho_o \theta_o u_o L^2}\right] \frac{\partial^2 \bar{T}}{\partial x^2} \quad (11)$$

$$- \frac{\partial}{\partial z}(\overline{\rho \theta w}) - \left[\frac{\rho_f T_o}{\rho_o \theta_o}\right] \frac{\partial}{\partial z}(\overline{\rho' w T}) + \left[\frac{k T_o}{c_p \rho_o \theta_o u_o h}\right] \frac{\partial^2 \bar{T}}{\partial z^2}$$

$$+ \left[\frac{Q_o h}{c_p \rho_o \theta_o u_o}\right] \Omega.$$

Over a diurnal cycle, changes in the mean temperature, represented by T_o, are smaller than the short term fluctuations. Typical values are

$T_o=.5°C$, $\theta_o=1°C$, $c_p=1\frac{cm^2}{s^2 °C}$, $k=1.4x10^{-3}\ \frac{cm^2}{s}$, $Q_o=$

$5x10^{-5}\ \frac{cal}{cm^3 sec}$. Then,

$$\frac{hT_o}{\theta_o u_o t_o}=5x10^{-4},\quad \frac{hT_o U_o}{L\theta_o u_o}=5x10^{-4},\quad \frac{\rho_f h}{\rho_o u_o t_o}=3x10^{-7},\quad \frac{\rho_f U_o h}{\rho_o u_o L}=3x10^{-7},$$

$$\frac{h}{L}=5x10^{-4},\quad \frac{\rho_f T_o h}{L\rho_o \theta_o}=7.5x10^{-8},\quad \frac{kT_o h}{c_p \rho_o \theta_o u_o L^2}=1.8x10^{-14}$$

$$\frac{\rho_f T_o}{\rho_o \theta_o}=1.5x10^{-4},\quad \frac{kT_o}{c_p \rho_o \theta_o u_o h}=7x10^{-8},\quad \frac{Q_o h}{c_p \rho_o \theta_o u_o}=5x10^{-3}.$$

To lowest order then, $\frac{\partial}{\partial z}(\overline{\theta w}) = 0$, i.e., a constant flux layer exists near the boundary.

As the goal of this study is to predict changes in the mean temperature, all terms whose magnitude is of the order of $5x10^{-4}$ must be retained, yielding

$$\left[\frac{hT_o}{\theta_o u_o t_o}\right]\overline{\frac{\partial \rho T}{\partial t}} + \left[\frac{hT_o U_o}{\theta_o u_o L}\right]\left[\frac{\partial}{\partial x}(\overline{T}\overline{U}) + \frac{\partial}{\partial z}(\overline{T}\overline{W})\right] = -\left[\frac{h}{L}\right]\frac{\partial}{\partial x}(\overline{\theta u}) - \frac{\partial}{\partial z}(\overline{\theta w}) + \left[\frac{Q_o h}{c_p \rho_o \theta_o u_o}\right] Q. \tag{12}$$

Obviously, molecular conduction of heat is negligible as are terms associated with the density fluctuations. Density variations are important only in their effect on

w_o and the vertical turbulent heat flux. The solar heating source is the largest second order term, and local changes in temperature, advection, and horizontal turbulent fluxes are second order effects of approximately equal magnitude.

This ordering is manifest in the difficulties encountered in attempts to describe vertical mixing processes on the basis of measurements of local temperature changes (see, e.g., Stommel, et al, 1969; Bowden, et al, 1970). Local changes of temperature are very small, and conditions must be extremely favorable if horizontal advection is to be neglected. This also accounts for most of the successes and limitations of one-dimensional thermocline models when applied to the diurnal time scale. To first order, the problem is one-dimensional, but to predict temperature changes one should also include horizontal fluxes of heat. It will be shown in Chapter 4, that horizontal advective and turbulent fluxes can be eliminated from the heat conservation equation by averaging horizontally over the lake surface. The effects of horizontal fluxes on the horizontally averaged temperature profile is generally small, though not always insignificant.

To introduce the effects of rotation, the three-dimensional form for the x-momentum equation, consistent with the previous scaling, is introduced:

$$\left[\frac{1}{f_o t_o}\right]\frac{\partial\bar{\rho}U}{\partial t} + Ro\left\{\frac{\partial}{\partial x}(\bar{\rho}U^2) + \frac{\partial}{\partial y}(\bar{\rho}UV) + \frac{\partial}{\partial z}(\bar{\rho}UW)\right\} = f_s\bar{\rho}V$$

$$+\left[\frac{\rho_f u_o}{\rho_o U_o}\right]f_s(\overline{\rho' v}) - \left[\frac{gs}{U_o f_o}\right]\frac{\partial\bar{p}}{\partial x} - \left[\frac{u_o^2}{f_o U_o h}\right]\left\{\frac{\partial}{\partial z}(\rho uw) - \left[\frac{h}{L}\right]\frac{\partial}{\partial x}(\overline{\rho u^2})\right.$$

$$\left. - \left[\frac{h}{L}\right]\frac{\partial}{\partial y}(\overline{\rho uv})\right\} - \left[\frac{\rho_f u_o}{\rho_o f_o h}\right]\frac{\partial}{\partial z}(U\overline{\rho' w}) \qquad (13)$$

where

$V_2 = V+v$, $f_o f_s = 2\Omega\sin\phi$, the Coriolis parameter, and the Rossby number, $R_o = \frac{U_o}{f_o L}$, with $f_o = 10^{-4}$. Then

$$\frac{1}{f_o t_o} = .1,\ Ro = .2,\ \frac{\rho_f u_o}{\rho_o U_o} = 1.5\times10^{-4},\ \frac{gs}{U_o f_o} = 5,\ \frac{u_o^2}{f_o U_o h} = 50,$$

$$\frac{u_o^2}{f_o U_o L} = 5\times10^{-2},\ \frac{\rho_f u_o}{\rho_o f_o h} = 3\times10^{-2}.$$

To zeroth order the epilimnion is a constant stress region. This order of approximation is adequate within ≈2m of the surface. To first order the three-dimensional equations of motion near the surface of the lake are

$$f\rho V - \frac{\partial\bar{p}}{\partial x} - \frac{\partial}{\partial z}(\rho\overline{uw}) = 0,\ f\rho U + \frac{\partial\bar{p}}{\partial y} + \frac{\partial}{\partial z}(\rho\overline{vw}) = 0\ ,$$

$$\frac{dp}{dz} = -\rho_o g.$$

To second order it is difficult to justify elimination of $\frac{\partial\bar{\rho}U}{\partial t}$, nonlinear terms prefaced by Ro, horizontal Reynolds stress divergence, or interaction of $\overline{\rho' w}$ which is generally eliminated through the Boussinesq approximation.

Note that the balance of forces is hardly geostrophic, which is the case when $\frac{gs}{U_o f_o} \approx 1$, and all other dimensionless parameters are $<<1$. The local and advective accelerations are small, but not insignificant. The relative importance of local accelerations vis-a-vis the Coriolis acceleration depends crucially on the time scale, t_o, chosen here to be 10^5 s, slightly longer than one day. If the time scale of interest were the inertial period, $\frac{2\pi}{f_o}$, or less, local accelerations could not be neglected.

Both the heat conservation equation and the equations of motion stress the importance of advection and horizontal mixing on the diurnal scale. Advective terms are small compared to the vertical turbulent fluxes, but of the same order as the local changes (of temperature or momentum).

The scaling of the thermal energy equation favors local changes in temperature on the seasonal scale: T_o=18°C, θ_o=2°C, t_o=30 days; h=20 m, U_o=20 $\frac{cm}{sec}$, L=100 km (a horizontal dimension of the lake), u_o=5 $\frac{cm}{sec}$. Here T_o is a differential temperature scale valid for temporal or vertical variations. Horizontal variations, however, rarely exceed 5°C. Let the horizontal temperature variation, T_{oh}=5°c. Then

$$\frac{hT_o}{\theta_o u_o t_o}=7\times10^{-4},\quad \frac{hT_o h U_o}{\theta_o u_o L}=2\times10^{-3},\quad \frac{h}{L}=2\times10^{-4}.$$

The value of the advective flux is still large, but this estimate is based on the assumption that $\overline{T}$ and U are well correlated over the period of interest. Because of the sidewall boundaries of lakes, $\overline{T}$ and U cannot remain well correlated over periods longer than the period of the gravest mode of internal gravity waves, generally of order 10 days in large lakes during the stratified season. The time-integrated advective flux will nearly vanish over a period of 30 days or more. In the seasonal cycle, then, one expects horizontal fluxes to be of lesser importance than on the diurnal scale.

The final equation to be considered in this section is the turbulent kinetic energy conservation equation. The derivation of this equation is well known (see Kraus, 1972). The turbulent energy conservation equation is

$$\frac{1}{2}\frac{\partial}{\partial t}(\overline{v_j v_j}) = -\frac{\partial}{\partial x_j}\left\{\frac{1}{2}V_i\overline{v_j v_j} + \overline{v_i\left(\frac{1}{2}v_j v_j + \frac{p'}{\rho}\right)}\right\} - \overline{v_i v_j}\frac{\partial V_j}{\partial x_i} - \frac{g\overline{\rho' w}}{\rho} - \varepsilon \qquad (14)$$

where the lower case repeated subscripts denote summation, $v_j v_j = v_1 v_1 + v_2 v_2 + v_3 v_3$; $v_i, i,j=1,2,3$ are the components of the turbulent velocity fluctuations; V_i, are the components of the mean velocity averaged over the ensemble; ε is the dissipation,

$\varepsilon = \nu \left[\frac{\partial v_i}{\partial x_j} + \frac{\partial v_j}{\partial x_i} \frac{\partial v_j}{\partial x_i} \right] \approx \frac{u_o^3}{h} \varepsilon_s$ (Tennekes and Lumley, 1972). $\frac{u_o^3}{h}$ is a minimum estimate of dissipation since the length scale of energy containing eddies may be less than the layer depth, but not more.

Dropping the "s" subscripts,

$$\left[\frac{u_o^2}{t}\right] \frac{1}{2} \frac{\partial}{\partial t}(\overline{v_j v_j}) = -\left[\frac{U_o u_o^2}{L}\right] \frac{1}{2} \frac{\partial}{\partial x_j}(V_i \overline{v_j v_j}) - \left[\frac{u_o^3}{L}\right] \frac{1}{2} \frac{\partial}{\partial x_\alpha}(\overline{v_\alpha v_j v_j}) - \left[\frac{u_o^3}{h}\right] \frac{1}{2} \frac{\partial}{\partial x_3}(\overline{v_3 v_j v_j}) - \left[\frac{u_o^3}{L}\right] \frac{\partial}{\partial x_\alpha}\left(\frac{\overline{v_\alpha p'}}{\rho}\right) - \left[\frac{u_o^3}{h}\right] \frac{\partial}{\partial x_3} \frac{\overline{v_3 p'}}{\rho} - \left[\frac{U_o u_o^2}{L}\right] \left\{ \overline{v_\alpha v_\beta} \frac{\partial V_\beta}{\partial x_\alpha} + \overline{v_3^2} \frac{\partial V_3}{\partial x_3} \right\} - \left[\frac{u_o^2 U_o h}{L^2}\right] \overline{v_\alpha v_3} \frac{\partial V_3}{\partial x_\alpha} - \left[\frac{u_o^2 U_o}{h}\right] \overline{v_3 v_\alpha} \frac{\partial V_\alpha}{\partial x_3} - \left[\frac{u_o^3}{h}\right] \varepsilon - \left[\frac{g \rho_f u_o}{\rho o}\right] \frac{\overline{\rho' v_3}}{\rho} \qquad (15)$$

where $\alpha=1,2$ and $\beta=1,2$, are indexes for horizontal components.

With the same scaling parameters as given above for the diurnal scale,

$\frac{u_o^2}{t}=10^{-3}$, $\frac{U_o u_o^2}{L}=2\times10^{-3}$, $\frac{u_o^3}{L}=10^{-3}$, $\frac{u_o^3}{h}=1$, $\frac{u_o^2 U_o h}{L^2}=2\times10^{-6}$, $\frac{u_o^2 U_o}{h}=2$, $\frac{g\rho_f u_o}{\rho_o}=3$.

Retaining all terms of order 1 and larger leaves

$$- \overline{uw}\,\frac{\partial U}{\partial z} - \overline{vw}\,\frac{\partial V}{\partial z} - \quad - \frac{g\overline{\rho' w}}{\rho} - \frac{\partial}{\partial z}\left[\overline{w\left(\frac{q^2}{2} + \frac{p'}{\rho_o}\right)}\right] = 0 \qquad (16)$$

adopting standard vector notation, with $q^2=u^2+v^2+w^2$, the turbulent intensity.

Niiler (1975) arrived at the same equation by considering actual observations of the various terms in the turbulent energy equation. Of greatest significance for this work is the fact that the rate of change of turbulent intensity is quite small compared to the terms retained, which allows the assumption of a steady-state in turbulent kinetic energy. The term $\frac{g\overline{\rho' w}}{\rho}$ is the rate of change of potential energy which must accompany vertical mixing in a stably stratified fluid.

CHAPTER III

RECENT THEORETICAL STUDIES OF THE SEASONAL THERMOCLINE

Lake thermoclines arise from the same type of surface forcing and exchange processes as the seasonal thermocline of the ocean. Heating of the upper waters increases their buoyancy. Turbulent mixing, whose energy source is also at the water's upper surface, mixes the near surface water. At the lower boundary of the turbulent upper layer, entrainment of the relatively cool and quiescent lower water into the surface layer sharpens the density gradient and deepens the mixed layer.

An analogous, though inverted, process acts in the lower layers of the atmosphere. Most turbulence is generated by friction at the boundary and is damped by viscous dissipation and the conversion of kinetic to potential energy associated with the vertical flow of heat. The resultant boundary layer is well mixed, but there is a nearly discontinuous density jump, the inversion, at its upper boundary.

The interaction between the density stratification and the turbulence, affecting the vertical fluxes of thermal and mechanical energy, is the essential ingredient for the formation of a seasonal thermocline. This was demonstrated by Munk and Anderson (1948), who showed that the major features of the thermocline can be described

locally, i.e., by consideration of local surface heat fluxes and wind stress. This is evident in the lowest order approximation to the heat, momentum, and turbulent energy conservation equations presented in Chapter 2. On the other hand, the main or permanent thermocline of the oceans represents the response of the density field to the global circulation and heating patterns of the ocean, and cannot be described locally. Permanent thermoclines are not found in lakes because lakes are not large enough to encompass two dissimilar climatic regimes.

The similarity of physical processes in oceans, lakes, and the atmospheric boundary layer allows the limnologist to profit from the extensive studies of these other environments. The primary difference between oceans and lakes, as affects this problem, is the dependence of the density of ocean water on salinity. Most theoretical studies of ocean thermoclines have assumed the salinity to be nearly invariant. Under this condition the density depends only on temperature, so this work may be applied almost directly to lake thermoclines. A little more caution must be exercised in applying atmospheric studies to bodies of water. Here the primary differences appear to be the different relative depths of the mixed layer, the Ekman layer, and the constant flux layers (Kraus, 1972) and the considerable influence, in the

limnological problem, of turbulence generated by breaking waves at the surface.

Theoretical models of the near surface waters of lakes and oceans can be divided into two major subsets, in terms of the domain considered. These are (1) models of the coupled air-water system, and (2) models of the water only, with conditions in the atmosphere assumed to be known. Both of these types of model can be further subdivided as to closure hypothesis. Most often used closure hypotheses are of the eddy diffusion type or the mixed layer type.

An eddy diffusion closure hypothesis is based on the assumption that the turbulent flux $\overline{u_i \chi'}$ of any quantity $\chi = X+\chi'$, is proportional to the partial derivative of its mean in the ith direction,

$$\overline{u_i \chi'} = -K \frac{\partial X}{\partial x_i} \tag{17}$$

e.g., the vertical turbulent heat flux,

$$\overline{w\theta} = -K_z \frac{\partial T}{\partial z}. \tag{18}$$

The turbulent momentum flux, referred to as the Reynolds stress is

$$\overline{wu} = -A_z \frac{\partial U}{\partial z} \tag{19}$$

where A_z is the z-component of the eddy viscosity.

The implication and limitations of this approach are discussed in many texts (see Tennekes and Lumley, 1972)

and will not be discussed in detail. The inspiration for such a representation was the theory of molecular diffusion, and the hypothesis works best when the turbulent eddies causing most of the diffusion are small scale in relation to the domain of the problem.

From dimensional considerations one can show that $K \propto u\ell$, where u and ℓ are velocity and length scales of the most energetic eddies. ℓ is referred to as the mixing length.

In the constant stress layer encompassing the air-sea interface, the velocity scales as $u_* = \sqrt{\frac{\tau_o}{\rho_a}}$, in the atmosphere, and $w_* = \sqrt{\frac{\tau_o}{\rho_w}} = u_* \sqrt{\frac{\rho_a}{\rho_w}} \approx .03\ u_*$ in the water; while the length scale is proportional to the distance from the boundary, $|z_b|$.

The interaction of the turbulence with the density is often formulated as $K_z = f(Ri)$. This can be interpreted as a statement that the length scales of energy containing eddies are controlled by the stratification.

Some mixed layer models use a critical Ri hypothesis for closure. These are based on theories of dynamic instability, reviewed by Turner (1973), which predict instability of a sheared, stratified fluid if

$$Ri < Ri_{cr} \tag{20}$$

where Ri_{cr} is some critical Richardson number, taken generally from theory. When instability is indicated by

(20) the unstable region is mixed, generally causing an increase in Ri and a return to dynamic stability. That this process is important in mixing at lake thermoclines has been suggested by Mortimer (1961), and verified observationally by Kaye (1974).

The coupled models, still in their infancy, are undoubtedly important in our understanding of air-sea interaction. Their complexity of solution requires either considerable expenditures of computer time or crude simplifying assumptions. A few recent models of this type will be discussed briefly.

Pandolfo (1969), solved a coupled set of conservation equations in the atmospheric and oceanic planetary boundary layers. Quantities conserved were heat and momentum in both the air and water, salinity in the water, and water vapor in the atmosphere. Eddy exchange coefficients, K_z, and A_z for diffusivity and viscosity respectively, were taken to be prescribed functions of Ri and the vertical coordinate. Effects of surface gravity waves on K_z and A_z were also considered. The wind speed at the top of the planetary boundary layer was assumed to be known. The integration of the model equations revealed motions with diurnal period in the atmopsheric boundary layer and inertial currents in the water. The integration simulated five days of real time.

Walmsley (1973) used a one-dimensional eddy diffusion type coupled model to study air-sea interaction in the Gulf of St. Lawrence. The model is similar to that of Pandolfo (1969). Discrepancies between observed and predicted thermal structure resulted from horizontal advection of heat, which was ignored in the one-dimensional model.

Yeh (1974) extended these concepts somewhat by introduction of the turbulent energy conservation equation, which enabled him to determine K_z under well known assumptions of turbulence similarity theory. The mixing length was assumed to increase linearly near the ground and to asymptotically approach a constant value at a height of the same order as the turbulent Ekman layer thickness ($\sim\frac{u*}{f}$). This mixing length formulation is due to Blackadar (1962).

A coupled three dimensional air-lake model was proposed by Jacobs and Pandolfo (1974a), built upon the foundation of Pandolfo (1969). Radiation fluxes in the atmosphere were computed from detailed actinometric formulae which account for the effects of atmospheric water vapor and cloudiness in several layers.

The large demands on computation time of this coupled three-dimensional model is evidenced by the time span of simulations reported in Jacobs and Pandolfo (1974b) and Jacobs and Brown (1974). The three-dimensional free

surface model was used to simulate one diurnal cycle. A slightly simpler three-dimensional model with a rigid air-sea interface was run for two diurnal cycles, and an analogous one-dimensional model was used for several four day simulations. The computation cost prohibited longer integrations.

Uncoupled models employing eddy diffusion assumptions for closure have the longest history of the thermocline models. As previously noted, the first model to include the dominant physical mechanisms, wind mixing and the suppression of this turbulent energy by a stable stratification, was the steady-state theory of Munk and Anderson (1948). Under the assumptions that $(K_z, A_z) = f(Ri)$, and the heat flux is directed downward, they solved a modified Ekman layer problem. The downward heat flux ensures $Ri>0$ everywhere, necessary because the functions, f, are only valid for $Ri>0$. The inadequacy of eddy diffusion concepts for describing convective mixing is a considerable theoretical and practical problem. Convective cells may have the same vertical scale as the epilimnion, in which case the eddy diffusion approximation, (17), is not valid.

Kraus and Rooth (1961) attempted to include convective mixing in an eddy diffusion model, by assuming that a convectively unstable region is mixed instantaneously.

They recognized that penetrative solar heating, combined with a generally upward surface heat flux, results in a convectively unstable layer near the surface, and emphasized the important role of convective mixing in maintaining the upper mixed layer. Ertel (1954) had first modelled the effect of convective mixing in lakes, but without considering the effects of the stable stratification in the thermocline. Kraus and Rooth's (1961) model is inapplicable to lakes because they assume a steady state maintained by steady upwelling. Although upwelling may reinforce the strong thermal gradient in some parts of the ocean, the formation of a seasonal thermocline does not require upwelling. In lakes, upwelling is intermittent and restricted horizontally.

Further study of the diurnal cycle of convection in the upper ocean was made by Foster (1971). Foster solved the continuity equation and the heat conservation equation in two-dimensions with diurnally varying penetrative solar heating and constant surface heat loss. Foster (1971) assumed constant eddy exchange coefficients, K_z and A_z. The forcing was ideal, and results were not compared in detail with observations. The work provides an estimate of the scales of convective cells and velocities.

The application of one-dimensional eddy diffusion models to lakes has been performed most notably by

Sundaram and Rehm (1971, 1972, 1973). They assumed all heating is applied at the upper boundary, i.e., they ignored the penetration of solar radiation into the lake. All surface heat fluxes were expressed in terms of an equilibrium temperature, T_e, such that

$$Q_s = K_e(T_e - T_s)$$

where Q_s is the surface heat flux, K_e is a heat exchange coefficient, and T_s is surface temperature.

The basic equation solved is

$$\frac{\partial T}{\partial t} = \frac{\partial}{\partial z}(K_z \frac{\partial T}{\partial z})$$

which is the eddy diffusion form of eq. (12) if horizontal fluxes of heat are ignored and there are no internal sources or sinks of heat. $K_z = f(Ri)$, and $Ri = Ri(\frac{\partial T}{\partial z}, \frac{\partial U}{\partial z})$, so the equation is non-linear.

The equations of motion were not solved, but the authors recognized that the mixing, as embodied in $K_z(Ri)$, is dependent on the velocity field. To estimate Ri without solving the equations of motion calls for sweeping assumptions about the structure of the velocity field. Sundaram and Rehm (1971) assumed the local surface wind stress and the distance from the surface determine the shear, and used

$$Ri_s = \frac{\alpha g z^2 \frac{\partial T}{\partial z}}{w^{*2}} , \qquad (21)$$

where $\alpha = \frac{1}{\rho_o} \frac{\partial \rho}{\partial T}$, which is equal to

$$Ri = \frac{\alpha g \frac{\partial T}{\partial z}}{(\frac{\partial U}{\partial z})^2}$$

if

$$\frac{\partial U}{\partial z} = \frac{w_*}{z} .$$

This last equation is similar to the expression

$$\frac{\partial U}{\partial z} = \frac{u_*}{k_v z} ,$$

valid under neutral stratification in the atmospheric boundary layer, where k_v is the von Karman constant. The eddy diffusivity, K_z, was then calculated from mixing length hypotheses of the form

$$K_z = K_{zo}(1 + \sigma_1 Ri)^{-1} \qquad (22a)$$

or

$$K_z = K_{zo}(1 - \sigma_2 Ri) \qquad (22b)$$

where $\sigma_1, \sigma_2 > 0$. K_{zo}, independent of z in Sundaram and Rehm (1971), is the eddy diffusivity expected under neutral stratification.

This is analogous to the similarity hypothesis discussed above

$$K_z \propto u\ell ,$$

with the length scale limited by the stable stratification.

In and below the thermocline, the turbulent intensity q^2 from eq. (16), is much less than in the epilimnion. Consequently the scale velocity, u, is smaller in the hypolimnion than the epilimnion. In the deeper layers of the lake, K_{zo}, as defined by Sundaram and Rehm (1971) is not a valid estimate of the neutral diffusivity. To parameterize this, they added the constraint that (22a) or (22b) holds from the surface down to a depth at which $K_z \leq K_m$, where K_m was specified a priori. K_m is of the same order as the molecular conductivity. Below that depth, $K_z = K_m$.

In Sundaram and Rehm (1973) this framework was extended to times, e.g., late summer and fall, when the heat flux in the epilimnion may be upward, and convective mixing occurs. This was parameterized by requiring that any statically unstable region be completely and instantaneously mixed. This assumption ignores the process of penetrative convection, which is known to occur when a convective region is bounded by stably stratified fluid. Convective elements tend to overshoot their depth of neutral buoyancy. Some of their kinetic energy is used to increase the potential energy of the system by mixing heat downward. Some of this energy may be used to generate internal waves. Sundaram and Rehm (1973) compared temperature predictions with observed conditions in Lake Cayuga.

The most recent, and perhaps the most rigorous, eddy diffusion model is that of Mellor and Durbin (1975). The equations solved by Mellor and Durbin (1975) were the equations of motion and the heat conservation equation, with the added constraint of the turbulent energy equation. The turbulent energy constraint allows for a more rigorous computation of the diffusion coefficient in a manner similar to that of Yeh (1974). Mellor and Durbin (1975) calculated the mixing length from the turbulent energy balance while Yeh (1974) prescribed it a priori. They compared the model predictions with observations for a sixty day period at Ocean Station Papa.

An alternative approach to the eddy diffusion closure hypothesis is the mixed layer approach first introduced by Kitaigorodskiy (1960). This approach is based on the observed uniformity of water properties above the thermocline, in the region which has been called the upper mixed layer. By integrating the conservation equations over the mixed layer, one need only specify fluxes at the surface and the bottom of the mixed layer. All mixed layer models tacitly assume some particular shape of the velocity and temperature profiles, just as Sundaram and Rehm (1971) assumed a shape for the velocity profile. The theory should be applicable to any body of water exhibiting the assumed profile shape. In most cases,

the assumed shape is flexible enough to approximate observed profiles in most bodies of water during seasons of interest.

The mixed layer theories have received some observational support in the past decade, as evidence has mounted that a sheared, stably stratified fluid, such as a lake, naturally tends toward a density profile resembling a stacked set of mixed layers in which the density is nearly uniform, separated by regions of large density gradient. The gradient regions are so thin that they often appear to be interfaces of density discontinuity. Such a density stratification cannot be predicted by eddy diffusivity considerations.

Furthermore, mixed layer models have been shown to be capable of describing convective mixing in a more straightforward manner than eddy diffusion theories. An eddy diffusion hypothesis can only be valid when the scale of eddies performing the mixing is much smaller than the domain of the problem. Langmuir cells and eddies generated by convection have length scales comparable to the epilimnion thickness. These large scale cells can transport heat through an isothermal layer and can even cause transport against the gradient (see, e.g., Deardorff, Willis and Lilly, 1969). Large scale cellular motion is known to be important in epilimnion mixing

(Scott, et. al., 1969). Eddy exchange coefficients cannot describe this phenomenon.

Kraus and Turner (1967) introduced the first time dependent model of the mixed layer type. Heat and turbulent kinetic energy were conserved in the mixed layer with no leakage of either to deeper waters. They considered the seasonal scale of temperature changes. The equations used were (12), without the advective terms or the horizontal turbulent flux, and (16). Fluxes of heat and kinetic energy at the surface are dependent on atmospheric conditions, presumed known.

Turbulent energy production in the mixed layer associated with the action of the wind, represented by G*, where

$$G^* = -\rho_o \left\{ \int_{-h}^{o} \overline{uw} \frac{\partial U}{\partial z} dz + \overline{w\left(\frac{p'}{\rho} + \frac{q^2}{2}\right)} \Big|_{z=-h}^{z=0} \right\}, \tag{23}$$

was assumed to be approximated by $\tau_o w_*$, and the dissipation of turbulent energy in the mixed layer,

$$D^* = \int_{-h}^{o} \epsilon \, dz \tag{24}$$

was neglected.

The turbulent heat flux at the bottom of the mixed layer, z=-h, was assumed to be used to warm entrained water to the temperature of the mixed layer,

$$- \overline{w\theta}\Big|_{-h} = \Lambda(T_s - T_h)\frac{dh}{dt},$$

$$\Lambda = \begin{cases} 1, & \frac{dh}{dt} \geq 0 \\ 0, & \frac{dh}{dt} < 0 \end{cases}$$

If all the turbulent energy generated by the wind is needed to mix the surface layer, no entrainment will occur and the heat flux at z=-h is zero. In this case, which occurs when the surface heat flux is increasing or the wind speed is decreasing, the mixed layer shrinks, and $\frac{dh}{dt}<0$.

Geisler and Kraus (1969), applying their study to the atmospheric boundary layer, solved a similar heat conservation equation (without sources or sinks) and the equations of motion for a horizontally homogeneous mixed layer moving as a slab. They assumed that the change of potential energy associated with the vertical flux of heat was proportional to the turbulent energy generated near the surface. This is a crucial assumption used in a number of mixed layer models including those of Kraus and Turner (1967), Denman (1973), Niiler (1975), and Edwards and Darbyshire (1973). The assumption was initially verified in laboratory experiments by Turner (1968) and Kato and Phillips (1969). However, recent experiments by Linden (1975) have disputed this hypothesis, indicating instead that the increase in potential

energy is proportional to the turbulent intensity at the thermocline, which is not linearly porportional to the turbulent energy generated at the surface.

From the turbulent energy equation, (16),

$$-\overline{uw}\,\frac{\partial U}{\partial z} - \frac{\partial}{\partial z}\overline{[w(\frac{q^2}{2} + \frac{p'}{\rho})]} = \frac{g\overline{\rho'w}}{\rho} + \varepsilon, \tag{25}$$

when V=0.

Integrating from z=-h to z=0

$$-\int_{-h}^{o} \overline{uw}\,\frac{\partial U}{\partial z}dz - \overline{[w(\frac{q^2}{2} + \frac{p'}{\rho})]}_o = \frac{g}{\rho}\int_{-h}^{o} \overline{\rho'w}\,dz + \int_{-h}^{o} \varepsilon dz \tag{26}$$

under the assumption that

$$\overline{[w(\frac{q^2}{2} + \frac{p'}{\rho})]}\Bigg|_{-h} = 0$$

since the fluctuating quantities will be small near the thermocline. Using the definitions (23) and (24)

$$G^* - D^* = \frac{g}{\rho}\int_{-h}^{o} \overline{\rho'w}\,dz \tag{27}$$

A number of theorists (e.g., Denman, 1973) hypothesize that

$$G^* - D^* = m\tau_o w_{sfc} \tag{28}$$

where τ_o is the surface momentum flux, w_{sfc} is a surface velocity scale, and m is assumed to be a constant. In the context of Linden's (1975) experiment, this assumption would be satisfied if the rate of increase of potential energy were proportional to the rate of energy production by an oscillating grid at the top of the experimental

tank. However, the experiments show that this condition is not satisfied, and that a more careful accounting of the dissipation in the layer is required.

Nihoul (1973) suggested that the misleading interpretation of the earlier experiments may have resulted from the much larger Brunt-Vaisala frequency, $N = \sqrt{\frac{g}{\rho}\frac{\partial \rho}{\partial z}}$, prevailing in the experiments of Kato and Phillips (1969) as compared with the actual stratification in surface waters of oceans and lakes. One might expect that turbulence would be damped primarily by interactions with the stratification in the experimental system and not by viscous dissipation. Thus the importance of the dissipation term in the mixed layer of oceans and lakes may have been underestimated. Nihoul (1973) used the turbulence similarity hypothesis $\varepsilon \alpha \frac{u^3}{h}$, where h is the mixed layer depth, and the forms

$$A_z = \alpha_o{}^2 h^2 \left|\frac{\partial u}{\partial z}\right|$$

$$K_z = \frac{4}{3}\alpha_o{}^2 h^2 \left|\frac{\partial u}{\partial z}\right|$$

where α_o is a constant, or order 10^{-1}, to solve the equation of motion (one-dimensional, non-rotating), a buoyancy conservation equation, and the kinetic energy equation. The results show the initial development from a linear profile under an imposed wind stress.

Mixed layer models in which the equations of motion are solved, e.g., Pollard, et al (1973), indicate a more rapid deepening of the mixed layer during the first day after the onset of strong winds, than do those, e.g., Denman (1973), in which only the turbulent energy and heat are conserved. This rapid entrainment results from shear instability at the thermocline associated with inertial currents. By careful consideration of the underlying assumptions of mixed layer models, Niiler (1975) has constructed a model in which momentum, heat, and turbulent energy are all conserved and found that the Denman (1973) and Pollard, et al (1973) models are special cases of his more general treatment. In Niiler's model, shear instability is the predominant mechanism responsible for mixed layer deepening at times less than the inertial period, while turbulent mixing caused by small scale eddies (i.e., penetrative convection, turbulent entrainment) is the dominant mechanism for longer time scales.

Although Niiler's (1975) model and that of Pollard et al (1973) solve the equations of motion, they are not capable of prescribing horizontal advection, because they consider a horizontally homogeneous fluid. Aside from the neglect of horizontal fluxes, the equations used in all recent models are consistent with the scaling of

Chapter 2. None of the models which solve the equations of motion have been verified by simulations using relevant observations.

Kitaigorodskiy and Miropolskiy (1970) solved a one-dimensional heat conservation equation, after fitting observed profiles of temperature in the thermocline to a polynomial in a "natural" coordinate system

$$\theta = \frac{[T_s - T(z,t)]}{T_s - T_H}$$

$$\eta = \frac{[z - h(t)]}{H - h(t)}$$

where T_s is the surface temperature, T_H is the temperature at z=-H far below the thermocline. T_H is independent of time. h is the mixed layer depth.

Kalatskiy (1973) used a critical Ri closure hypothesis to find analytical solutions to the heat conservation equation under various boundary and initial conditions.

Sundaram (1973) and Edwards and Darbyshire (1973) have applied the mixed layer models to lakes, but used the same closure hypothesis (28) found wanting in the ocean. This hypothesis is even less satisfying in lakes, since the turbulent energy coming from the wave field will depend not only on the wind speed, but also on the limited fetch. Edwards and Darbyshire (1973) examined the

behavior of the "constant", m, in (28) on the basis of detailed observations in Lake Bala, Wales. They found that m varied by more than an order of magnitude during an annual cycle, but used a constant value in their numerical simulation.

CHAPTER IV

A LAKE THERMOCLINE MODEL

In this chapter, a lake thermocline model is described which is built on the foundation laid by Kraus and Turner (1967) and Denman (1973). The model has been adapted for application to lakes and extended to include effects of atmospheric stability on the surface exchange, wave-breaking, and new formulations for production and dissipation of turbulent energy. This chapter has two sections. In the first, the governing equations will be derived, following closely the analysis of Denman (1973). The second section deals with the parameterization of the forcing terms in the governing equations. These cannot in general be found from first principles, but methods for estimating them from routinely observed quantities are adopted.

a. Derivation of model equations

The heat conservation equation from eq. (12), in three dimensional form is

$$\frac{\partial T}{\partial t} + \nabla\cdot(T\vec{U}) = -\nabla\cdot(\overline{\theta\vec{u}}) + \frac{Q}{\rho c_p}. \qquad (29)$$

To eliminate the horizontal advection terms, this equation is averaged over any horizontal plane in the lake, with A the area of the plane and dA an element of its surface,

$$\frac{\partial \hat{T}}{\partial t} + \frac{1}{A}\iint[\frac{\partial}{\partial x}(TU) + \frac{\partial}{\partial y}(TV)]dA + \frac{\partial}{\partial z}(\hat{TW}) = -\frac{1}{A}\iint[\frac{\partial}{\partial x}(\overline{\theta u}) + \frac{\partial}{\partial y}(\overline{\theta u})]dA - \frac{\partial}{\partial z}(\hat{\overline{\theta w}}) + \frac{\hat{Q}}{\rho c_p} \quad (30)$$

where

$$\hat{T} = \frac{1}{A}\iint T dA,$$

represents a horizontally averaged variable. As the velocity and the turbulent heat flux normal to the boundaries are zero, and as a consequence of the divergence theorem in two dimensions

$$\iint[\frac{\partial}{\partial x}(TU) + \frac{\partial}{\partial y}(TV)]dA = \oint(T\vec{U}\cdot\hat{n})ds = 0, \text{ and}$$

$$\iint[\frac{\partial}{\partial x}(\overline{\theta u}) + \frac{\partial}{\partial y}(\overline{\theta v})]dA = \oint(\overline{\theta u}\cdot\hat{n})ds = 0,$$

where the line integral is taken around the depth contour which bounds the plane and $\hat{n}$ is normal to that contour. Then, eq. (30) becomes

$$\frac{\partial \hat{T}}{\partial t} + \frac{\partial}{\partial z}(\hat{TW}) = -\frac{\partial}{\partial z}(\hat{\overline{\theta w}}) + \frac{Q}{\rho c_p} \quad . \quad (31)$$

The second term on the left is associated with the upwelling of cold water which is known to be an important, though intermittent, phenomenon in lakes. The scaling showed it to be a small term, but of the same order of magnitude as the rate of change of temperature. With little justification, save convenience, this term will be neglected in building the model. Effects of this approximation will be discussed in Chapter 6.

The only significant internal source of heat is due to the conversion of radiant solar energy to heat. As discussed in Chapter 1, this flux of radiant energy may be represented, to a reasonable approximation, as

$$I = S^* e^{\beta z}$$

where S^* is the penetrating component, $S^* = I_o(1-A_r)$, A_r is the albedo, and I_o is the incident radiation.

The rate of solar heating is the convergence of the upward flux, $-I$,

$$\frac{\partial I}{\partial z} = \beta S^* e^{\beta z} \quad . \tag{32}$$

Thus the heat conservation equation, after horizontal averaging and neglect of upwelling and downwelling is

$$\frac{\partial T}{\partial t} + \frac{\partial}{\partial z}(\overline{w\theta}) = \frac{\beta S^* e^{\beta z}}{\rho_o c_p} \tag{33}$$

where the ^'s denoting horizontal averages have been deleted.

The turbulent kinetic energy conservation equation (16) may be horizontally averaged without change in form, and dropping the ^'s, with the understanding that all quantities represent horizontal averages over the whole lake, (16) becomes

$$- \overline{uw}\,\frac{\partial U}{\partial z} - \overline{vw}\,\frac{\partial V}{\partial z} - \frac{\partial}{\partial z}\left[\overline{w'\left(\frac{p'}{\rho_o} + \frac{q^2}{2}\right)}\right] - \varepsilon = g\alpha(\overline{w\theta}) \tag{34}$$

where $\alpha = \frac{1}{\rho_o}\frac{\partial \rho}{\partial T}$ implies $\rho' = \alpha\theta\rho_o$.

These equations are to be satisfied for the surface mixed layer, defined as the region, extending downward from the lake's surface, in which the temperature and the concentration of any other passive contaminants are independent of depth. Below this region the turbulent kinetic energy is assumed to be very small, and the flux of turbulent energy from the mixed layer to deeper waters is neglected. This ideal picture of a turbulent well-mixed upper layer resting on a quiescent thermocline region is well established by observations (Grant, et al, 1968). Integrating (34) from the bottom of the mixed layer, z=-h, to the surface, z=0, yields

$$- \int_{-h}^{o} [\overline{uw}\,\frac{\partial U}{\partial z} + \overline{vw}\,\frac{\partial V}{\partial z}]dz - \overline{w(\frac{p'}{\rho_o} + \frac{q^2}{2}}\Big|_{z=0} + \overline{w(\frac{p'}{\rho_o} + \frac{q^2}{2}}\Big|_{z=-h} - \int_{-h}^{o} \varepsilon dz = \alpha g \int_{-h}^{o} \overline{w\theta} dz \ . \tag{35}$$

The term,

$$\overline{w(\frac{p'}{\rho_o} + \frac{q^2}{2}}\Big|_{z=-h} \ ,$$

supplies energy to internal waves at the thermocline. These internal waves are capable of radiating energy away from the mixed layer (Townsend, 1965). Linden (1975) has shown that this term is important in laboratory models of a similar system, but to date no satisfactory

method of estimating the loss in oceanic or lake environments is available. Consequently it is assumed that

$$\overline{w'\left(\frac{p'}{\rho_o} + \frac{q^2}{2}\right)}\Bigg|_{z=-h} = 0 \ . \tag{36}$$

Following Denman (1973), let

$$G^* = -\rho_o \int_{-h}^{o} \left[\overline{uw}\,\frac{\partial U}{\partial z} + \overline{vw}\,\frac{\partial V}{\partial z}\right] dz - \overline{\rho_o w\left(\frac{p'}{\rho_o} + \frac{q^2}{2}\right)}\Bigg|_{z=0}, \tag{37}$$

$$D^* = \rho_o \int_{-h}^{o} \varepsilon dz, \tag{38}$$

$$W^* = \rho_o \alpha g \int_{-h}^{o} \overline{w\theta} dz \ . \tag{39}$$

Then G* is the rate of kinetic energy input by the wind, D* is the rate of kinetic energy dissipation in the mixed layer, and W* is the rate of conversion of kinetic energy to potential energy associated with the vertical turbulent flux of heat through the layer.

Under assumption (36) and definitions (37-39), Eq. (35) becomes

$$G^* - D^* = W^*, \tag{40}$$

which is a statement that the excess of production over dissipation in the layer is used to increase its potential energy.

Integration of equation (33) from z to the surface yields

$$\int_z^o \frac{\partial T}{\partial t} dz + \int_z^o \frac{\partial}{\partial z}(\overline{w\theta}) dz = \int_z^o \frac{S^* e^{\beta z}}{\rho_o c_p} dz$$

$$- z\frac{dT_s}{dt} - \overline{w\theta}\Big|_z = \frac{S^*}{\rho_o c_p}(1-e^{\beta z}) - \overline{w\theta}\Big|_o \qquad (41)$$

If (41) is applied for z=-h

$$h\frac{dT_s}{dt} - \overline{w\theta}\Big|_{-h} = \frac{S^*}{\rho_o c_p}(1-e^{-\beta h}) - \overline{w\theta}\Big|_o \qquad (42)$$

The upper boundary condition on the heat flux is

$$\overline{w\theta}\Big|_o = - \frac{B^*}{\rho_o c_p} , \qquad (43)$$

where B* (cal $cm^{-2}sec^{-1}$) is the net transfer of heat from the air to lake as a result of infrared radiation, and sensible and latent heat exchange.

When the mixed layer is deepening, cold water, at temperature T_{-h}, just below z=-h is swept up into the mixed layer, and the heat flux at z=-h is used to warm this water to the temperature of the mixed layer. A small amount of heat leaks through the mixed layer and into the hypolimnion. This leakage of heat, associated with diffusive processes in the thermocline, has not previously been treated in a mixed layer model.

For z<-h, it is assumed that the heat flux can be expressed in terms of eddy diffusivity. As discussed in Chapter 3, an eddy diffusion assumption is not justified in the mixed layer because the mixing elements have length scales equal to the layer depth. In the thermocline and

hypolimnion, large scale vertical motions are rare or non-existent. Vertical motions are suppressed by the stable stratification of the thermocline. Known heat sources of the hypolimnion are not distributed so as to lead to convective instability.

Thus, for $z<-h$

$$-\overline{w\theta} = K_z \frac{\partial T}{\partial z} . \tag{44}$$

If one considers the interface at $z=-h$ to have thickness δ and to extend from $-h-\frac{\delta}{2}$ to $-h+\frac{\delta}{2}$, then integrating (33) from $-h-\delta$ to $-h+\delta$ yields

$$2\delta\frac{\partial T}{\partial t} + (T_s - T_{-h-\delta})\frac{\partial h}{\partial t} + \overline{w\theta}\Big|_{-h+\delta} - \overline{w\theta}\Big|_{-h-\delta} = \frac{S^* e^{\beta z}}{\rho_o c_p}\Bigg|_{-h-\delta}^{-h+\delta}$$

$$2\delta\frac{\partial T}{\partial t} + (T_s - T_{-h-\delta})\frac{\partial h}{\partial t} + \overline{w\theta}\Big|_{-h+\delta} + K_z\frac{\partial T}{\partial z}\Big|_{-h-\delta} = \frac{S^* e^{\beta z}}{\rho_o c_p}\Bigg|_{-h-\delta}^{-h+\delta}$$

in the limit as $\delta\to 0$, and assuming the thermocline is a level surface.

$$(T_s - T_{-h})\frac{dh}{dt} + \overline{w\theta}\Big|_{-h} + K_z\frac{\partial T}{\partial z}\Big|_{-h-\delta} = 0. \tag{45}$$

For convenience, let $T_{-h} = T_h$

$$\overline{w\theta}\Big|_{-h} = -H\frac{dh}{dt}(T_s - T_h) - K_z\frac{\partial T}{\partial z}\Big|_{-h} \tag{46}$$

where

$$H = \begin{cases} 1, & \frac{dh}{dt}\geq 0 \\ 0, & \frac{dh}{dt}<0 . \end{cases}$$

This introduction of the Heaviside function, H, makes (46) uniformly valid in situations when the

turbulent energy at the bottom of the epilimnion is insufficient to cause entrainment. In that situation the depth of the surface layer decreases and

$$\overline{w\theta}\Big|_{-h} = -K_z \frac{\partial T}{\partial z}\Big|_{-h}.$$

The first term on the right of (46) accounts for the heating of the water entrained into the mixed layer. Its temperature must increase from T_h to T_s. The step function ensures that "unmixing" does not occur.

Applying the boundary conditions (43) and (46) to eq. (42) yields

$$h\frac{dT_s}{dt} + H\frac{dh}{dt}(T_s - T_h) + K_z \frac{\partial T}{\partial z}\Big|_{-h} = S(1-e^{-\beta h}) + B \qquad (47)$$

under the transformation

$$[S^*, B^*] = \rho_o c_p [S, B].$$

Applying the heat conservation equation, (33), below the mixed layer with K_z independent of z yields

$$\frac{\partial T}{\partial t} = K_z \frac{\partial^2 T}{\partial z^2} + \beta S e^{\beta z} . \qquad (48)$$

At the moving interface z=-h(t), the total derivative of T_h is

$$\frac{d}{dt}T_h = \frac{\partial}{\partial t}T_h - \frac{dh}{dt}\frac{\partial T}{\partial z}\Big|_{-h}$$

$$\frac{dT_h}{dt} = K_z \frac{\partial^2 T}{\partial z^2}\Big|_{-h} + \beta S e^{-\beta h} - \frac{dh}{dt}\frac{\partial T}{\partial z}\Big|_{-h} . \qquad (49)$$

Integration of (33) twice with respect to z introduces the interaction between the turbulence and the stratification, specifically through the proportionality between the heat flux integral and the rate of conversion of kinetic to potential energy, W*.

$$\int_{-h}^{o} (\overline{w\theta})dz = \frac{h^2}{2}\frac{dT_s}{dt} - (S+B)h + \frac{S}{\beta}(1-e^{-\beta h}) = \frac{W^*}{g\alpha\rho_o} \tag{50}$$

where (39), the definition of W* has been used.

Then (40) and (50) yield

$$\frac{dT_s}{dt} = \frac{2}{h^2}[-(G-D) + (S+B)h - \frac{S}{\beta}(1-e^{-\beta h})] \tag{51}$$

under the transformation $[G^*,D^*,W^*]=g\alpha\rho_o[G,D,W]$.

Then (51) can be used to eliminate $\frac{dT_s}{dt}$ from (47) yielding

$$H\frac{dh}{dt} = \frac{2[(G-D) + \frac{S}{\beta}(1-e^{-\beta h})] - h[B+S(1-e^{-\beta h}) + K_z\frac{\partial T}{\partial z}\Big|_{-h}]}{h(T_s-T_h)} \tag{52}$$

Eqs. (49), (51) and (52) specify the development of the mixed layer.

Eq. (48) must be satisfied for $z<-h$.

The boundary conditions for the solution of (48) are

$$\frac{\partial T}{\partial z} = 0, \quad z = -d \tag{53}$$

where d is the mean depth of the lake, and

$$T = T_h, \quad z = -h \tag{54}$$

b. Representation of the forcing functions

Through the derivation of the eqs. (48), (49), (51), (52), (53) and (54), the development of the model has been quite similar to the analysis of Denman (1973), with the only change involving the diffusion below the mixed layer and the subsequent leakage of heat, $K_z \frac{\partial T}{\partial z}\Big|_{-h}$, into the hypolimnion. The most significant differences between the previous model of Denman (1973) and the present work lies in the representation of the various forcing functions G*, D*, S* and B*. The method of computation of these quantities from the meteorological inputs and the formulation of K_z, the hypolimnion diffusion coefficient will be discussed in detail below.

S*, the solar radiation flux just below the air-sea interface, is calculated by standard actinometric formulae. The vertical distribution and types of clouds are not considered in detail. The water vapor content, dust content and cloudiness of the atmosphere are capsulized in two parameters, atmospheric transmission coefficient and total sky cover. Different types of clouds have different optical characteristics, but these differences are accounted for only by climatological estimates as a function of latitude (Budyko, 1956).

The incident shortwave (solar) radiation flux at the surface, I_o, may be direct or scattered by the atmosphere

$$I_o = I_d + I_s \tag{55}$$

where

$$I_d = 3x10^{-2}\cos(\theta_z)P^{m_o}[1-(1-K')n]\,(\text{cal cm}^{-2}\text{sec}^{-1}) \tag{56}$$

where θ_z is the sun's zenith angle; P is the atmospheric transmission coefficient, assumed constant; $m_o=[\cos(\theta)]^{-1}$, is the optical air mass; n is the total cloud cover; K' is a function of latitude (Budyko, 1956), tabulated by Kraus (1972), based on differences in typical cloud types with latitude; $3x10^{-2}$(cal $cm^{-2}sec^{-1}$) is the "meteorological solar constant" suggested by Sivkov (1971); and

$$I_s = .38(3x10^{-2} - I_d)\cos(\theta_z). \tag{57}$$

This form for the scattered radiation is preferred by Sivkov (1971).

This formulation for I_o has been tested for cloudless skies and found to be in excellent agreement with observations.

The penetrating component of solar radiation, S*, consists of the incident radiation less the reflected,

$$S^* = I_o(1-A_r)$$

where A_r is the albedo of the sea surface.

The reflectance of a water surface is related to the flux of radiation from different regions of the sky. The scattered radiation is often assumed to be isotropic, i.e.,

equal amounts of radiation come from all directions in the sky, while the direct radiation comes only from the direction of the sun. Thus the zenith angle of the sun and the relative contributions of direct and scattered radiation control the albedo of the sea surface. Variations in the state of the sea surface, as long as it isn't frozen, have been shown to have little effect on the albedo (Degtyarev, et al, 1964). The relative contribution of direct and scattered radiation depends on the zenith angle and the cloud cover. Thus, A_r may be related to the zenith angle and $r = \frac{I_s}{I_o}$, or alternatively to the zenith angle and the cloud cover. The latter approach has been used in this work.

Pivovarov, et al (1965) suggested the following empirical formula for $A_r(\theta)$ under cloudless skies

$$A_r = \frac{a^*}{\cos(\theta) + b^*} \tag{58}$$

where $a^*=b^*=.04$.

The author has found that the same form adequately fits observations (Deacon and Stevenson, 1968) of albedo under varying cloud cover if a* and b* are considered to be functions of cloud cover as tabulated in Table 1.

The error in S* incurred by the use of (58) is less than 3%, for $\theta<80°$. For $\theta>80°$, it is assumed that $A_r=.25$. Any error in A_r at large zenith angle will be relatively unimportant since I_o is very small for $\theta>80°$.

Table 1. Albedo Coefficients

n	a*	b*
<.5	.04	.04
.5 - .88	.044	.15
.88 - 1.	.117	1.0

B* is the surface heat flux by infrared radiation, sensible and latent heat exchange,

$$B^* = R_\ell + Q_s + Q_\ell \tag{59}$$

with the convention, (43), that B* is positive when the lake is gaining heat from the atmosphere.

It is assumed that

$$R_\ell = -1.334\times10^{-12}T_s^4(.39 - .05\sqrt{e_a})(1 - C_L n^2)\,\text{cal cm}^{-2}\text{sec}^{-1} \tag{60}$$

a form recommended by Budyko (1956) where e_a is the water vapor pressure in the air at a few meters above the surface, and C_L is an empirically determined function of latitude.

The expression inside the first parentheses of (60) accounts for the downward flux of radiation from the atmosphere, under the assumption that the air temperature is nearly T_s. The second parenthetic expression accounts for the effect of clouds. The coefficient C_L is tabulated by Kraus (1972).

Bulk transfer formulae are used for computation of the turbulent exchanges, Q_s and Q_ℓ.

$$Q_s = \rho_a h_z c_p (T_z - T_s) U_z \tag{61}$$

$$Q_\ell = \rho_a d_z L_e (q_z - q_s) U_z \tag{62}$$

q_z, T_z and U_z, are specific humidity, temperature and wind speed at some height, z, above the lake surface. T_s is the lake surface temperature and q_s is the saturation specific humidity at T_s; ρ_a, c_p are density and specific heat, respectively, of air; h_z and d_z are transfer coefficients for sensible and latent heat, respectively; and L_e is the latent heat of evaporation of water.

It is assumed that $h_z=d_z=g(Ri_b)$ where

$$Ri_b \simeq \frac{g}{T} z \frac{T_z - T_o}{(U_z)^2} \quad ,$$

and the function $g(Ri_b)$ is derived by Deardorff (1968). $h_{10}(0) = d_{10}(0) = 1.3 \times 10^{-3}$, at neutral stratification.

G*,D*, the rates of production and dissipation of turbulent kinetic energy, remain the most difficult terms to estimate because of the absence of (1) a complete theory of turbulent exchange in natural bodies of water, and (2) relevant observations.

Beginning with Kraus and Turner (1967), most mixed layer models have been based on the assumption that all terms in the turbulent energy equation, (40), are

proportional to $\tau_o w_{sfc}$, where τ_o is the surface momentum flux (equal to the stress at, e.g., 10m above the surface) and w_{sfc} is a surface velocity scale. w_{sfc} has been assumed to be w_* (Kraus and Turner, 1967; Niiler, 1975); the wind speed at 10m, U_{10} (Denman, 1973; Turner, 1969); or the surface current speed U_s (Edwards and Darbyshire, 1973). The difference between these choices of w_{sfc} is unimportant since U_s and w_* are approximately proportional to U_{10}. The estimates of each of these previous studies can be restated in terms of Denman (1973) as

$$G^* - D^* = m\tau_o U_{10} = W^* \qquad (63)$$

where m is assumed to be a universal constant.

Since $\tau \propto U^2_{10}$, the rate of increase of potential energy, W^*, is assumed proportional to the cube of the wind speed. m can be computed from observations of the rate of increase of potential energy of a water column associated with the passage of a storm. Table 2 summarizes a number of observations from which m has been calculated. Even though errors involved in these computations are large, it is clear that m is not a universal constant and the use of (63) is not warranted. The method by which m is predicted under the precepts of the current model will be presented later in this chapter. The observations of Edwards and Darbyshire (1973) and

Table 2. Variation of the Coefficient m.

	h (m)	fetch (km)	U_{10} (m/sec)	time span (day)	m(obs)$^{+}$	m(est.[91])$^{+}$
Dutton and Bryson, (1962)	9	3	12	3	$.3\times10^{-3}$	3.4×10^{-3}
Edwards and Darbyshire [7/14-10/14], (1973)	14	2.5	5	90	$.3\times10^{-3}$	1.1×10^{-3}
Edwards and Darbyshire [5/25-7/4], (1973)	7	2.5	5	40	$.5\times10^{-3}$	2.3×10^{-3}
Denman and Miyake, (1973)	40	∞	7	40	1.2×10^{-3}	3.0×10^{-3}
Halpern, (1974)	20	∞	12	1	3.9×10^{-3}	5.6×10^{-3}
Stommel, et al [3/17], (1969)	23	∞	6.5	.2	7.7×10^{-3}	3.4×10^{-3}
Stommel, et al [3/14], (1969)	16	∞	11	.2	15.4×10^{-3}	5.8×10^{-3}

$^{+}$estimated error is $\pm2\times10^{-3}$

Stommel, et al (1969) have been separated into two subsets corresponding to significantly different environmental conditions. Infinite fetch is indicated for situations in which the wave field was not fetch-limited.

(63) may be interpreted as a statement that the rate of dissipation of turbulent energy is proportional to the rate of production of energy by the shear flow (Turner, 1973). There are a number of reasons why this hypothesis must fail as a description of the kinetic energy balance. Consider the interactions which are likely to occur on a

cool, calm night (U_{10}=0). The lake surface must lose heat to the atmosphere, initiating convective motions. (63) implies that all terms vanish in this situation. These conditions would actually lead to convective motion ($W^*<0$) and subsequent viscous dissipation ($D^*>0$) while $G^*=0$. Indeed, dissipation of convective motion is always ignored in application of (63). To the contrary, Turner (1973) argues that convective motion is effectively dissipated within the convective region.

Another reason why (63) is inadequate is the neglect of any consideration of the wave field. The kinetic energy associated with the wave field is generally much greater than that associated with the shear flow. Although wave energy is not turbulent and not available for mixing, it can become available through wave breaking and other nonlinear wave decay mechanisms. The rate of energy lost from the wave field is postulated by Hasselmann (1974) to be proportional to the energy in the wave field. The energy in the wave field is not uniquely related to the local wind speed. Other controlling factors are fetch, duration of the wind and advection of wave energy.

Linden (1975) has shown that (63) is invalid because it implies that conversion of kinetic energy to potential energy by entrainment at z=-h is independent of h.

(63) implies a fixed fraction of the surface energy input $\tau_o u_s$ is converted to potential energy. Linden's experiments indicate that the fraction of surface energy converted to potential energy decreases as h increases because of an increase of D* with h. Generation of turbulent energy by the wind, G*, can be considered a surface phenomenon, while the energy dissipation is distributed throughout the layer.

These diverse criticisms all point to the abandoning of (63) by more careful consideration of wave breaking and the dissipation of turbulent energy. Formulation of a rational alternative to (63) has been the major focus of this dissertation.

Consider G*-D* to have 5 major components:

1) G^*_s, production of turbulence by the shear flow
2) G^*_w, production of turbulence by breaking waves and other non-linear wave decay mechanisms
3) D^*_w, dissipation of the turbulence associated with wave breaking
4) D^*_s, dissipation of turbulence generated by the shear flow
5) D^*_c, dissipation of convectively produced turbulence.

The direct interaction of the turbulence with the density field, W* from eq. (39), is eliminated from the model equations through application of eq. (50).

Assuming linearity,

$$G^*-D^* = G^*_s + G^*_w - D^*_w - D^*_s - D^*_c. \qquad (64)$$

Non-linear interaction between these components may play some, as yet unknown, role in the energy balance. (64) is a first approximation which may be improved as knowledge of oceanic turbulence increases.

Before proceeding with definitions of the various components of (64) a brief discussion of momentum and energy exchange at the air-sea interface is in order. The momentum flux, τ_o, is independent of z in a shallow region encompassing both sides of the interface, for $-1m \lesssim z \lesssim 20m$ (Kraus, 1972).

The momentum flux at the interface is accomplished by tangential shear and by pressure fluctuations in phase with the vertical velocity. At a smooth boundary all the momentum flux is by shear, while at a rough boundary the stress is supported by pressure variations at the boundary. Since the air-sea interface is aerodynamically rough under all but the lightest winds (rough if $U_{10} > 3^{m/sec}$, Wu, 1969) most of the momentum flux is supported by normal pressures. Since the interface is free to move, these pressure variations generate waves. Beginning with Stewart's (1961) semi-quantitative considerations of the momentum flux to waves and continuing through the extensive observations of the JONSWAP experiment (Hasselmann, et al,

1973; Hasselmann, 1974) most investigators have concluded that the largest part of the momentum flux at the air-sea interface goes initially into the wave field through the $\overline{wp'}$ correlation term. Some of this momentum is rapidly channeled to turbulence and the mean flow through wave breaking and other wave decay processes.

Define

$$\tau_o = \tau_s + \tau_w \tag{65}$$

where τ_s is the momentum flux supported by shear, and τ_w is the momentum flux supported by $\overline{wp'}$, i.e., the flux to the wave field.

The interface energy flux to the shear flow and its associated turbulence is $\dot{E}_s = \vec{\tau}_s \cdot \vec{U}_s$, where U_s is the interface velocity, and the energy flux to waves is $\dot{E}_w = \vec{\tau}_w \cdot \vec{c}$ where $\vec{c}$ is the phase velocity of the waves. Assuming that stress and velocity vectors are parallel,

$$\dot{E}_s = \tau_s U_s, \tag{66}$$

$$\dot{E}_w = \tau_w c \ . \tag{67}$$

It is assumed that all of the energy flux, supported by shear, $\dot{E}_s$, generates turbulence in the water and is initially available for mixing. Thus

$$G^*_s = \tau_s U_s, \tag{68}$$

where

$$\tau_s = \tau_o\left(1 - \frac{\tau_w}{\tau_o}\right). \tag{69}$$

$\frac{\tau_w}{\tau_o}$, the ratio of wave momentum flux to total stress, has been the subject of intensive investigation over the past decade. Dobson (1971) observed the $\overline{p'w}$ correlation over waves and concluded that $\frac{\tau_w}{\tau_o} = .9$. Hasselmann (1974) analyzed the JONSWAP data to determine the energy flux vs. wave number associated with wave-wave interactions, wave breaking, and τ_wc, and concluded that, under fetch-limited conditions, $.5 < \frac{\tau_w}{\tau_o} < 1.0$.

As there are reasons to believe that Dobson's estimate is too high (Snyder, 1974), it is assumed that

$$\frac{\tau_w}{\tau_o} = .8 \ , \tag{70}$$

which, from (69), implies

$$\tau_s = .2\tau_o. \tag{71}$$

τ_o can be estimated by a bulk transfer formula,

$$\tau_o = \rho_a C_z U^2_z \tag{72}$$

where $C_{10}=1.3\text{x}10^{-3}$ under neutral atmospheric stability. At different heights, z,

$$\frac{C_z}{C_{10}} = \left(\frac{\ln \frac{10}{z_o}}{\ln \frac{z}{z_o}}\right)^2$$

where z_o, is determined by the expression

$$z_o = 10 \exp[-\frac{k_v}{\sqrt{C_{10}}}] \text{ (m)}$$

where k_v is the von Karman constant, k_v=.4.

C_z is assumed to vary with atmospheric stability as formulated by Deardorff (1968) and Businger, et al (1971).

Further it is assumed that

$$U_s = .035U_{10} \text{ (Wu, 1975).} \tag{73}$$

It is anticipated that $\frac{\tau_w}{\tau_o}$, and $U_s(U_{10})$ may vary with previous wind and wave history, fetch, and atmospheric stability. Such variations are neglected.

The wave mixed layer. Theoretical descriptions of wave produced turbulence are inadequate for estimation of the residual, G^*_w-D^*_w. Benilov's (1973) analysis is perhaps the most complete description, but he makes the assumption G^*_w=D^*_w, which can only be valid if there is no buoyancy flux, that is, if W*=0. For consideration of the structure of wave produced turbulence, this is a reasonable assumption since

$$G^*_w \simeq D^*_w >> |G^*_w - D^*_w| \ . \tag{74}$$

The rate of generation of turbulent energy by wave breaking is quite large, but, because of the limited length scales of the turbulence associated with wave breaking, this energy is rapidly dissipated by viscous processes. (For a more complete discussion, see Phillips,

1969; observational evidence is provided by Stewart and Grant, 1962.) Consequently the effects of this turbulence are limited to a shallow region whose depth should scale with wave parameters.

(74) suggests that independent estimates of G^*_w and D^*_w require considerable precision if the residual is to be predicted adequately. Current theoretical or empirical descriptions do not afford the required precision. Independent estimation is not required since these terms always appear in the combination $G^*_w - D^*_w$. Consequently an estimate of the difference was sought.

Laboratory experiments by Dobroklonskiy and Kontoboytseva (1973) show that the turbulent mixed layer associated with a monochromatic wave field is proportional to the wave height. The depth of this mixed layer is roughly 1.2 times the wave height. These experimental results are not directly applicable to the natural system because the wave field was monochromatic, and there was no wind. Both of these differences between the experimental conditions and the actual conditions at the lake's surface would tend to encourage wave breaking at the lake surface. Nonlinear interaction of waves with different phase speeds encourages breaking at lower significant wave heights at a lake surface than for monochromatic waves. The presence of wind shear at the lake surface

causes waves to break at lower heights than in the absence of wind (Banner and Phillips, 1974).

Observations of temperature microstructure (Ostapoff and Worthem, 1974; Woods, 1968) indicate that a wave mixed layer exists in the ocean. These observations place an upper limit on the effects of wave breaking, for it is impossible to isolate the contribution of wave breaking to the mixing of this homogeneous layer. In the context of the present work, "wave-mixed layer" is defined as a homogeneous region of depth less than the large scale seasonal thermocline whose depth is observed to be correlated with wave height, and which is mixed predominantly by wave action. This layer, distinct from the rest of the mixed layer by a small temperature jump ($\Delta T \leq .1°C$), generally exists only in the day time.

Although the experimental evidence is certainly not complete, it is hypothesized that a wave mixed layer exists of depth, h_{wm}, proportional to the significant wave height, $H_{1/3}$, i.e.,

$$h_{wm} = aH_{1/3} \ . \tag{75}$$

From the observational evidence cited above, $1.2 \leq a \leq 4$. Eq. (75) implies that the depth of the wave mixed layer is independent of the solar heating which tends to stabilize the layer. That is, the depth of the mixed region is independent of the buoyancy flux implicit

in the mixing. The justification for this curious property is found in the local similarity theory of turbulence in stratified fluids. There is evidence (see Phillips, 1969) that the effects of buoyancy on turbulence is negligible for wave-numbers, $\kappa > \kappa_b$, where

$$\kappa_b = C^{3/4} \sqrt{\frac{N^3}{\varepsilon}} , \tag{76}$$

$N = \sqrt{\frac{g}{\rho} \frac{\partial \rho}{\partial z}}$, the Brunt-Vaisala frequency, and C is a constant. This result was first derived by Lumley (1964).

Consider typical values of N and ε for the wave mixed layer

$N \approx 5.4 \times 10^{-3} \text{sec}^{-1}$ (Woods, 1968)

$\varepsilon \approx .042$ erg $\text{cm}^{-3}\text{sec}^{-1}$ (Stewart and Grant, 1962)

$\kappa_b \approx 1.9 \times 10^{-3} C^{3/4} \text{cm}^{-1}$.

It is reasonable to assume a length scale for turbulence generated by wave breaking of the same order as the wave height.

$$\kappa_{wb} \approx \frac{1}{H_{1/3}} \approx 2 \times 10^{-2} \text{cm}^{-1}$$

is an appropriate estimate for the observations of Steward and Grant (1962). If, as is expected, C is of order 1 then $\kappa_{wb} >> \kappa_b$. Consequently, turbulence in the wave-mixed layer is independent of the buoyancy flux.

Qualitatively, the picture drawn here is of highly energetic, but small scale turbulence. Because of its high energy it overwhelms any stratification near the surface. Its small length scale ensures rapid dissipation and restricts the depth of its influence.

It is also assumed that $(G^*_w - D^*_w)$, the energy available for mixing from the wave field, is the energy required to mix a layer of depth h_{wm}. This can be calculated from the heat inputs to the region as a function of depth and time by finding the difference in the rate of change of potential energy of the layer for the case of no mixing and the case of complete mixing. The potential energy of the layer is changing as a function of time because of the internal heat source and the surface heat flux, in addition to the changes accomplished by the turbulent mixing. In isolating the process of wave mixing, the heat flux out of the bottom of the layer is ignored since it is assumed that this flux is accomplished by large eddies associated with the shear flow and convection.

If there were no turbulence in the region $0>z>-h_{wm}$ the rate of change of its potential energy per unit area would be

$$\frac{dP.E.}{dt} = \frac{d}{dt}\int_{-h_{wm}}^{o} \rho g z dz$$

$$= g\left[\int_{-h_{wm}}^{o} z\frac{d\rho}{dt}dz - \rho_o h_{wm}\frac{dh_{wm}}{dt}\right]$$

if $\overline{w\theta} = \overline{U} = \overline{V} = \overline{W} = 0$, then $\frac{\partial}{\partial t} = \frac{d}{dt}$, $\frac{dT}{dt} = \beta S e^{\beta z} + 2B\delta(z)$, where it is convenient to consider the surface flux as a generalized source, using the Dirac delta function, $\delta(z)$ having the following properties

$$\delta(z) = 0, \quad z \neq 0$$

$$\int_{-\zeta}^{\zeta} \delta(z)dz = 1, \quad \zeta \neq 0$$

$$\delta(z) = \delta(-z) .$$

$$\frac{d\rho}{dt} = \frac{d\rho}{dT}\frac{dT}{dt} = \rho_o \alpha[\beta S e^{\beta z} + 2B\delta(z)], \tag{77}$$

where $\alpha = \frac{1}{\rho_o}\frac{\partial \rho}{\partial T}$.

Then

$$\frac{dP.E.}{dt} = g\left\{\int_{-h_{wm}}^{o} \rho_o \alpha z[\beta S e^{\beta z} + 2B\delta(z)]dz - \rho_o h_{wm}\frac{dh_{wm}}{dt}\right\} .$$

α is a slowly varying function of temperature and therefore of z. Assuming $\alpha \approx$ constant introduces an error of less than 10%. Then

$$\frac{dP.E.}{dt} = \rho_o g\alpha\left\{\int_{-h_{wm}}^{o} z\beta S e^{\beta z}dz + \int_{-h_{wm}}^{o} z2B\delta(z)dz\right\} - \rho_o g h_{wm}\frac{dh_{wm}}{dt}$$

$$= \alpha\rho_o g\left\{\frac{Se^{\beta z}}{\beta}(\beta z - 1)\Big|_{-h_{wm}}^{o}\right\} - \rho_o g h_{wm}\frac{dh_{wm}}{dt} ,$$

and

$$\frac{dP.E.}{dt} = \rho_o g \alpha[-\frac{S}{\beta} + \frac{Se^{-\beta h_{wm}}}{\beta}(1 + \beta h_{wm})] - \rho_o g h_{wm} \frac{dh_{wm}}{dt} \qquad (78)$$

is the expression for the rate of change of potential energy of a column from $0>z>-h_{wm}$ if no turbulent mixing occurred.

If the layer is completely mixed,

$$\bar{\rho} = \frac{1}{h_{wm}} \int_{-h_{wm}}^{o} \rho dz \ , \qquad (79)$$

and so

$$\frac{d\bar{\rho}}{dt} = \frac{d}{dt} \frac{1}{h_{wm}} \int_{-h_{wm}}^{o} \rho dz \ .$$

Differentiation of the product yields

$$\frac{d\bar{\rho}}{dt} = \frac{1}{h_{wm}} \frac{d}{dt} \int_{-h_{wm}}^{o} \rho dz - \left[\frac{1}{h_{wm}}\right]^2 \frac{dh_{wm}}{dt} \int_{-h_{wm}}^{o} \rho dz \ .$$

Leibniz rule implies

$$\frac{d\bar{\rho}}{dt} = \frac{1}{h_{wm}} \int_{-h_{wm}}^{o} \frac{d\rho}{dt} dz + \frac{\rho_o}{h_{wm}} \frac{dh_{wm}}{dt}$$

$$- \left[\frac{1}{h_{wm}}\right]^2 \frac{dh_{wm}}{dt} \int_{-h_{wm}}^{o} \rho dz \ .$$

Substitution from (77) and (79) yields

$$\frac{d\bar{\rho}}{dt} = \frac{1}{h_{wm}} \left\{ \int_{-h_{wm}}^{o} \rho_o \alpha [\beta S e^{\beta z} + 2B\delta(z)] dz + \frac{dh_{wm}}{dt} [\rho_o - \bar{\rho}] \right\}$$

$$= \frac{1}{h_{wm}} \left\{ \rho_o \alpha [S(1-e^{-\beta h_{wm}}) + B] + (\rho_o - \bar{\rho}) \frac{dh_{wm}}{dt} \right\} .$$

Typical values in c.g.s units are

$\alpha=10^{-4}$, $S=10^{-2}$, $h=10^{2}$, $c_p=1$, $B=10^{-2}$, $\rho_o-\bar{\rho}=10^{-5}$, $\frac{dh_{wm}}{dt}=10^{-3}$.

Terms involving S, $B=0(10^{-6})$, and terms involving $(\rho_o-\bar{\rho})=0(10^{-8})$. Thus the last term can be safely neglected, and

$$\frac{d\bar{\rho}}{dt} = \frac{\rho_o\alpha}{h_{wm}}[S(1-e^{-\beta h_{wm}}) + B]. \tag{80}$$

Then the rate of change of P.E. for the completely mixed layer is

$$\frac{dP.E.}{dt} = \frac{d}{dt}\int_{-h_{wm}}^{o} \bar{\rho}gzdz .$$

Applying Leibniz rule yields

$$\frac{dP.E.}{dt} = \int_{-h_{wm}}^{o} gz\frac{d\bar{\rho}}{dt}dz - g\rho_o h_{wm}\frac{dh_{wm}}{dt} ,$$

and substituting from (80) yields

$$\begin{aligned}\frac{dP.E.}{dt} &= \frac{\alpha\rho_o g}{h_{wm}}\int_{-h_{wm}}^{o}[S(1-e^{-\beta h_{wm}}) + B]zdz - g\rho_o h_{wm}\frac{dh_{wm}}{dt} \\ &= \frac{-\alpha\rho_o g}{2}[S(1-e^{-\beta h_{wm}}) + B]h_{wm} - g\rho_o h_{wm}\frac{dh_{wm}}{dt} .\end{aligned} \tag{81}$$

The rate of change associated with the mixing is

$$\left.\frac{dP.E.}{dt}\right|_{mixed} - \left.\frac{dP.E.}{dt}\right|_{unmixed} = \left.\frac{dP.E.}{dt}\right|_{mixing}$$

$$\left.\frac{dP.E.}{dt}\right|_{mixing} = -g\alpha\rho_o\left[\frac{S}{2}(1-e^{-\beta h_{wm}}) + \frac{B}{2}\right]h_{wm}$$

$$-\frac{S}{\beta} + \frac{Se^{-\beta h_{wm}}}{\beta}(1+h_{wm}) = -g\alpha\rho_o\left\{\frac{1}{2}\left[S(1+e^{-\beta h_{wm}}) + B\right]h_{wm}\right.$$

$$\left. -\frac{S}{\beta}(1-e^{-\beta h_{wm}})\right\} = G^*_w - D^*_w \quad . \tag{82}$$

The significant wave height, $H_{1/3}$, is estimated by assuming that the wave field is fetch-limited. Using the empirical formulae of Bretschneider (1966) cast in the dimensionally consistent form of Hasselmann, et al (1973),

$$H_{1/3} = \begin{cases} 2.4\times10^{-3}F_o^{1/2}\left(\frac{U_{10}^2}{g}\right)(m), & F_o<1.4\times10^4 \\ .28\,\frac{U_{10}^2}{g}, & F_o\geq 1.4\times10^4 \end{cases}$$

where $F_o=\frac{gF}{U_{10}^2}$, and F is the fetch distance. The approximation for fully developed seas, $F_o\geq 1.4\times10^4$, is from Kraus (1972).

The remaining dissipation terms, D^*_s and D^*_c are calculated according to the turbulence similarity hypothesis

$$\varepsilon\alpha\frac{u^3}{\ell} \tag{83}$$

where u and ℓ are characteristic velocity and length scales for the large energy containing eddies

Characteristic velocity scales for shear produced turbulence, u'_s, and convectively produced turbulence, u'_c are

$$u'_s = w_* = \sqrt{\frac{\tau_o}{\rho_w}} \tag{84}$$

$$u'_c = (g\alpha B^* h_c)^{1/3} , \tag{85}$$

where h_c is the depth of the convective region

$$h_c = \begin{cases} h, & \lambda_c > h \\ \lambda_c, & 0 < \lambda_c > h \\ 0, & \lambda_c < 0 \end{cases} \tag{86}$$

where $\lambda_c = -\beta \ln(\frac{S^*+B^*}{S^*})$, λ_c is the depth of a convectively unstable region for solar heating, S*, penetrating to a scale depth of β^{-1}, and a surface heat loss, B*.

The convective velocity scale (85) is due to Deardorff (1970) while (86) was found by Kraus and Rooth (1961).

A length scale for shear produced turbulence is

$$\begin{aligned} \ell &= kz, \quad z \leq \delta_e \\ &= k\delta_e, \quad z \geq \delta_e \end{aligned} \tag{87}$$

where $\delta_e \approx .3\frac{w_*}{f}$ is the depth of the turbulent Ekman boundary layer with $f = 2\Omega \sin\phi$, the Coriolis parameter. Functional forms of this type for ℓ have been used successfully in the atmospheric boundary layer (e.g., Blackadar, 1962). The dependence of the length scale on rotation tends to stabilize the mixed layer depth at δ_e under high winds, since for $h < \delta_e$,

$$\int_{-h}^{o} \varepsilon dz \propto \ln h ,$$

while, for $h > \delta_e$,

$$\int_{-h}^{0} \varepsilon dz \propto h \ .$$

The length scale assumed for the convectively produced turbulence is h_c (Deardorff and Willis, 1967; Ostapoff and Worthem, 1974).

The observations of Stewart and Grant (1962) indicate that dissipation in the wave mixed layer is an order of magnitude larger than that expected by similarity theory if the turbulence were produced by the shear flow. This large dissipation rate is due to turbulence caused by wave breaking. Consequently, shear and convectively produced turbulence is assumed to be insignificant compared to wave generated turbulence in the region $-h_{wm} < z < 0$.

Thus

$$D^*_s + D^*_c = \Lambda(h_c - h_{wm}) \int_{-h_c}^{-h_{wm}} r_c g \alpha B^* dz + \int_{-(h,\delta_e)_{min}}^{-h_{wm}} r_s \frac{w_*^3}{k_v z} \tag{88}$$

$$+ \Lambda(h - \delta_e) \int_{-h}^{-\delta_e} r_s \frac{w_*^3}{k_v \delta_e} dz$$

where

$$\Lambda(x) = \begin{cases} 1, & x > 0 \\ 0, & x \leq 0 \end{cases}, \text{ and } (h,\delta)_{min} = \begin{cases} h, & h < \delta_e \\ \delta_e, & h > \delta_e \end{cases} .$$

The constants of proportionality r_s and r_c, required to complete (83) have been determined by analysis of observations by Stewart and Grant (1962), and Grant, et al (1968) for shear produced turbulence; and experiments

in Rayleigh convection by Deardorff and Willis (1967) for r_c, whence, r_s=.5 and r_c=2.7.

When $h<\delta_e$, which is typical for lakes,

$$G^*-D^* = \tau_s U_s - \frac{r_s}{k_v} w_*^3 \ln\left(\frac{h}{h_{wm}}\right) - r_c g\alpha B^* (h_c - h_{wm}) + (G^*_w - D^*_w) \quad (89)$$

U_s=.035U_{10}, $h_{wm}=aH_{1/3}$, τ_s=.2$\rho_a C_{10} U_{10}^2$.

$G^*_w-D^*_w$ is given by (82)

for the case S*=B*=0,

$$G^*-D^* = \tau_s U_s - \frac{r_s}{k_v} w_*^3 \ln\left(\frac{h}{h_{wm}}\right) . \quad (90)$$

The constant coefficient, m, used by Denman (1973) in eq. (63) has no significance for the present model. However, as considerable previous research has been expressed in terms of m, the present model will be expressed in these terms also. For the very simple case expressed by (90),

$$m = \frac{\tau_s U_s - \frac{r_s}{k} w_*^3 \ln\left(\frac{h}{h_{wm}}\right)}{\tau_o U_{10}} \quad (91)$$

$$= [7-1.63 \ln\left(\frac{h}{h_{wm}}\right)] \times 10^{-3} \text{ with } B^*, S^* = 0$$

For the set of observations for which m has been determined, listed in Table 2, there is a wide variation in environmental conditions and available information relevant to estimation of the surface fluxes. The

observed value of m from Denman and Miyake (1973) is the value which yields adequate simulation of T(z,t) from the model of Denman (1973), which does account for the surface heat fluxes. On the other hand, Dutton and Bryson (1962) only state that the skies were cloudless and winds ranged from 20-30 kts. over the three day period. Any flux of heat into the observed water column contributes to changes in potential energy of the column. Dutton and Bryson's observations of the temperature structure of Trout Lake in Wisconsin were made on June 24 and 27, with the days clear and windy. The expected insolation under these conditions leads to a decrease in potential energy of the lake which may be of greater magnitude than the effects of the wind. Only Denman and Miyake (1973) and Edwards and Darbyshire (1973) account for effects of net heat flux on the potential energy. Similarly, estimation of m from (91) is subject to error through the assumptions, $S^*=B^*=0$; and as a result of uncertainty in estimation of h($\pm$3m) etc., such that the absolute error in estimation of m by either technique must be $\simeq \pm 2\times10^{-3}$. Although the estimated values of m, given in Table 2, do not exhibit the wide range observed, the correlation between estimated and observed values of m is .71.

During the stratified season, hypolimnion diffusion is very weak, with diffusion coefficients approaching molecular. Kullenberg (1971) proposed an empirical form

for the vertical diffusivity based on dye experiments in the Kattegat. The formula is

$$K_z = c_k U_a^2 N^{-2} \left|\frac{dU}{dz}\right| \tag{92}$$

where U_a=wind speed, $N^2=\frac{g}{\rho}\frac{\partial \rho}{\partial z}$, and $\frac{dU}{dz}$ is the vertical shear of the horizontal current. The formula was later verified by Kullenberg, et al (1973) in Lake Ontario, but with a slightly smaller value for the constant c_k. The value of c_k from the Lake Ontario experiments has been adopted for the lake thermocline model. As the model ignores the mean currents, there is no information available to it concerning the shear. An approximation appropriate for a stably stratified turbulent boundary layer (Deacon and Webb, 1962) has been adopted,

$$\frac{dU}{dz} = \frac{w_\star}{k_v z_b}(1 + 10Ri)^{1/2}$$

where z_b is the distance to the nearest boundary and

$$Ri = \frac{N^2}{\left|\frac{dU}{dz}\right|^2} = \frac{N^2 k_v^2 z_b^2}{w_\star^2 (1 + 10Ri)}$$

This empirical relation can be solved to obtain an approximate Richardson number

$$Ri = -5 + \sqrt{25 + \frac{N^2 k_v^2 z_b^2}{w_\star^2}}$$

and thus $\frac{dU}{dz}$ can be determined from known quantities.

Comparison of this formulation with the shear observed by Kullenberg (1971) indicates that the shear can be estimated within 50% of the measured value.

K_z is calculated at several depths below the mixed layer. The smallest diffusivity so calculated is assumed to apply throughout the hypolimnion. Diffusivities of less than 3 times molecular are not allowed. This procedure is not considered completely satisfactory since w_* is not a realistic turbulent intensity scale below the thermocline, and K_z is probably not independent of depth. However, the diffusivity is so small that errors of an order of magnitude would not significantly affect the results.

The ratio, a, of wave mixed layer depth, to significant wave height, is the least well known of the model parameters and was considered a free parameter, its value determined by correspondence of model predictions to observed conditions. The only constraint was $1<a<4$, as mentioned above. The procedure indicated that the model best simulates observed thermal structure if $a=2$. This value was adopted and used in all simulations reported herein. All other coefficients have been observed, or calculated with varying degrees of precision by various investigators. The best estimate known to the author has been chosen for use in the numerical simulation. A summary

of parameter values used in numerical simulations is given in Table 3.

Table 3. Parameter values

$a = \frac{h_{wm}}{H_{1/3}}$	2.0
$\frac{\tau_w}{\tau_o}$	.8
C_{10}(neutral)	1.3×10^{-3}
h_{10}(neutral)	1.3×10^{-3}
d_{10}(neutral)	1.3×10^{-3}
r_s	.5
r_c	2.7
"meteorological" solar constant	$3 \times 10^{-2} \frac{cal}{cm^2 sec}$
$\frac{H_{1/3}\, g}{F_o^{1/2}\, U_{10}^2}$, fetch-limited	2.4×10^{-3}
$\frac{H_{1/3}\, g}{U_{10}^2}$, fully-developed waves	.28
k_v	.4
$\frac{U_s}{U_{10}}$	.035
c_k	2×10^{-8}

CHAPTER VI

METHOD OF SOLUTION

The equations to be solved are three ordinary differential equations for the mixed layer parameters T_s, h, T_h, eqs. (51), (52), (49); the partial differential equation (48) for T(z,t), $z<-h$; and the boundary conditions represented by (53) and (54). h, marking the boundary of the two domains, and T_h, the temperature there, are time dependent and their determination is a part of the solution. All of these equations are to be satisfied simultaneously. A technique for simultaneous solution of this system is unknown to the author, but fortunately there is a separation of time scales over which significant changes can occur in the regions $z>-h$, and $z<-h$.

A diffusive time scale is $\tau = \frac{\Delta z^2}{K}$, where τ is, e.g., a time scale for changes in the boundary conditions, and z is a distance from the boundary at which those changes will be significantly felt. Below the mixed layer, in the domain of (48), $K \approx .2 \frac{cm^2}{sec}$, $\tau \approx 10^4$sec, then $\Delta z \simeq 40$cm. Thus changes on the time scale of 10^4sec will be significant only within 40cm of the boundary. However, for $z>-h$, $K \approx \infty$, implying that changes in the boundary conditions, of any time scale, are felt instantaneously throughout the mixed layer. This suggests the following algorithm for

solution of the system of equations by finite difference techniques:

(1) Solve (48) from initial conditions over an interval of time, $\Delta t \leq \tau$, with $\Delta z > 40cm$, holding h, T_h constant.

(2) Solve (49), (51), (52) over a similar time interval with

$$\left[\frac{\partial T}{\partial z}, \frac{\partial^2 T}{\partial z^2}\right]_{-h}$$

provided by step (1).

(3) Use new h, T_h generated by (2) for integration of (48) over Δt.

(4) Repeat (2), etc.

Thus, variations of h and T_h are accounted for in solution of the mixed layer equations, but rapid, i.e., $\tau \leq 10^4$sec. variations in these parameters are safely ignored in solution of (48), and the solution proceeds alternately between the two domains.

The mixed layer ordinary equations, (49), (51), and (52), are solved by a variable step fourth order Runge-Kutta algorithm adapted for this problem from an IBM, Scientific Subroutine Package (SSP) subroutine. At each time step the solution at $t + \Delta t$ is found. Then the interval, Δt, is halved and the solution is found again at $t + 2(\frac{\Delta t}{2})$. If the difference between the two results is greater than some specified error bound, ζ, the

interval is halved and a similar process, is repeated. If the difference is less than $\zeta/50$, the interval is doubled. If the difference is greater than ζ for

$$\Delta t = \frac{1}{2^{10}}(\Delta ti),$$

where Δti is the initial step, the subroutine returns to the main program with an error message. Δti is the maximum step allowed. The Runge-Kutta algorithm is unconditionally stable.

(48) is solved via a Crank-Nicholson scheme which is also unconditionally stable.

When $\frac{dh}{dt}<0$, eq. (52) reduces to a non-linear algebraic equation,

$$h = \frac{2[(G-D) + \frac{S}{\beta}(1-e^{-\beta h})]}{B+S(1-e^{-\beta h}) + K_z\frac{\partial T}{\partial z}\Big|_{-h}}$$

which is solved by Newton's iterative technique.

This technique requires a first guess of h, h_o, given by the linear approximation

$$h_o = \frac{2[(G-D) + \frac{S}{\beta}]}{B+S} .$$

The algorithms for application of Newton's iterative scheme were also adapted from SSP subroutines.

A routine check on the accuracy of these techniques has been made by comparing the heat flux integral

$$Q_i(t) = \int_o^t (S+B)dt$$

with the enthalpy change of the water column,

$$H_i(t) = \rho c_p \int_{-D}^{o} [T(z,t) - T(z,0)]dz \ .$$

These integrals are computed numerically since S and B are known at discrete values of t, t_i, and T is only known at discrete values of z, z_i.

The relative error in the heat conservation

$$E(t) = 2\frac{[Q_i(t) - H_i(t)]}{[Q_i(t) + H_i(t)]}$$

is found to be a generally decreasing function of t,

$$E(t_2) \leq E(t_1) \text{ for } t_2 >> t_1 \ ,$$

indicating that errors incurred are random and tend to cancel out in longer integrations.

For the shortest integrations reported here, for which t_{max}=1 day, $E(t_{max}) \approx 7\%$.

For the longer integrations, $t_{max} \geq 30$ days, $E(t_{max})$ ranges from .2% to 2%.

CHAPTER VI

MODEL VERIFICATION

The proposed model is expected to be valid for all freshwater lakes regardless of size. As no previous model properly treats the space scale dependency observed by Blanton (1973), the present model will be shown to be superior to previous models in its universal validity for lakes of different size.

Niiler (1975) concludes that mixed layer models which ignore inertial currents are not valid for time scales of the order of the inertial period. However, Denman and Miyake (1973) verify a model similar to that presented here for time scales of the order of the inertial period, so one might hope that the model is valid on the diurnal, as well as the seasonal scale.

Observational programs in which all of the required input data have been measured in conjunction with adequate lake temperature profiles are rare. Only two such sets were available to the author: (1) the International Field Year for the Great Lakes (IFYGL) experiment, and (2) observations on Llyn Cwellyn, a small lake in Wales (Darbyshire and Colclough, 1972). Lake Ontario has a surface area of $1.8 \times 10^4 km^2$ while the surface area of Llyn Cwellyn is 1 km^2, providing ample variation in spatial scale. The Lake Ontario observations

extend over seven months with observations of all necessary parameters at several locations around, over, and in the lake. Horizontally averaged surface conditions and temperature profiles may be obtained from the raw data on an hourly basis during much of the period extending from May through November of 1972.

The observations on Llyn Cwellyn, on the other hand, consist of temperature profiles at one location in the lake at half hour intervals. Continuous records of the surface meteorological conditions at one station are available, but the length of the record is only one day. In this chapter the results of model simulations of thermal structure for these two cases will be discussed.

IFYGL. IFYGL was a large, international, cooperative experiment designed to provide comprehensive observations of physical, chemical, meteorological, and biological parameters in Lake Ontario over an annual cycle. In addition to baseline observations of currents, water temperature, and meteorological variables over the whole basin, a number of specialized or local experiments were conducted by various American and Canadian scientists. The primary IFYGL data base utilized in this study was the archive of the Physical Data Collection System (PDCS). The PDCS sensors were deployed from moored buoys and towers, and the resultant records are time series of observations from fixed points. Figure 2

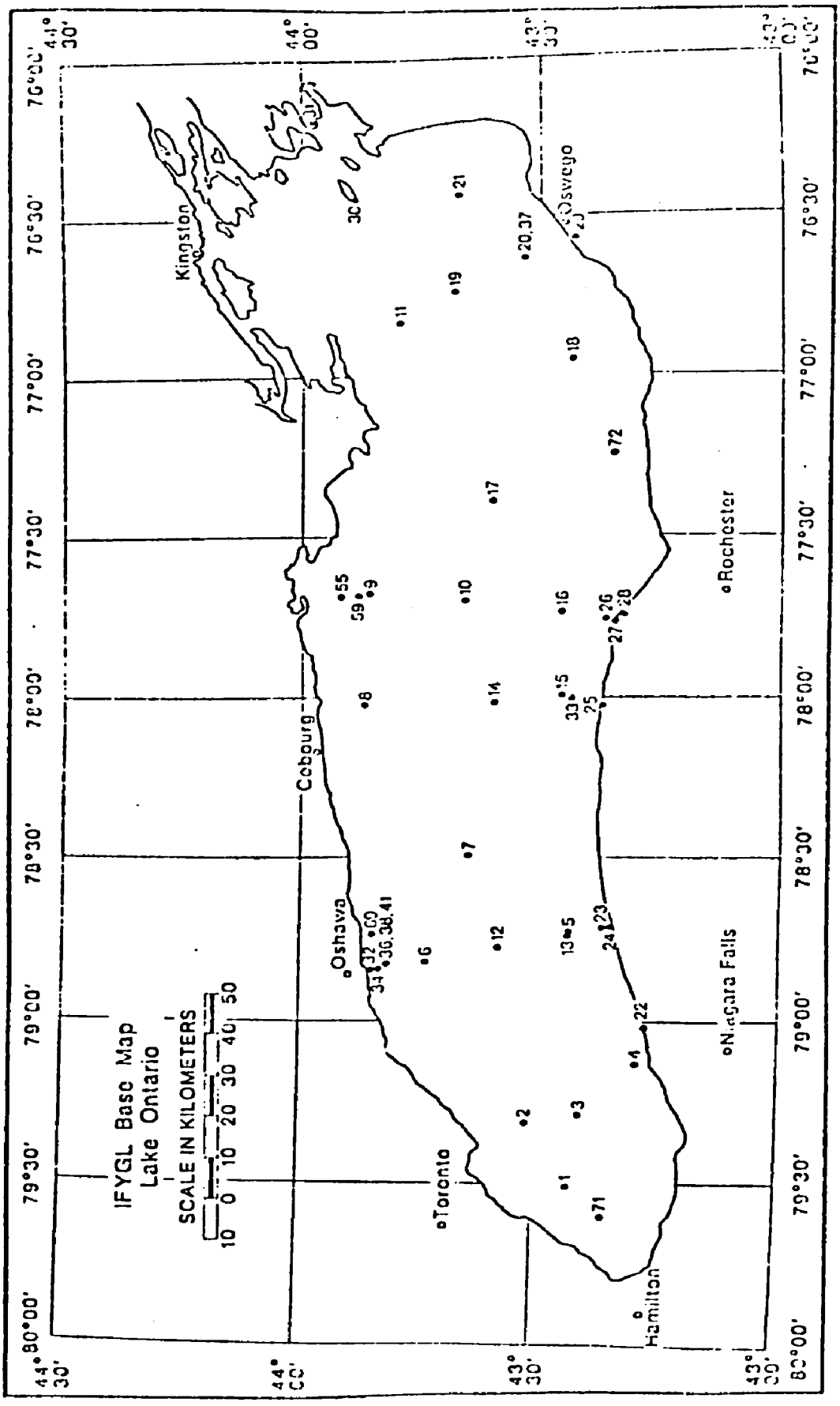


Fig. 2. Map of Lake Ontario showing the stations of the IFYGL Physical Data Collection System.

is a map of Lake Ontario with PDCS station positions indicated. The sampling interval was 6 min. After preliminary editing, the hourly averaged data, on magnetic tape, were graciously provided by Dr. R. L. Pickett of NOAA, Great Lakes Environmental Research Laboratory.

The PDCS observations utilized are East and North components of wind velocity, air temperature, dew point temperature, and water temperature. The height above the lake surface at which the atmospheric sensors (one per station) were emplaced is known, but not uniform. Water temperature was obtained at up to 14 levels, at 5 m intervals for $z > -40$ m, every 10 m for $-40\text{m} \geq z \geq -60$ m and, at 75 m, 100 m, and 150 m. Stations in shallow water, $D \leq 20$ m, have greater vertical resolution in the temperature.

Also utilized were observations of cloud cover at weather stations near the lake in the U.S. and Canada. Total sky cover was reported hourly.

The IFYGL experiment represents an unprecedented body of limnological data. There is a temptation to design the model so as to utilize this special data set to its fullest. This might involve using the spatially distributed meteorological data to force the model locally before horizontal averaging, or using measured values of

radiation instead of empirical radiation formulae. However, the potential user of the model will probably have neither observations of horizontal variations of meteorological conditions over a lake, nor radiation observations. It is intended that input requirements be limited to routinely observed meteorological variables. Consequently, lake wide averages of all meteorological variables were obtained and used to compute the forcing functions, G, D, S, and B.

Atmospheric properties change rapidly in the vertical direction near the lake surface. Bulk transfer formulae require meteorological variables to be observed at some specific height, z. Consequently all observations were adjusted (via micrometeorological formulae) to a uniform height above the sea surface. The sensor heights for various platforms are listed in Table 4.

Table 4. PDCS Sensor Heights, IFYGL

Station Type	Air Temp. (m)	Wind (m)	Dew Point (m)
Land	1.5	10	1.5
Buoy (American)	3	3	3
Buoy (Canadian)	4*	4*	4*
Island	1.5	1.5	1.5
Shallow Tower	3	10	3
Deep Tower	3	10	3

Source: IFYGL Data Management, National Climatic Center,
*Fred Jenkins, personal communication

All values were adjusted to a height of 3 m. To approximate wind speed, temperature, and humidity at 3 m from observations at different levels, the following formulae were used.

$$U_3 = U_z + \frac{u_*}{k}[\ln\frac{3}{z} - \psi_1\Big|_3 + \psi_1\Big|_z]$$

$$T_3 = T_z + \theta_*[\ln\frac{3}{z} - \psi_2\Big|_3 + \psi_2\Big|_z]$$

$$q_3 = q_z + q_*[\ln\frac{3}{z} - \psi_2\Big|_3 + \psi_2\Big|_z]$$

where u_*, θ_*, and q_* are obtained from the relations

$$U_z = \frac{u_*}{k}[\ln\frac{z}{z_o} - \psi_1\Big|_z]$$

$$T_z - T_s = \theta_*[\ln\frac{z}{z_o} - \psi_2\Big|_z]$$

$$q_z - q_s = q^*[\ln\frac{z}{z_o} - \psi_2\Big|_z]$$

with $z_o = 1.5 \times 10^{-2}$cm over water and assume $z_o = 2$ cm for land stations.

For unstable stratification, ψ_1 and ψ_2 are given by Paulson (1967). Under stable conditions the formulations of Businger, et al (1971) have been used. ψ_1 and ψ_2 are functions of a stability parameter, e.g. z/L where L is the Monin-Obukhov length. z/L is approximated as 12 Rib as suggested by Deardorff (1968) where

$$\text{Rib} = \frac{gz}{T_z}\,\frac{T_z - T_s}{U^2_z}$$

The horizontal averaging technique, which was used for all variables, consisted of a weighted mean with the weights a function of spatial distribution. The lake surface, or the area within a specified depth contour for subsurface temperatures, was segmented into areas whose boundaries were equi-distant from two stations. Thus all points in, e.g., region 1 were closer to station 1 than to any other station. Then the observations from any one station was weighted by the area of its corresponding region.

Stations for which no data were reported were interpolated as the unweighted mean of the five nearest stations. If none of these five stations reported an observation, the station was dropped from consideration in the horizontal average.

This averaging process is utilized to eliminate a bias toward near shore areas likely to occur if all stations were accorded equal weights (see Fig. 2). Since cloud cover observations were only made from land, an unweighted mean was used which may be unrepresentative of over lake cloud cover. This bias should be most severe during mid-summer when the lakes are less cloudy than the adjacent land (Phillips and McCulloch, 1972).

The weather of IFYGL has been reviewed by Phillips (1974). The months chosen for simulation, July, August, and October will be described briefly here.

The months of July and August were characterized by seasonal weather and calm winds. According to Phillips (1974) monthly average wind speeds were below normal during July and August at several weather stations adjacent to the lake. Record low monthly average wind speeds were recorded at Toronto Island Airport during both months. Nonetheless, there were stormy periods which elicited significant response in the lake. One of these was the cool, dry period of July 23-26 when hourly lake average winds reached 7 m/sec, generally from the west. The thermocline was tilted significantly. Surface temperature along the north shore decreased by 13°C from the 20th to the 26th (Arajs and Farooqui, 1974). Preceeding this storm the month of July had been warm and calm with the lake surface temperature increasing by about 10°C from the first to the twentieth.

August 4 saw the arrival of a very cool dry air mass with moderate winds and clear skies. Relatively cool air persisted until the twentieth. Winds were strong from Aug. 8-10, with hourly, lakewide mean speeds of 11.7 m/s on Aug. 9. From Aug. 21 to the end of August warm air and light winds persisted, although Aug. 28 was moderately windy. Humidity was high throughout the month, aside from the 4th and 5th. The data presented by Arajs and Farooqui (1974) also indicate upwelling on Aug. 10 and

28. These upwelling events should provide the severest tests of the model since whatever effect they may have on the mean thermal structure is not explicitly considered.

The month of October was somewhat windier than the mid-summer period of July and August. Daily lakewide mean wind speeds in excess of 9 m/sec occurred on October 9 and 17. Air temperatures were generally below the lake surface temperature after October 8. Mean air temperatures for October were between 2 and 3°C below normal throughout the Lake Ontario basin (Phillips, 1974). Upwelling accompanied the strong winds of the 8th and 9th, but unlike the mid-summer events, the thermocline never fully recovered from the tilt imparted by this storm. The 10° isotherm exhibits a tilt of 50 to 80 m from October 10 to the end of the month.

Besides the hourly lakewide mean meteorological inputs, the last remaining input parameter required for Lake Ontario is the solar radiation attenuation coefficient. The source for this parameter is an IFYGL study of the optical characteristics of Lake Ontario by Thompson, et al (1974). This study shows the variation of β with time during 1972, and indicates $\beta \approx .0056$ cm^{-1} during July and August, $\beta \approx .0044$ cm^{-1} during October.

The months of July and August are conducive to verification of the model on two counts. Because of the

intense stratification and relatively light winds of this period, the thermocline approximates a level surface. Although three upwelling events occurred during this period, they were intermittent. Even during these events the slope of the thermocline is considerably less than in October.

Secondly, the vertical spacing of temperature sensors was too great to permit resolution of a mixed layer if it's depth was less than 5 m. Only for h>5m will two sensors record nearly identical temperature, thus indicating the presence of a mixed layer. During July and August, 60% of the diurnally averaged profiles indicated a resolvable mixed layer. June profiles rarely show a mixed layer, although the explanation for this may be that its depth was less than 5 m.

The model was run for 62 days beginning July 1. The diurnally averaged surface meteorological conditions for the period are summarized in Fig. 3. The surface heat fluxes, S and B, (solid lines, scale on left) were model generated. The air-lake temperature difference (upper dashed line, scale on right) is computed from observations of air temperature (model input) and the model predictions of the lake surface temperature. Wind speed is as observed (lower dashed line, scale on right). B is negatively correlated with wind speed, positively correlated with T_a-T_l, and shows greater variability than S.

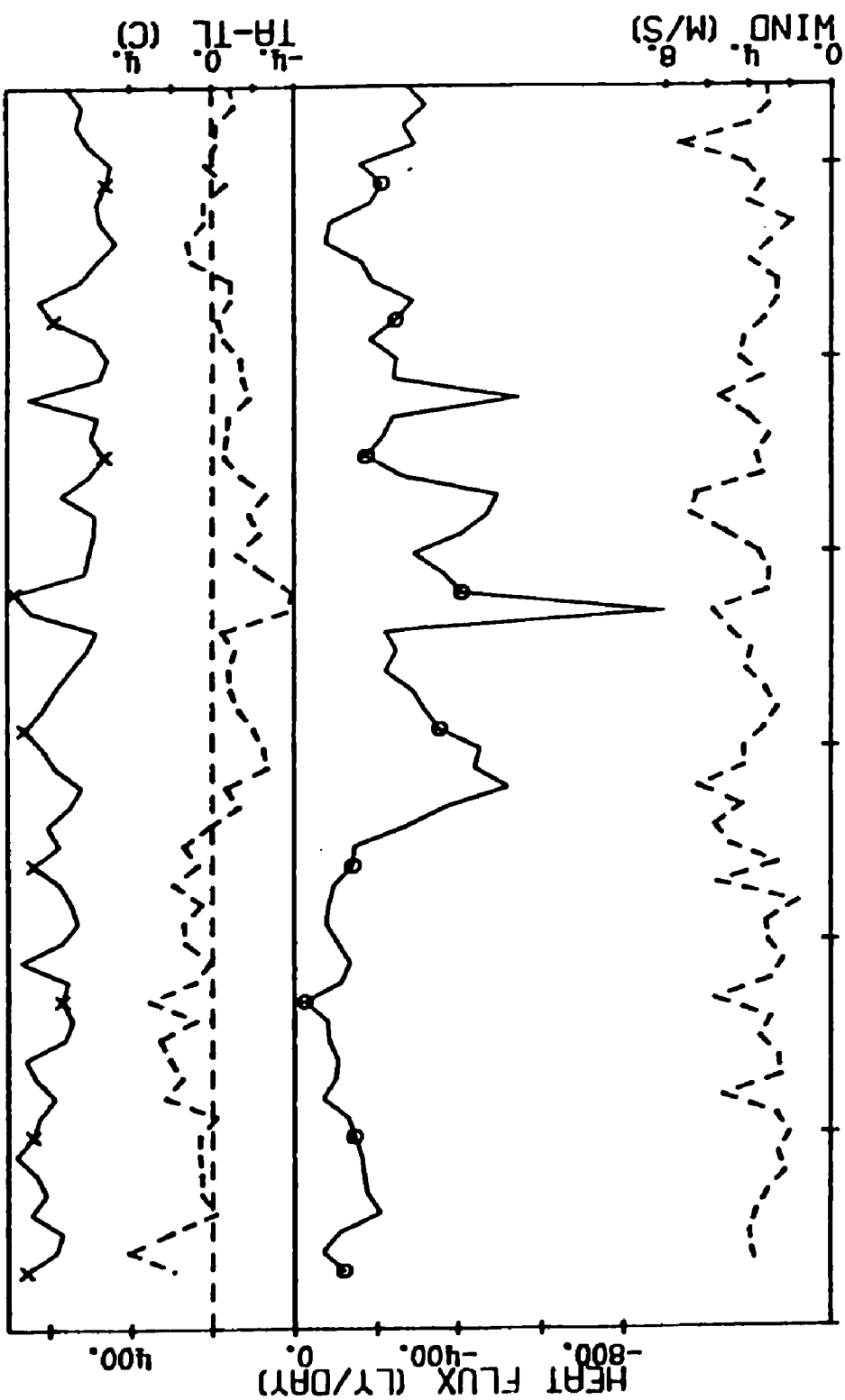


Fig. 3. Surface conditions, Lake Ontario, July and Aug., 1972. The upper solid line is insolation, S*, the lower solid line is the surface heat flux, B*. Both S* and B* are calculated by the model. The upper dashed line is the air-lake temperature difference, where Ta is observed while lake temperature is predicted by the model. The lower dashed line is the observed wind speed. All quantities are lakewide diurnal averages. Julian date 182 corresponds to July 1.

Fig. 4 shows a comparison of predicted and observed surface temperatures after diurnal averaging. Julian dates are used in the graphs depicting the July, August output. Julian date 182 corresponds to July 1. The agreement is excellent prior to date 205 (July 24), a period of upwelling, with a correlation between observed and predicted values of .99. After this time the correlation is reduced to .96, but is still considered satisfactory with a maximum error of 1.26°C at date 230 (Aug. 18). Overall the correlation is .98. The root mean square deviation of observed and predicted surface temperature is .41°C prior to 205, .58°C after 205, and .53°C over the 62 day period.

The comparison of observed and predicted mean temperature profiles is shown in Fig. 5. The initial profile (solid line with symbols at depths of observation) is shown in each graph as a reference. The solid lines are the observed profile, broken lines are profiles generated by the model. If one correlates the predicted and observed change in temperature from the initial to final profiles at 13 depths for which observations are available, the correlation is .995. The correlation of observed and predicted temperature changes from the initial profile to July 22 at the same depths is .994.

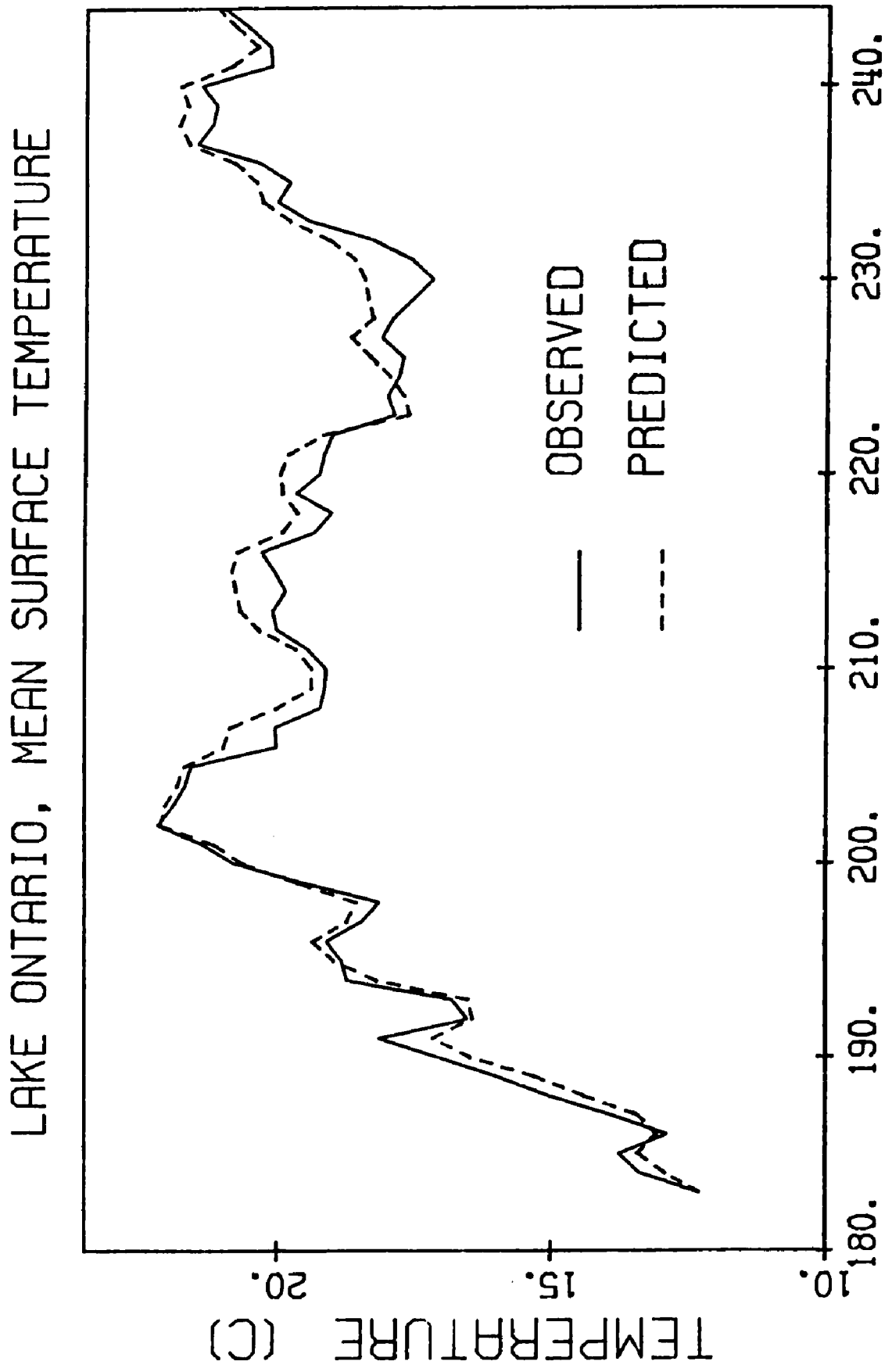


Fig. 4. Lake Ontario, July-Aug., 1972, mean surface temperature, lakewide diurnal average.

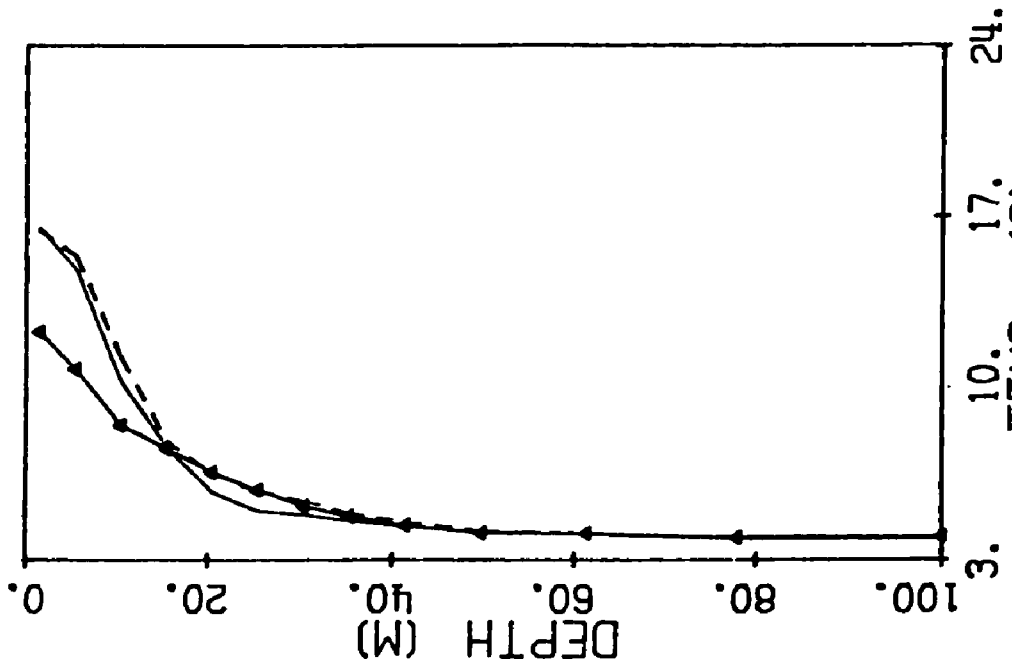


Fig. 5b. Same as 5a, initial profile (symbols), and observed and predicted for July 11.

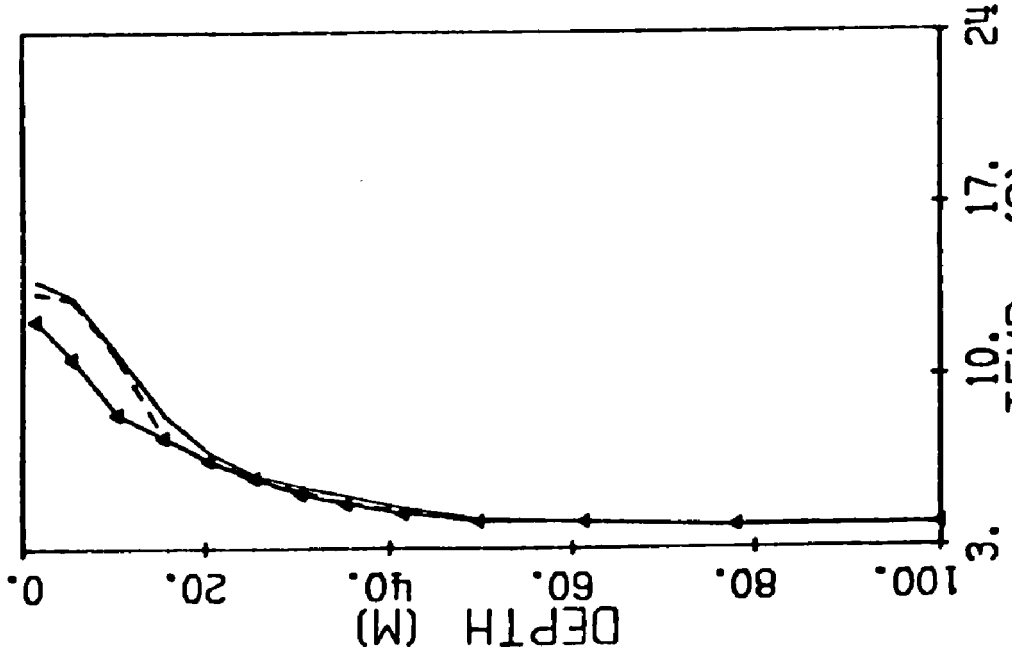


Fig. 5a. Lake Ontario mean temperature profile, line with symbols is July 1 (initial); solid line without symbols is July 6, observed; dashed line is July 6, model predicted.

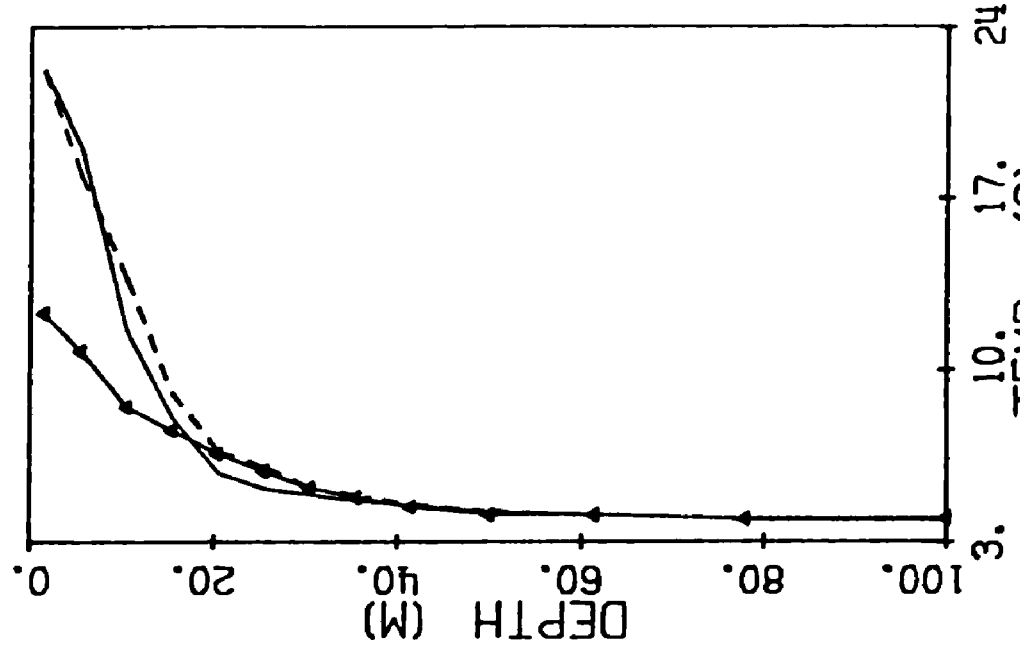


Fig. 5d. Same as 5a, initial profile (symbols), and observed and predicted for July 21.

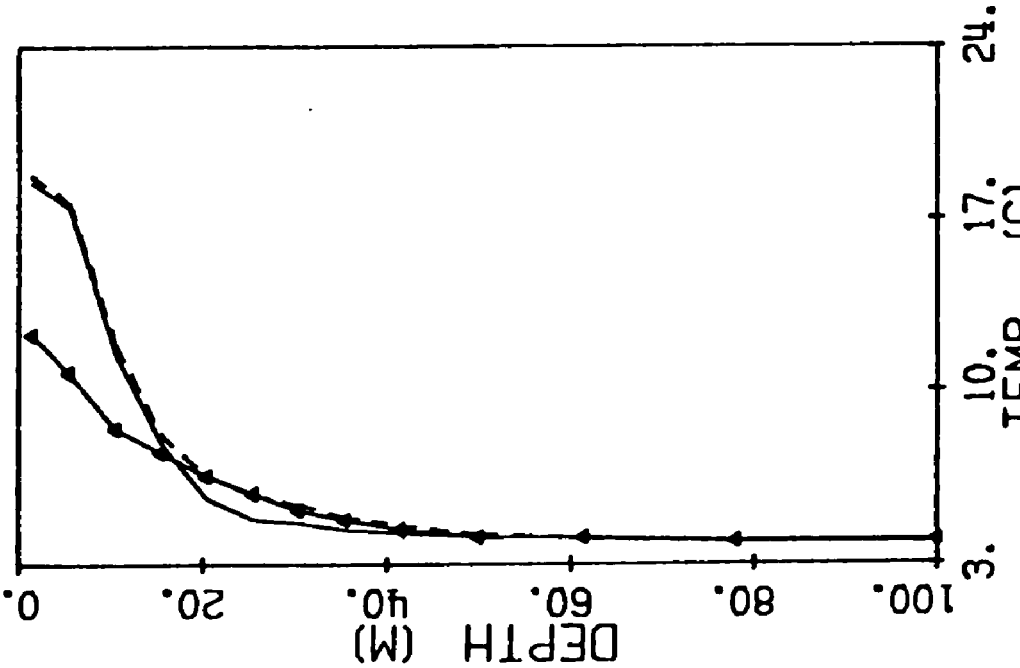


Fig. 5c. Same as 5a, initial profile (symbols), and observed and predicted for July 16.

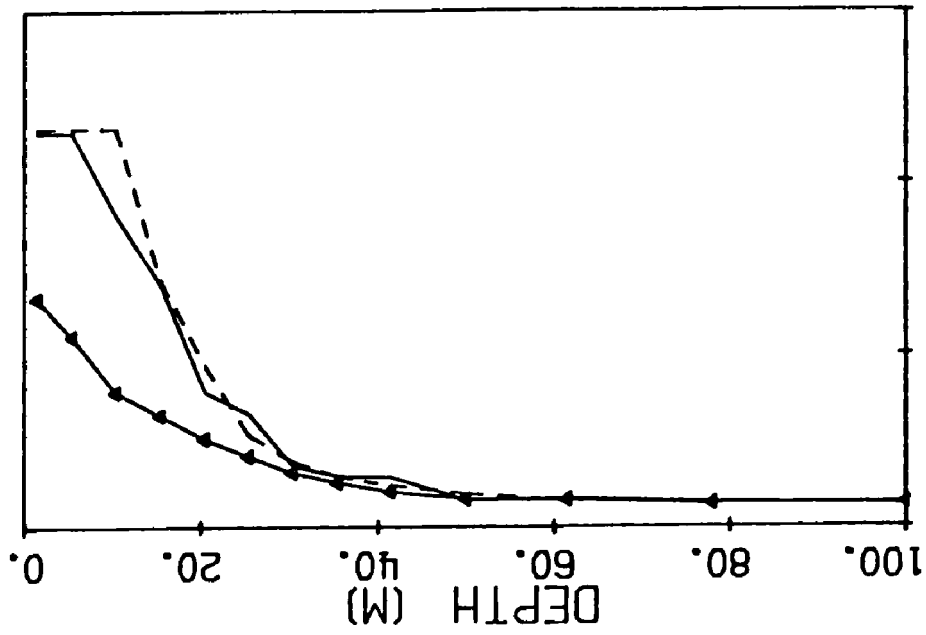


Fig. 5f. Same as 5a, initial profile (symbols), and observed and predicted for July 31.

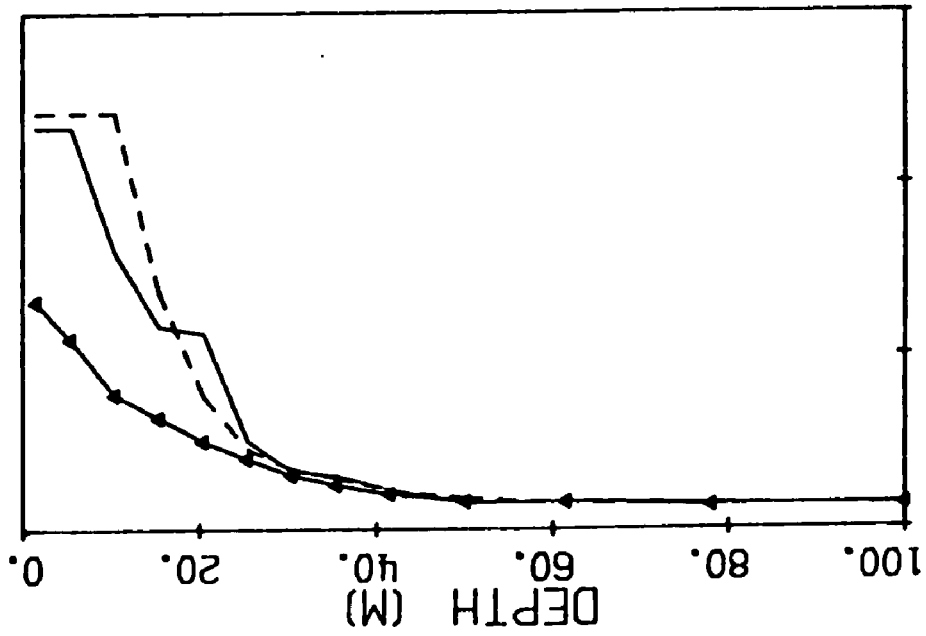


Fig. 5e. Same as 5a, initial profile (symbols), and observed and predicted for July 26.

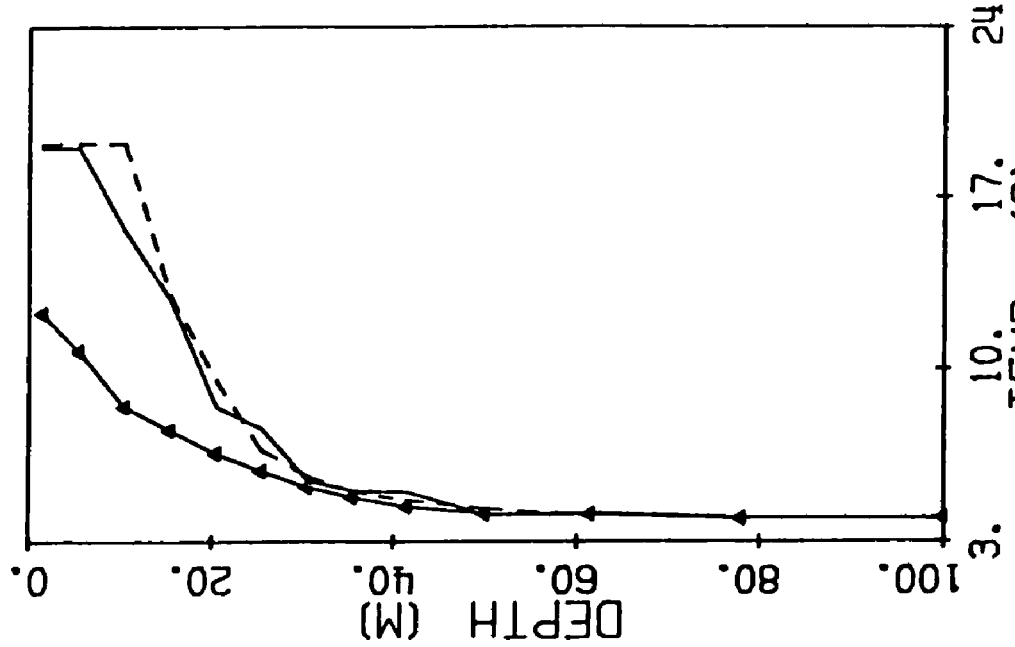


Fig. 5h. Same as 5a, initial profile (symbols), and observed and predicted for Aug. 10.

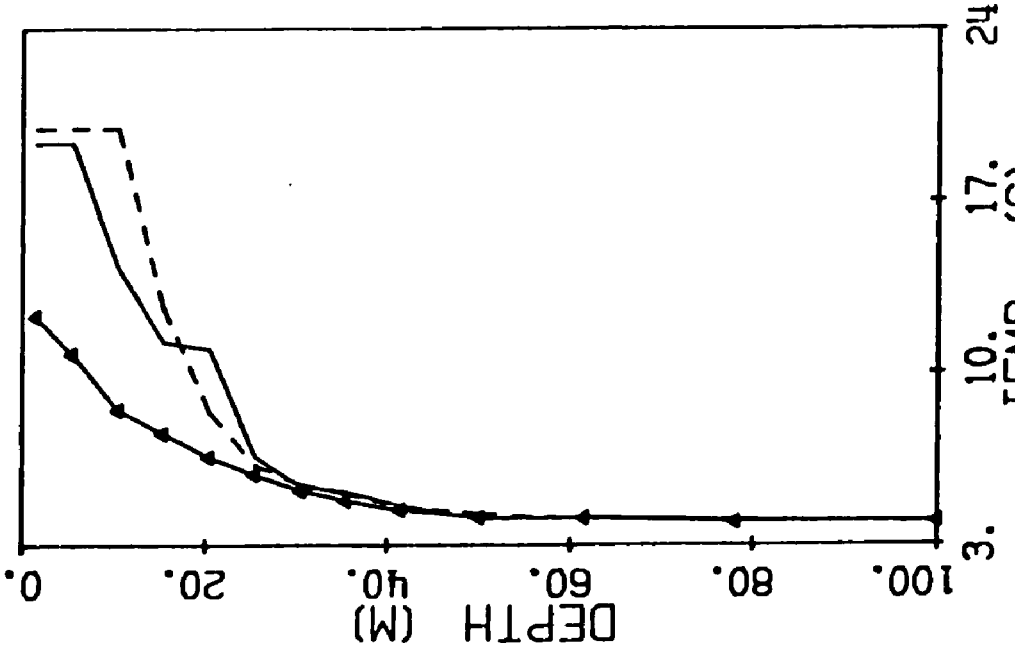


Fig. 5g. Same as 5a, initial profile (symbols), and observed and predicted for Aug. 5.

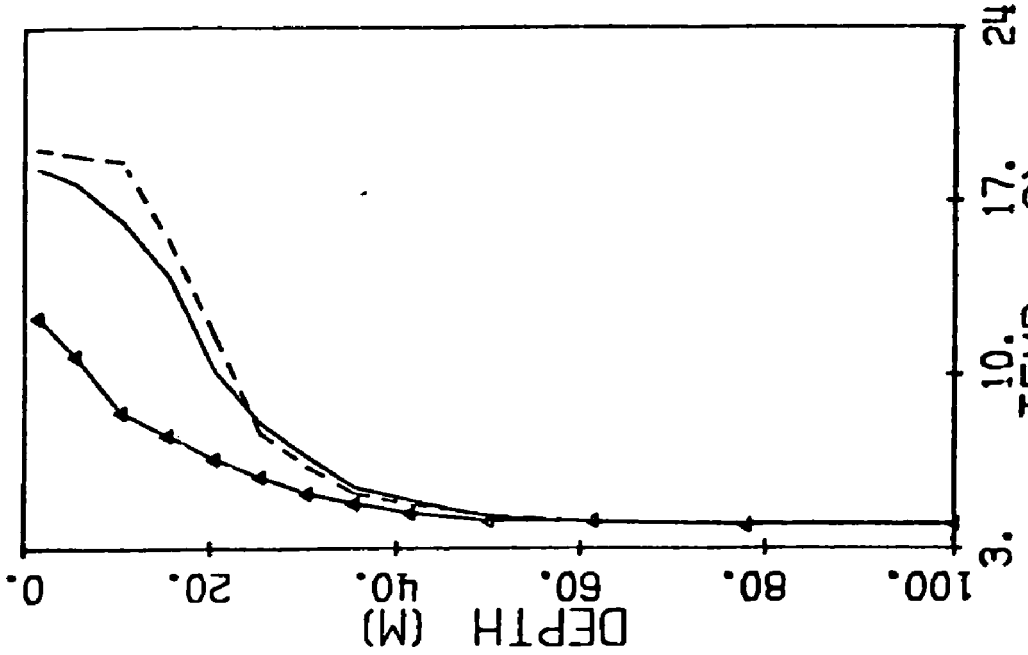


Fig. 5j. Same as 5a, initial profile (symbols), and observed and predicted for Aug. 20.

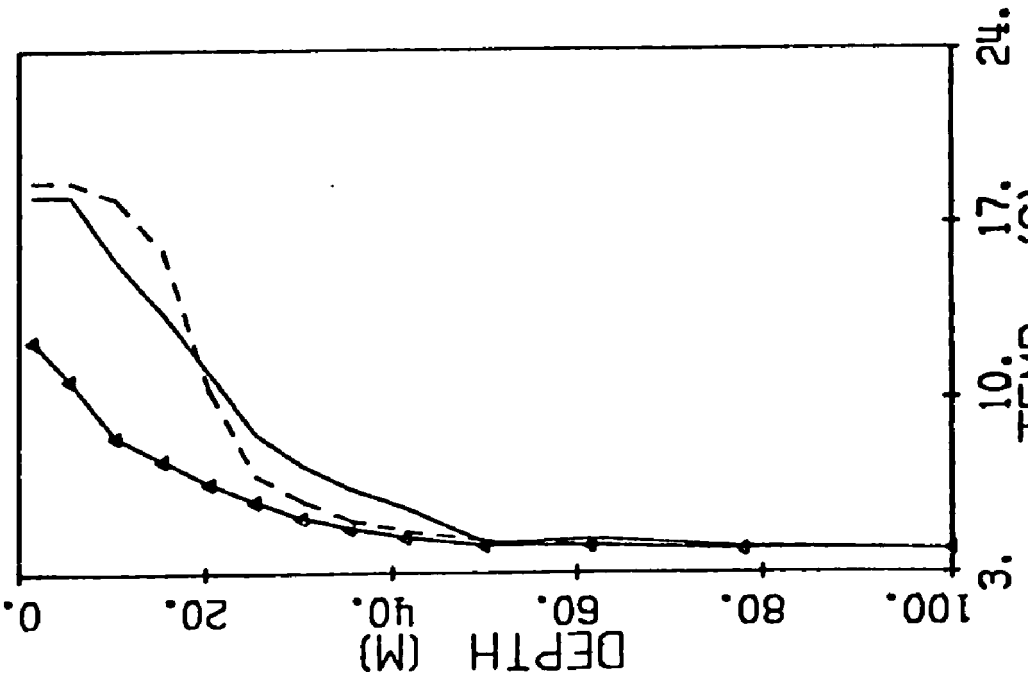


Fig. 5i. Same as 5a, initial profile (symbols), and observed and predicted for Aug. 15.

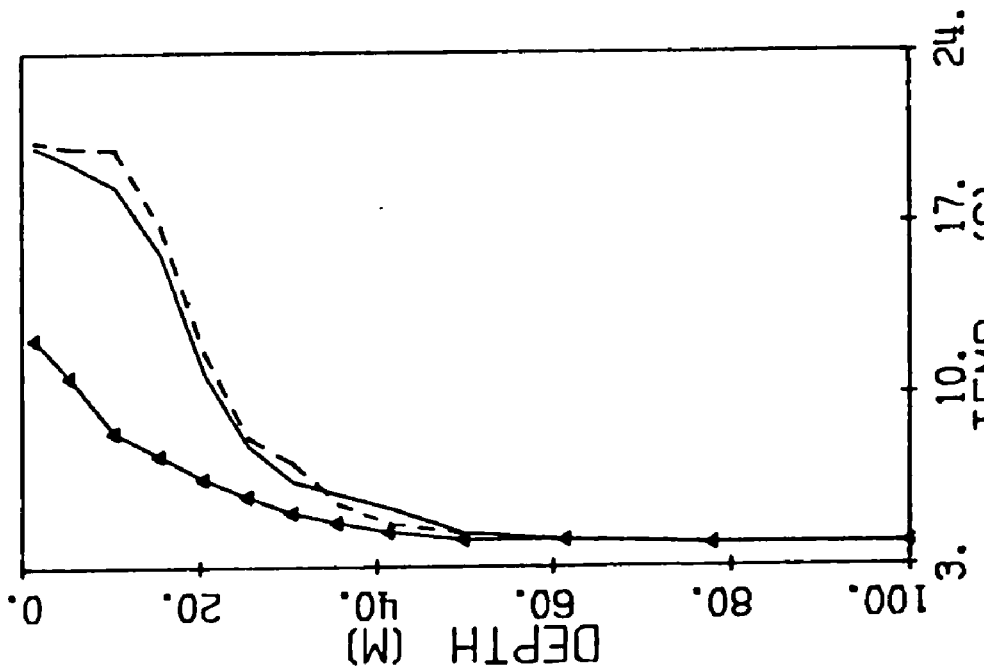


Fig. 5l. Same as 5z, initial profile (symbols), and observed and predicted for Aug. 30.

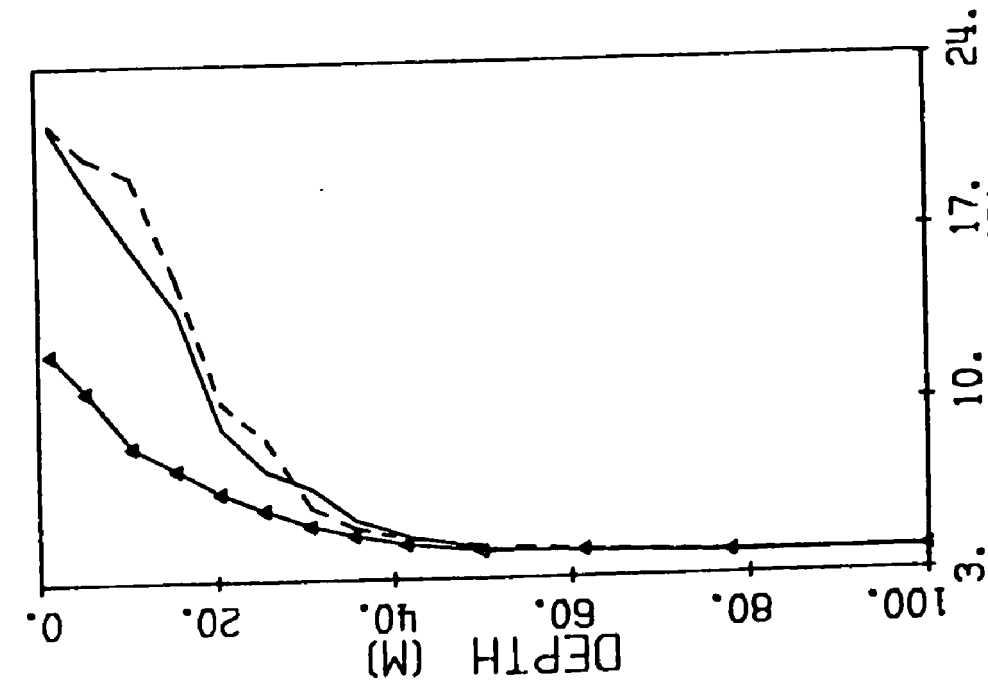


Fig. 5k. Same as 5a, initial profile (symbols), and observed and predicted for Aug. 25.

A more complete display of the model-generated temperature field in depth and time is shown in Fig. 6, a plot of diurnal mean isotherm depths vs. time. Fig. 7 is a similar plot for the diurnal lakewide mean isotherms as observed by the PDCS. In Fig. 7 dashed boxes enclose regions in depth and time for which the mean values may be unrepresentative of lakewide conditions because few sensors reported observations. For $z>-30m$ the mean values are considered unreliable if less than 4 stations reported. For $z<-30m$, where temperature gradients are smaller, two or more stations are considered sufficient.

Presentation of the diurnal averages is necessary in comparing the model predictions with results because the observations are not dense or uniform enough to take meaningful horizontal averages of the hourly values. In addition, the time span of the simulation, $\approx$1500 hours, yields too many data to adequately interpret on an hourly basis. To indicate the response of the model on shorter time scales, Fig. 8 shows predicted temperature vs. time at 4 depths. The diurnal component of the surface temperature is a clear feature, as is the time (date 222) when the mixed layer deepens past 15 m. Some anomalous changes in subsurface temperatures result from the linear interpolation scheme used to extract the temperatures at fixed depths from the raw output, which yields temperatures at a constant number of grid points with spacing,

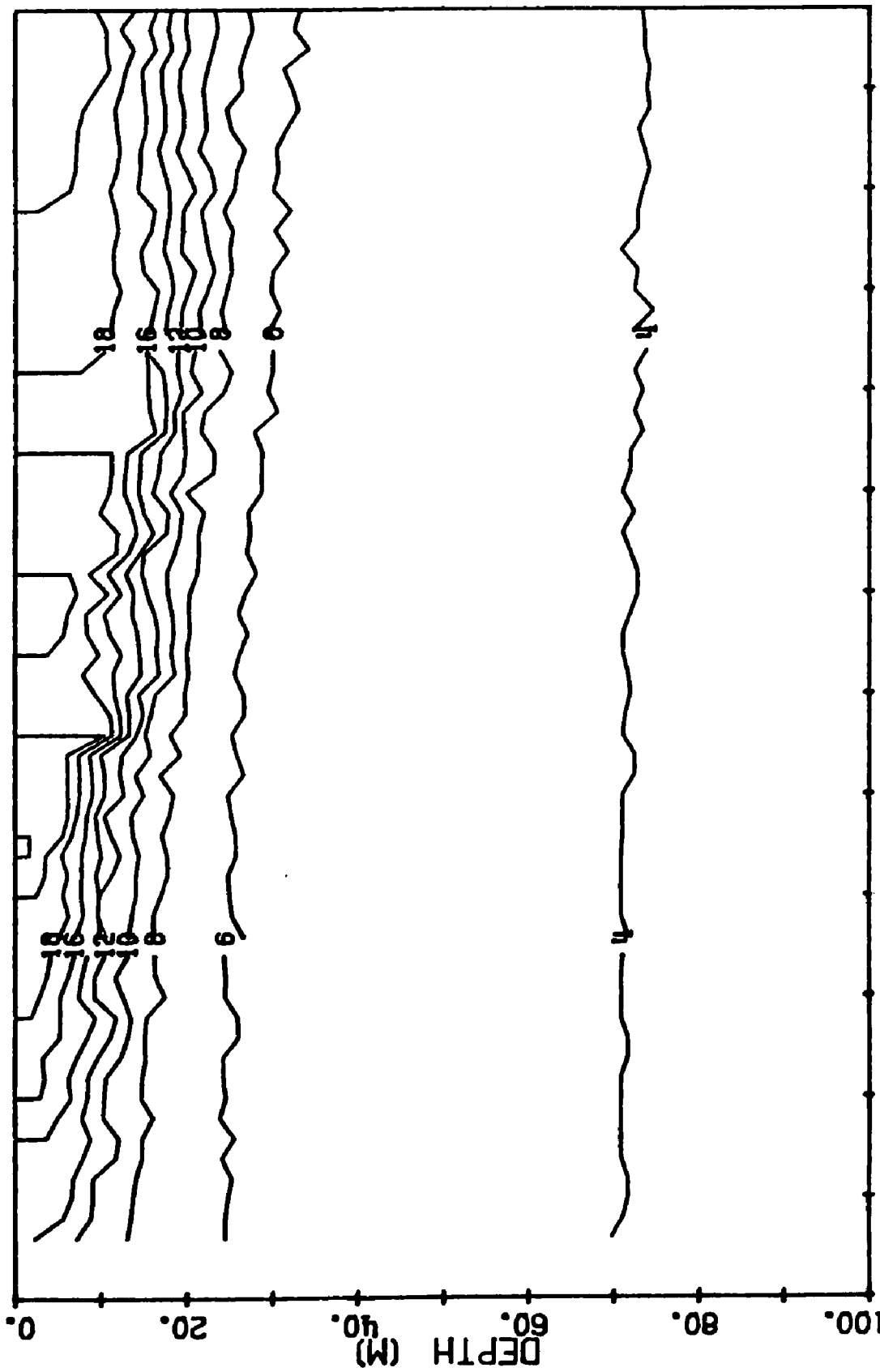


Fig. 6. Lake Ontario, July-Aug., 1972. Isotherm depths vs. time as predicted by the model. Contour interval is 2°C.

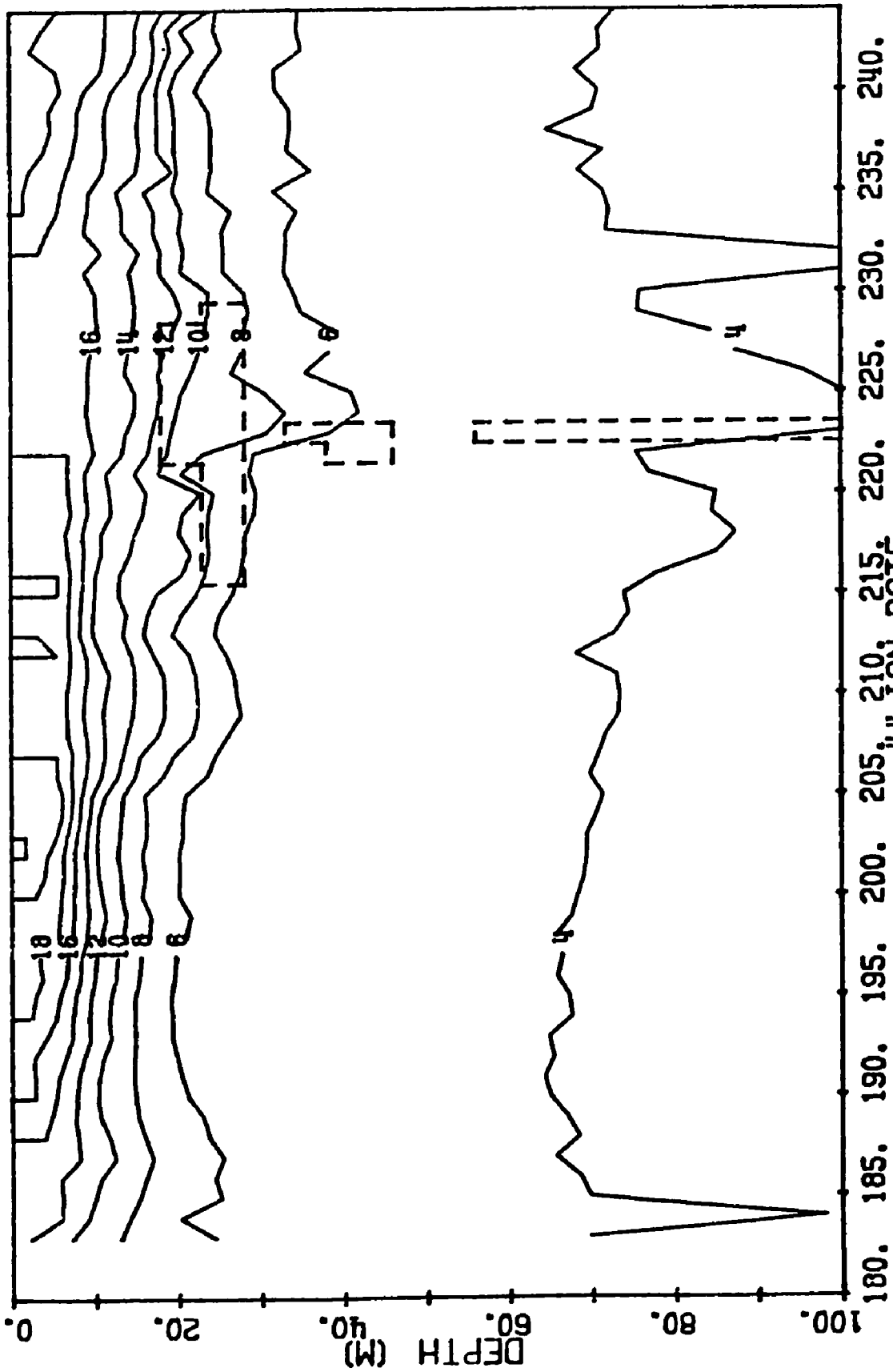


Fig. 7. Lake Ontario, July-Aug., 1972, lakewide mean isotherm depths vs. time as observed by PDCS. Sparsely observed regions in depth and time are enclosed by dashed boxes (see text). Contour interval is 2°C.

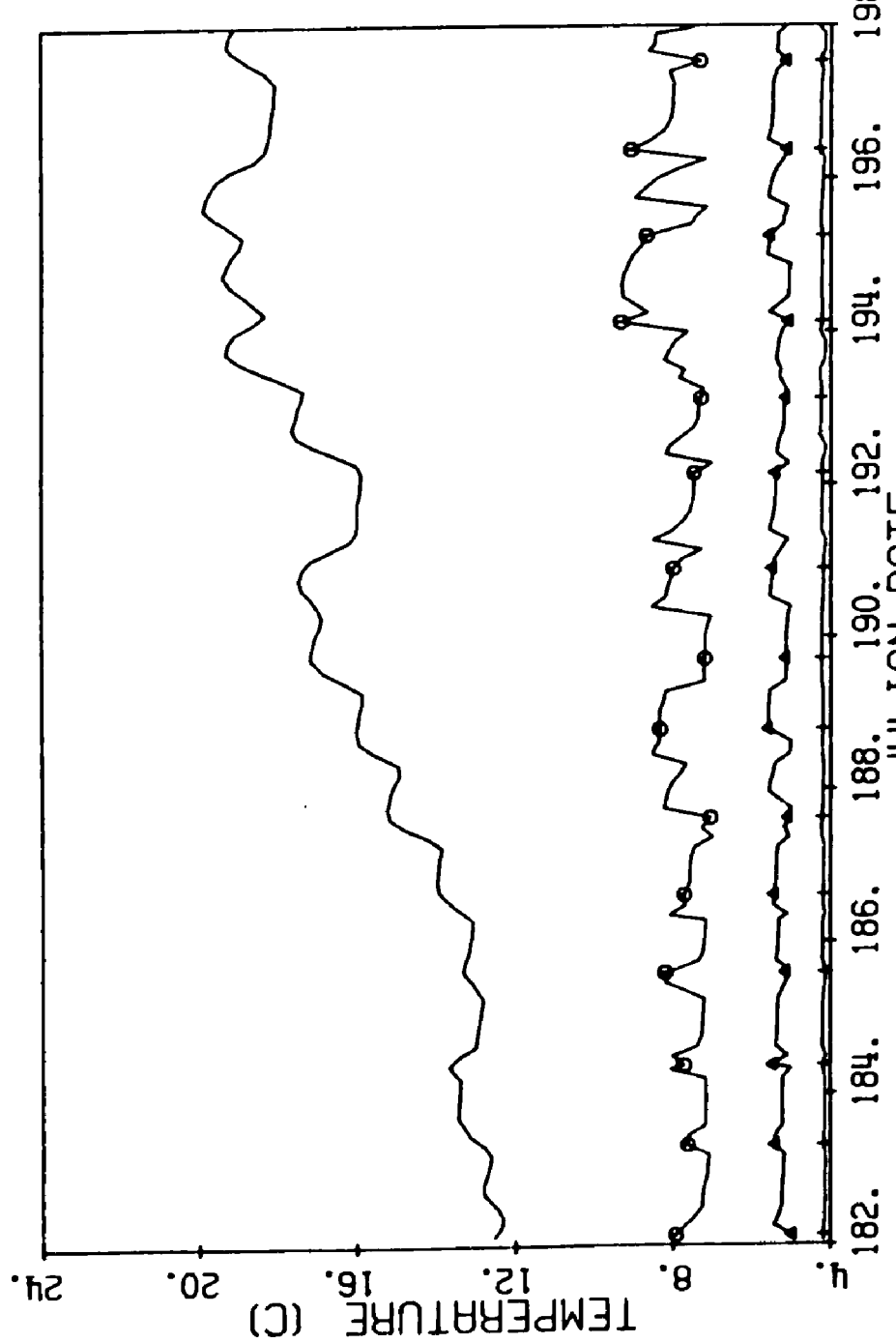


Fig. 8a. Lake Ontario, July-Aug., 1972, model predicted T vs. t at four depths. Upper line (without symbols) is surface temperature, line with circles is T (-15m), line with triangles is T (-30m), lower line with crosses is T (-60m)

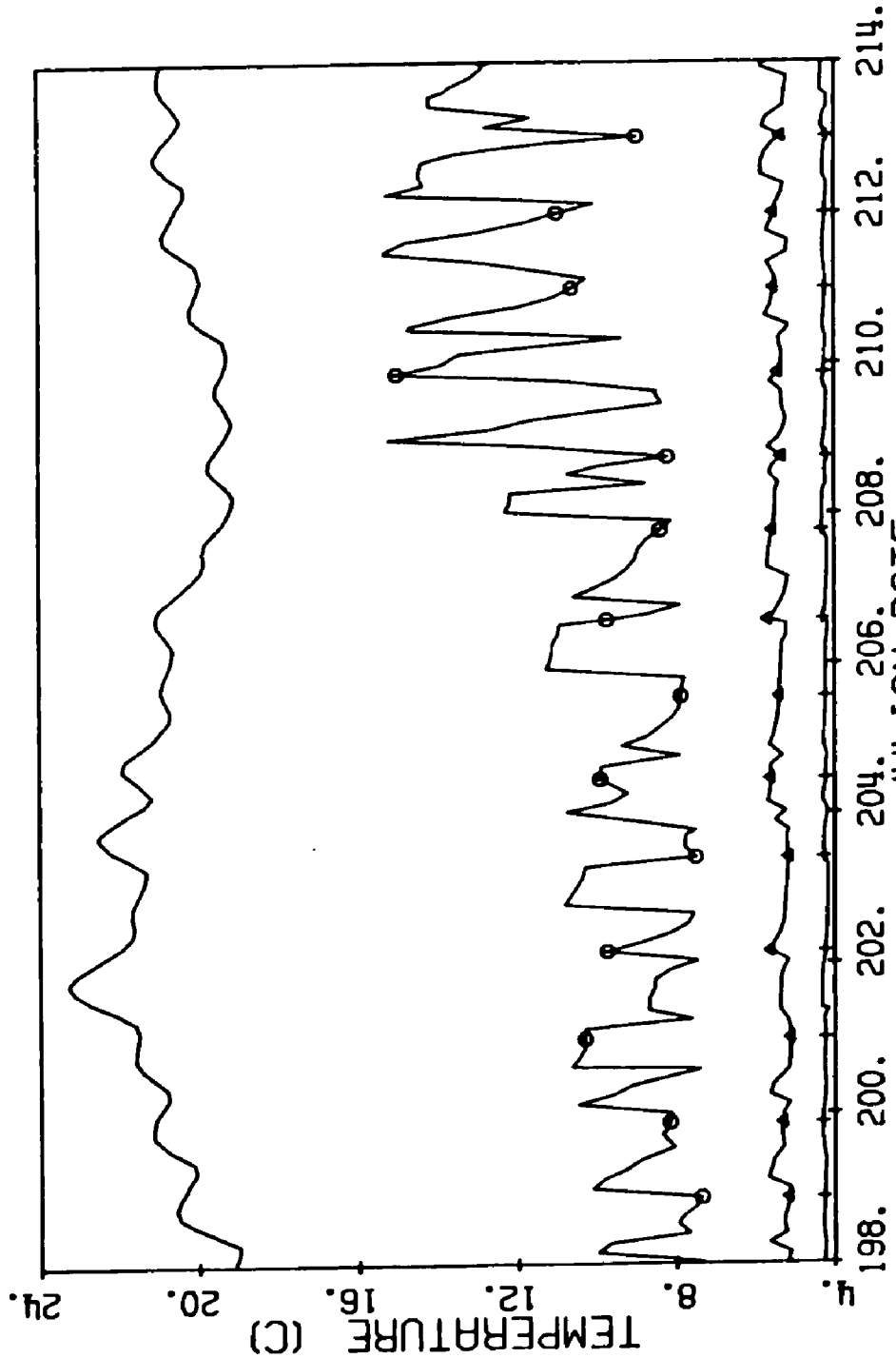

TEMPERATURE (C)
4.
8.
12.
16.
20.
24.
198.
200.
202.
204.
206.
208.
210.
212.
214.
JULIAN DATE

Fig. 8b. See 8a

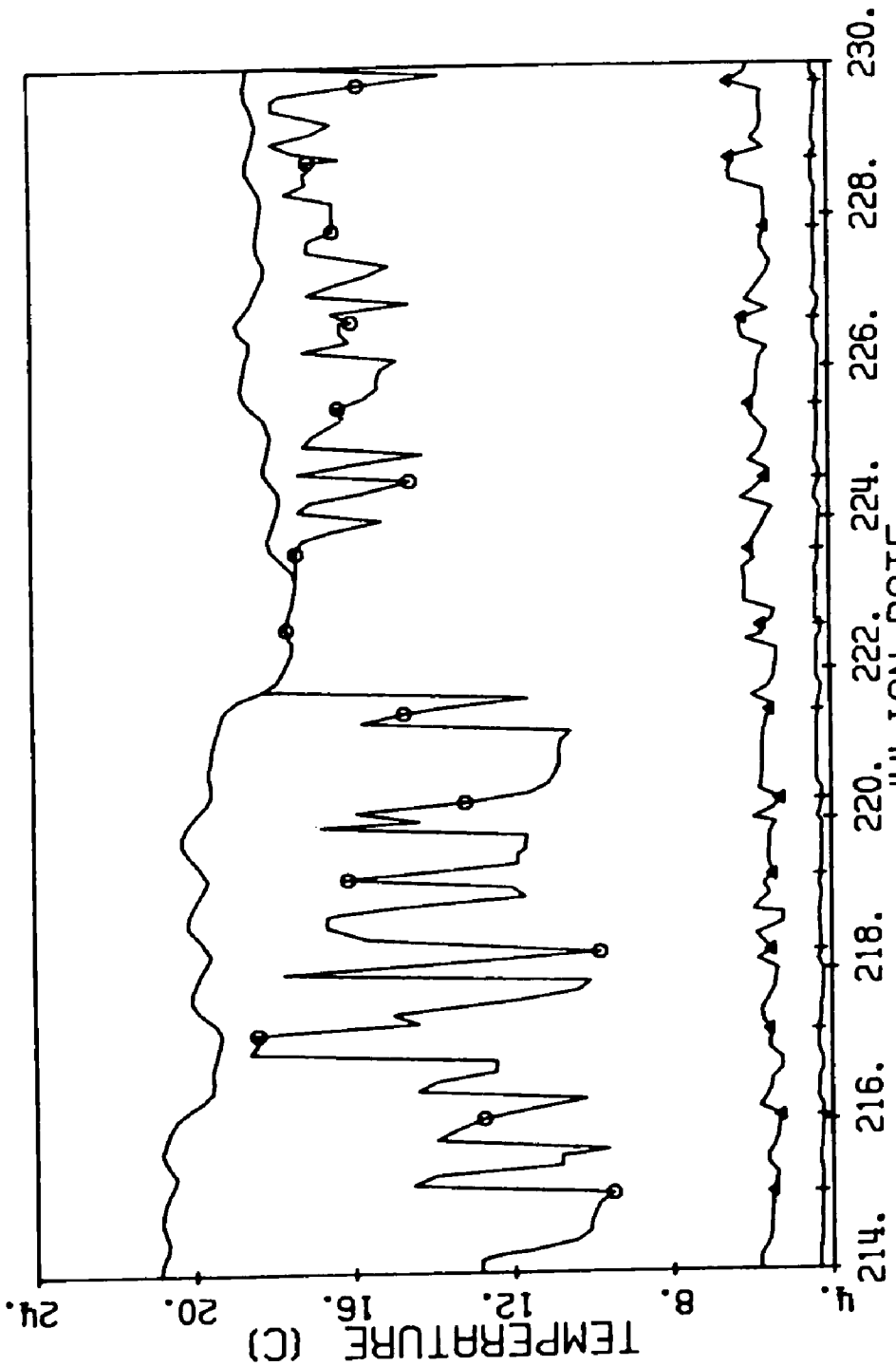

TEMPERATURE (C)
4.
8.
12.
16.
20.
24.
214.
216.
218.
220.
222.
224.
226.
228.
230.
JULIAN DATE

Fig. 8c. See 8a

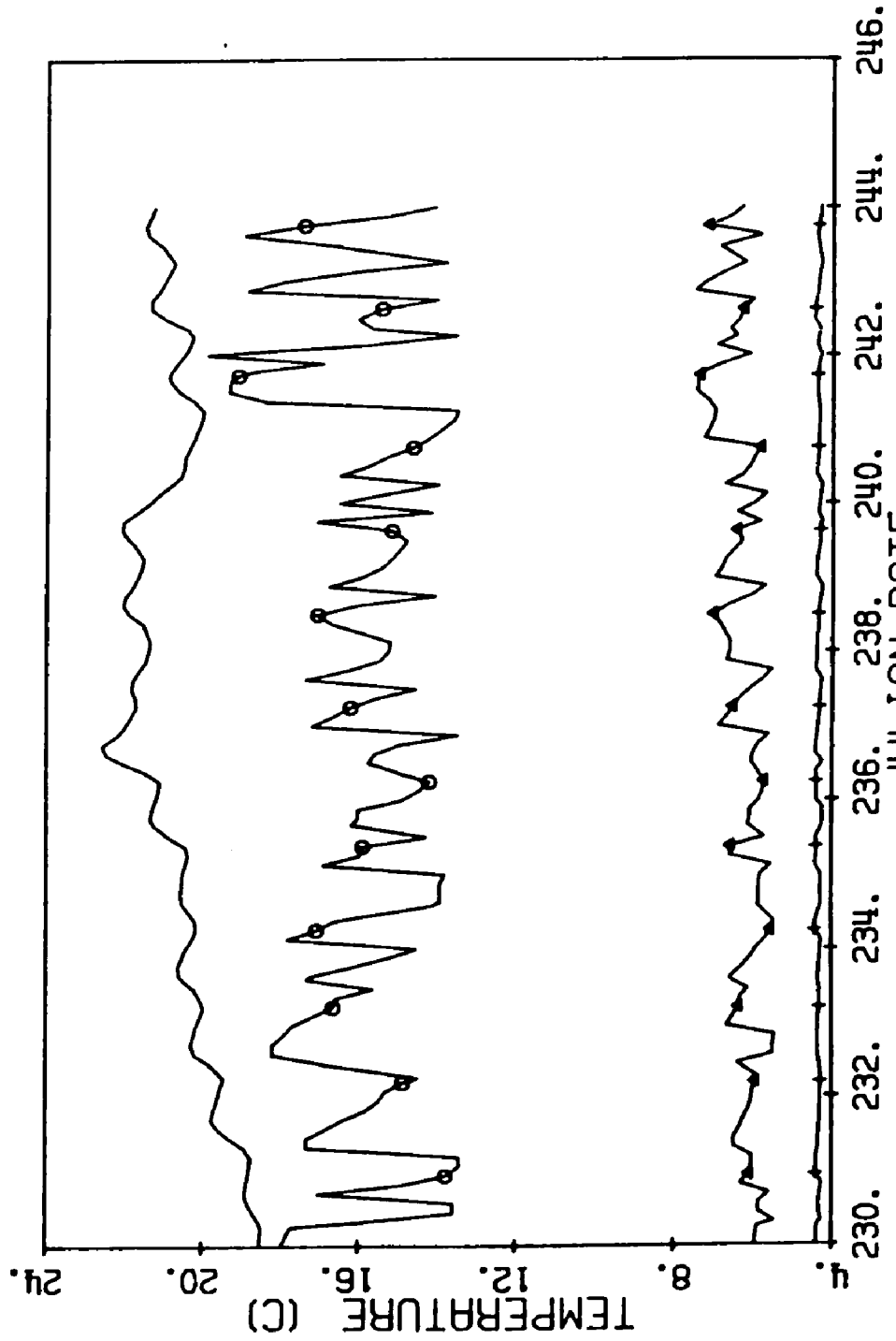

TEMPERATURE (C)
4.
8.
12.
16.
20.
24.
230.
232.
234.
236.
238.
240.
242.
244.
246.
JULIAN DATE

Fig. 8d. See 8a

$$\Delta z(t) = \frac{d-h(t)}{(M-1)}$$

where d, the mean depth, and M, the number of grid points, are constant.

In the month of October, a well defined mixed layer exists, which deepens from 20 to 35 m during the month. However the storm of Oct. 8-10 forces surface waters to the SE part of the lake, and unlike mid-summer, the thermocline does not return to a nearly level surface. Apparently the period of the internal seiche, greater under the reduced stratification of October, exceeds the time scale of variations in the wind field, and thus the thermocline assumes a fairly steady slope. Under these conditions, the one-dimensional assumptions of the model are called into question. It will be seen that the model still performs with reasonable facility in this case, although the predicted profiles do not approximate lake-wide mean profiles. Instead they are shown to approximate the vertical temperature distribution which would exist if isotherms were level, i.e., if there were no currents.

The surface conditions are shown in Fig. 9. As can be seen, most variations in the surface heat flux, S and B, are due to variations in B. These variations are negatively correlated with the wind speed and positively correlated with $T_a - T_l$.

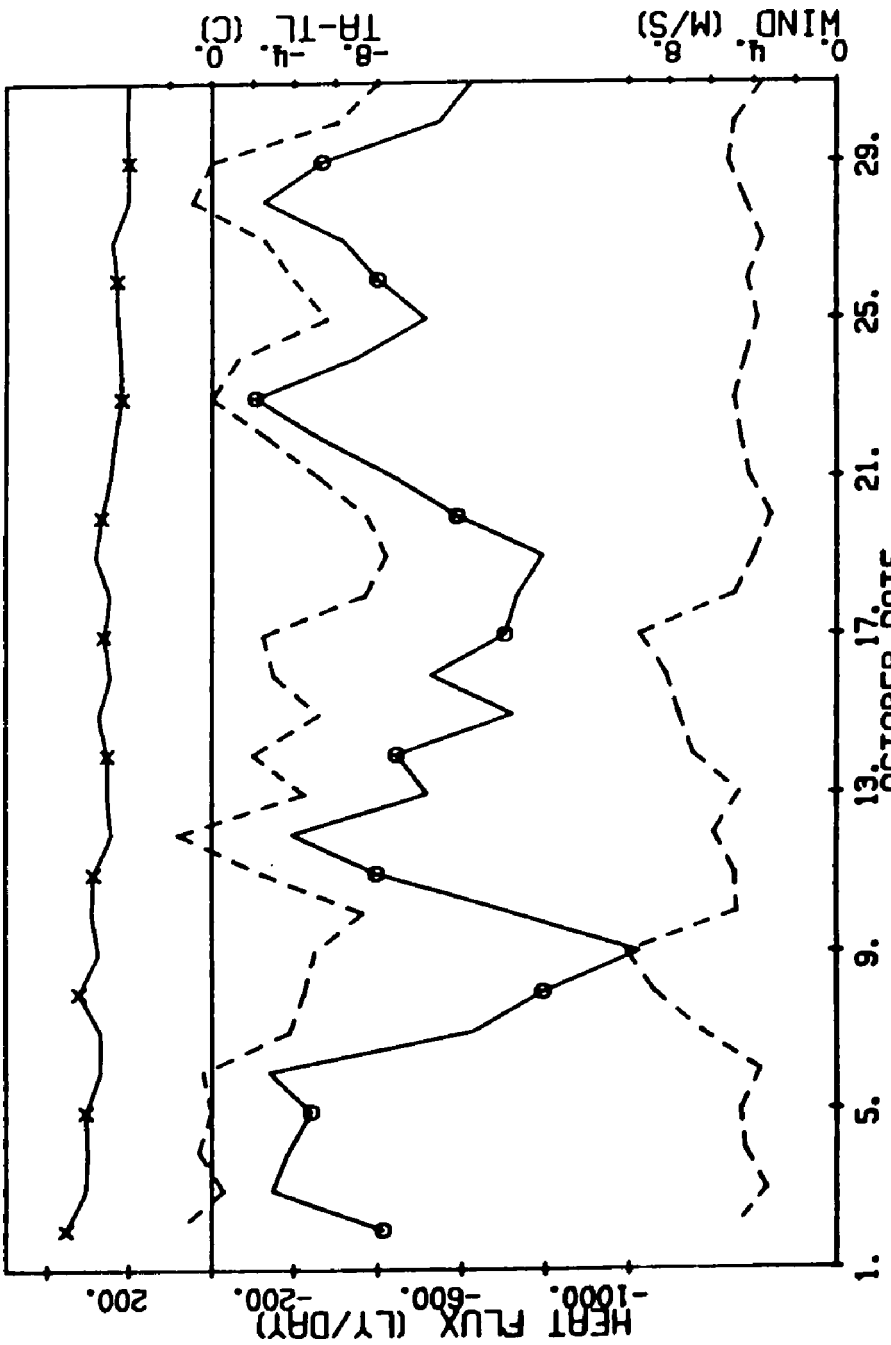


Fig. 9. Surface conditions, Lake Ontario, Oct. 1972, upper solid line is insolation, S*, lower solid line is surface heat loss, B*, both of which are model generated. The upper dashed line is air-lake temperature difference, T_a from PDCS observations while T_ℓ is model predicted. The lower dashed line is wind speed as observed by PDCS. All quantities are lakewide diurnal averages

Fig. 10 is a comparison of observed and predicted surface temperature. Their correlation is .988 for the month, .99 prior to the eleventh, .84 from Oct. 11-20 and .95 after the 21st. Again the upwelling is the probable culprit for the reduced predictive capability after the storm of the 8-10th. The root mean square deviation of predicted and observed surface temperatures is .47°C for the month of October, and only .13°C prior to the ninth.

Observations are less dense (spatially) in October than mid-summer. What is even more disturbing than their sparsity, is the bias toward the SE, downwelling, part of the lake after October 16. After this date, stations in Canadian waters only report temperature at the surface and 15 m; after the 20th only at 15 m. Complete vertical temperature profiles are available only from stations 16, 17, 20, 21, 23, and 26. Means constructed from the available observations are biased toward a downwelling part of the lake, where the mixed layer is ≈75 m deep. Nonetheless, the comparison between the predicted and mean temperature profiles is shown in Fig. 11.

It is difficult to eliminate this bias from the observations since there is relatively little information about the three dimensional temperature field in the lake during this period. 32-50 stationary sensors cannot tell you everything you want to know about the temperature of

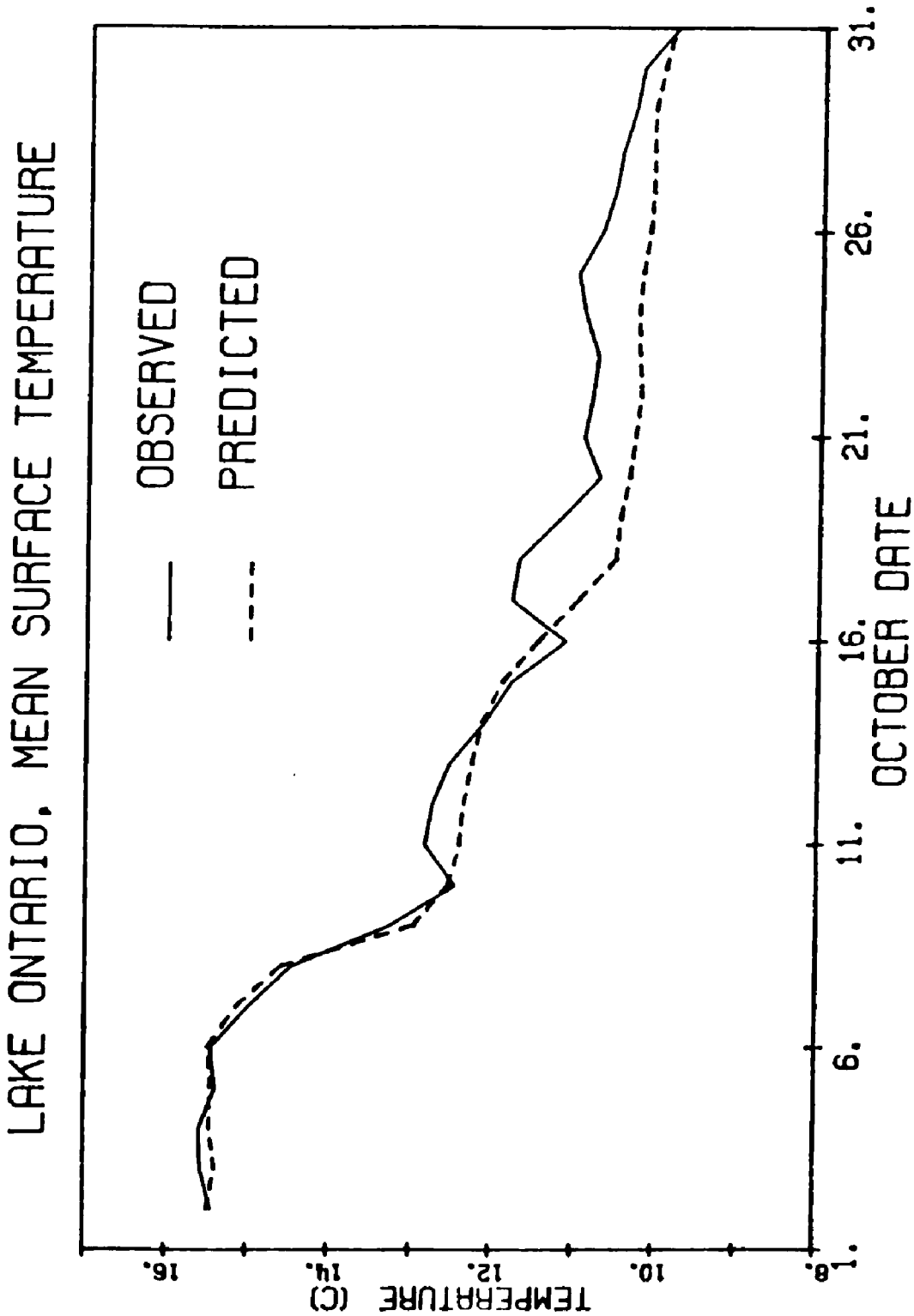


Fig. 10. Lake Ontario, Oct., 1972, mean surface temperature, lakewide diurnal average.

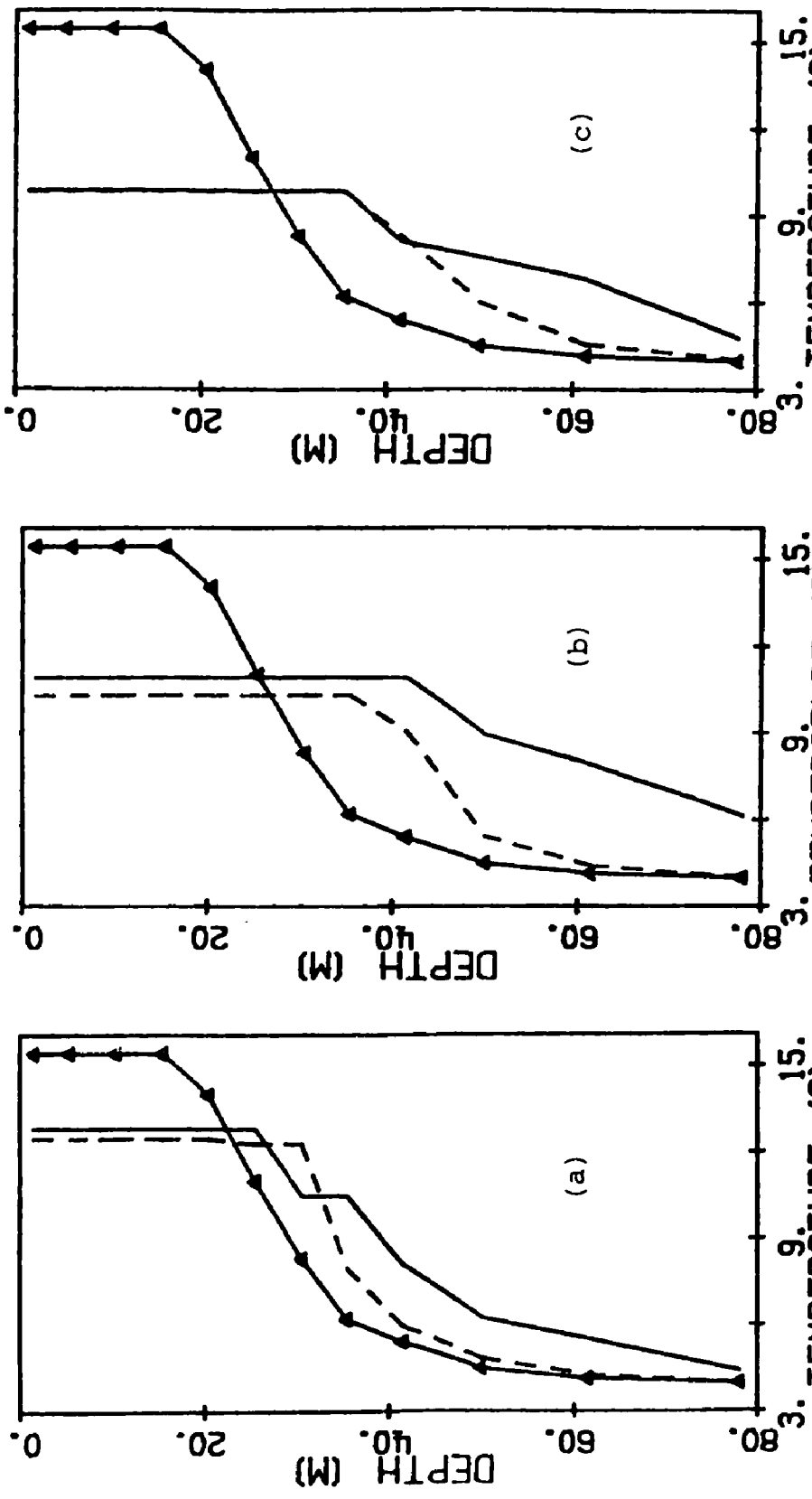


Fig. 11. Lake Ontario, mean temperature profiles, solid line with symbols is Oct. 1 (initial), solid line is observed and dashed is predicted for (a) Oct. 11, (b) Oct. 21 and (c) Oct. 31.

Lake Ontario. It is not possible to reconstruct an undisturbed temperature field (one for which isotherms and level surfaces coincide) from this data while conserving heat. Besides, such a temperature pattern would be quite unrealistic. On the other hand, the one-dimensional model is analogous to a cylindrical lake, having approximately the same shoreline as the real lake, but with a constant depth and horizontal isotherms. The three dimensional temperature distribution of this ideal lake is known, and hypothetical advection, accompanied by tilting of isotherms, can be accomplished while conserving heat. This is the procedure adopted here. The planar slope of a selected thermocline isotherm is estimated from the temperature observations by regression analysis. The corresponding isotherm is given the same slope in the ideal lake. All other isotherms are held parallel to the selected isotherm and their spacing is held constant. Then the ideal lake is sampled at the same locations as the observations reported, and an identically defined horizontal average is taken. Observations during this period were so sparse, that the slope of isotherms could be determined on only a few occasions, and the results of this analysis are shown in Figs. 12 and 13 which show the model profile, the observed mean profile, and the tilted model mean profile. Obviously, the correspondence is

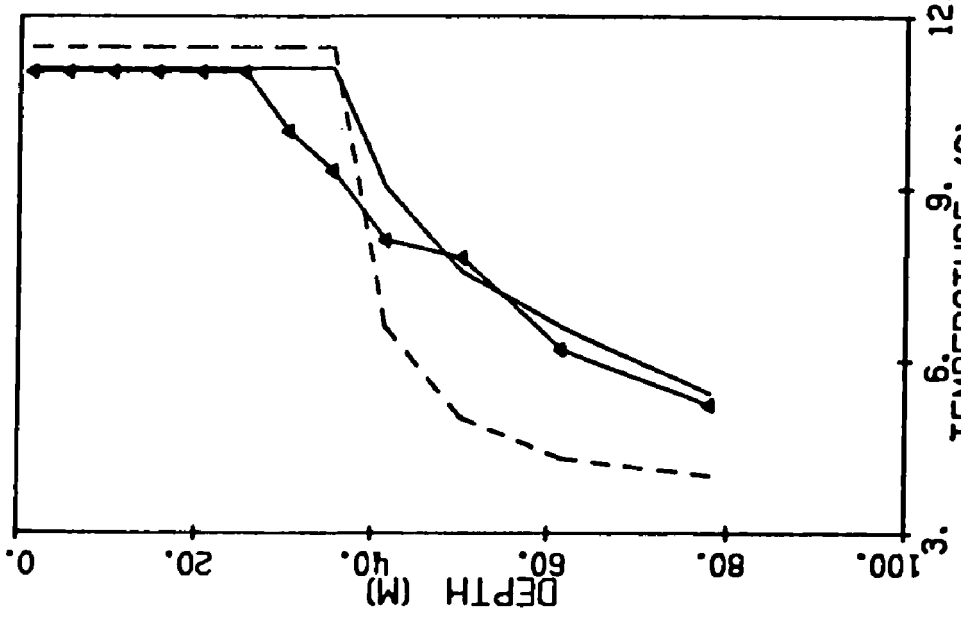


Fig. 12. Tilted model profile as discussed on p. 122 is solid line with symbols, solid line is observed mean profile and dashed line is untilted model profile for Oct. 16.

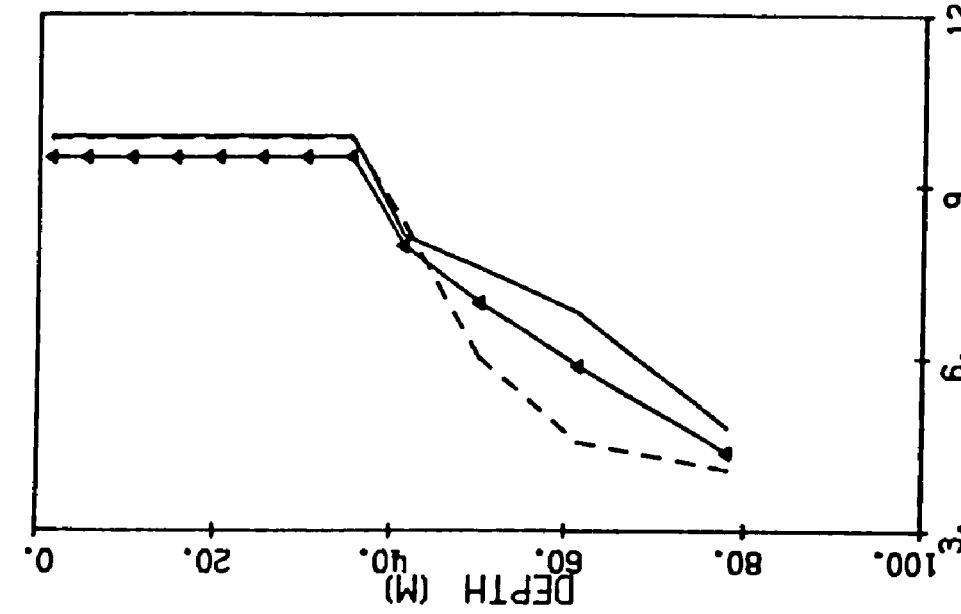


Fig. 13. Same as Fig. 12 for Oct. 31.

enhanced considerably by the procedure. The correlation between observed and predicted temperature changes from the initial profile at 12 depths is .945 (Oct. 16) and .980 (Oct. 31). After tilting the model, the correlations increase to .991 for Oct. 16 and .998 for Oct. 31.

This analysis is not intended to show that the model correctly predicts mean profiles during this month, for the "prediction" required knowledge of the actual temperature field. However, it does suggest that the undisturbed vertical temperature structure, i.e., the temperature profile expected if winds and currents vanished, is correctly modeled. This in turn implies that diffusive processes are adequately simulated while, obviously, advective processes are not.

Short term variations of the model are depicted in Fig. 14 showing the temperature vs. time at the surface, z=-15, -30, -60m.

Llyn Cwellyn. To demonstrate the validity of the model for lakes of varying surface area, the model was used to simulate the variation of T(z) in Llyn Cwellyn, a small lake (area = 1 km^2, mean depth = 18 m) in Wales. The input data is taken from Darbyshire and Colclough (1972) and covers a one day period, June 1, 1966, during which strong winds effected significant changes in the thermal structure of the lake. At 7 a.m., local time, the temperature profile was nearly linear from z=-1m to

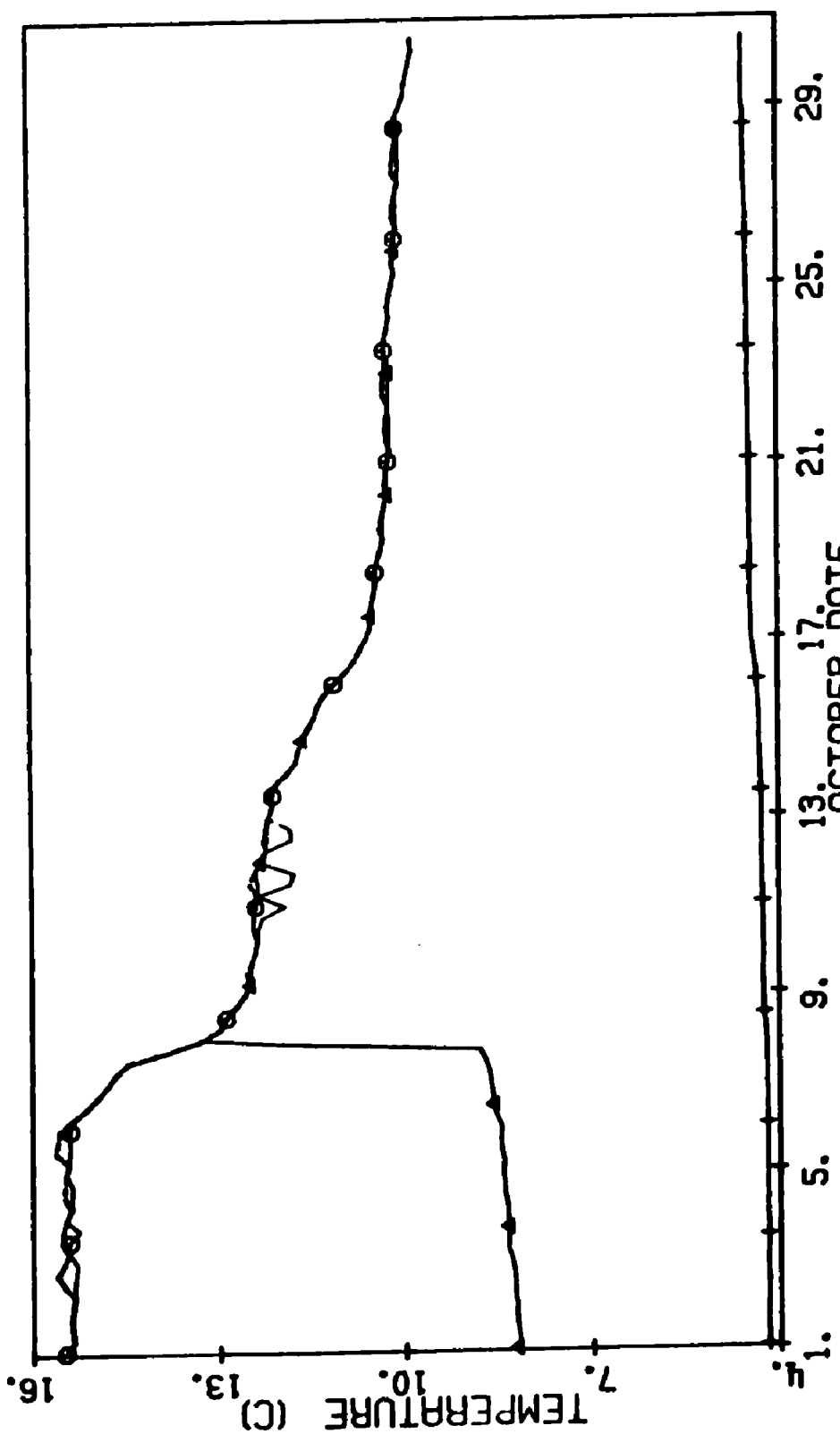


Fig. 14. Lake Ontario, Oct., 1972, model predicted T vs. t at four depths. Upper dashed line (without symbols) is T_s, line with circles is T(-15m), line with triangles is T(-30m), bottom line with crosses is T(-60m). Note entrainment of 30m water into mixed layer on Oct. 8. The diurnal component prominent in Fig. 8 is nearly absent here.

z=-14m, but by 6 p.m. a well mixed layer of depth, h=7m, was established atop a well defined thermocline. Temperature observations were made at one location only, site of the buoy shown in Fig. 15. Air temperatures were obtained at the same location while wind speeds were measured at the anemometer site. Because observations of water temperature were taken at one location only, advective heat fluxes cannot be averaged out, and some estimate of their magnitude must be made. Advective fluxes are relatively small, as noted by Darbyshire and Colclough (1972) and consequently this case was chosen for verification of the model. One way to discern advective heat fluxes is to examine the enthalpy of the column for anomalous changes, i.e. changes unrelated to the surface heat flux. Fig. 16 is a plot of the change of enthalpy from the initial state (hour 6) of the observed fluid column, and the surface heat flux computed by the bulk transfer formulae and radiation formula of Chapter 4. As no observations of atmospheric humidity are presented by Darbyshire and Colclough, it was assumed that the relative humidity was .9. This high value was used because of the proximity of the lake to the Atlantic Ocean from which the winds were blowing. As can be seen in Fig. 16 the rate of change of enthalpy of the sampled column corresponds closely to surface heating rate up to

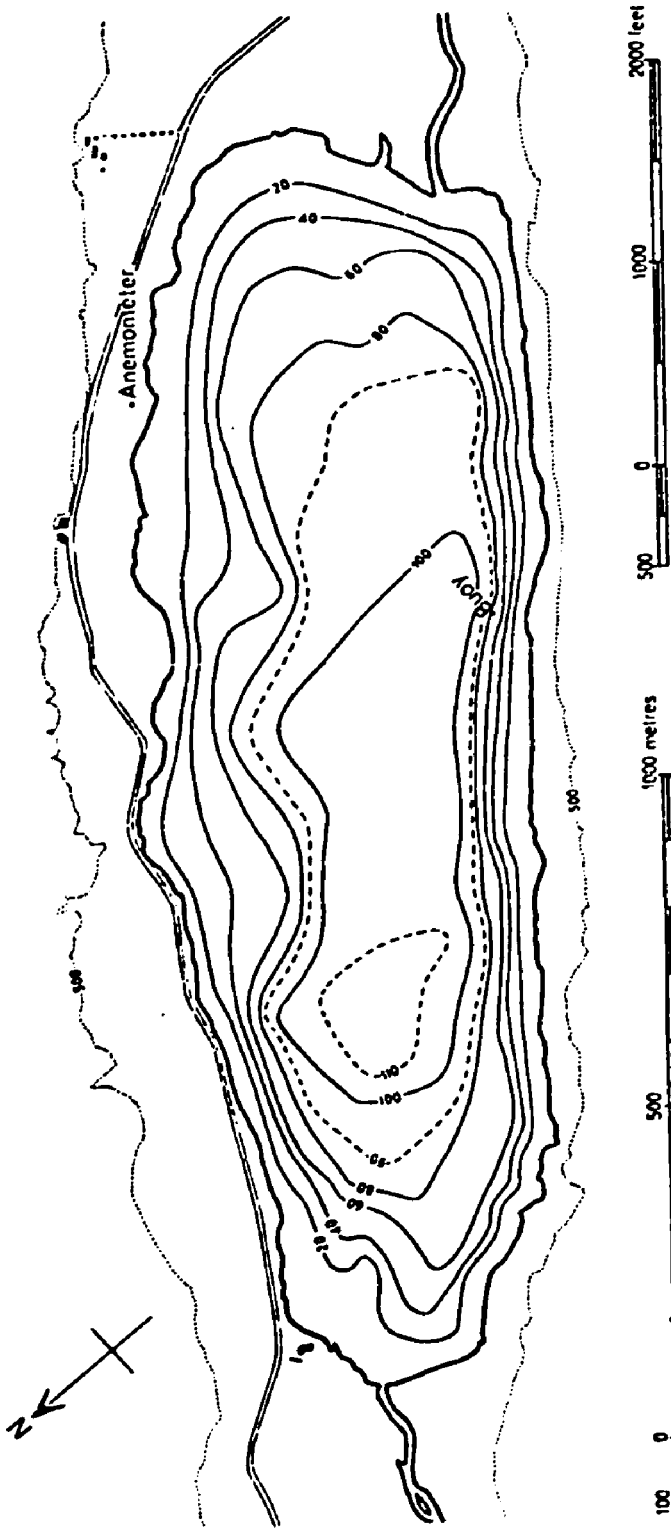


Fig. 15. Map of Llyn Cwellyn, Wales, contours in feet, reprinted from Darbyshire and Edwards, 1972.

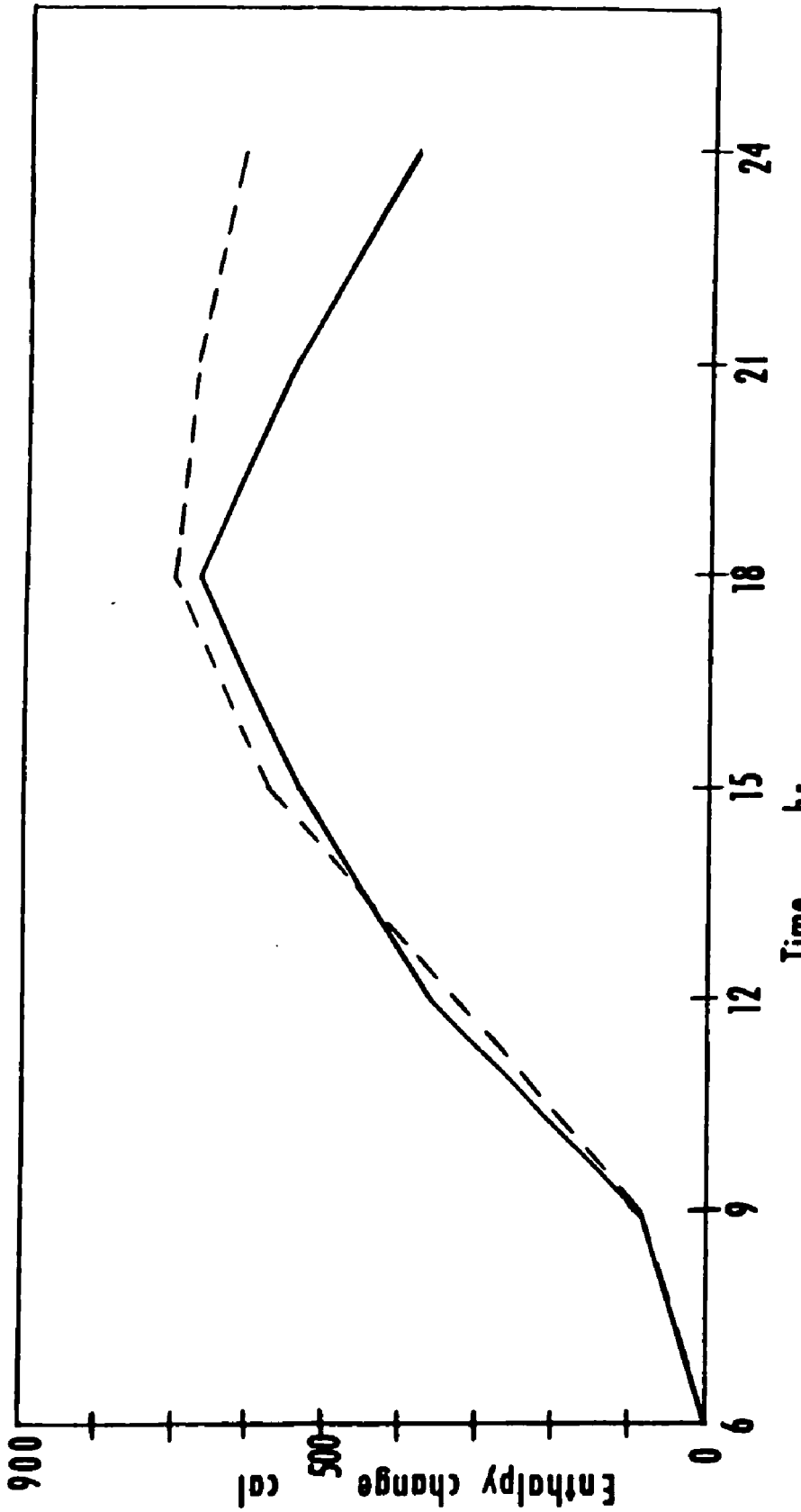


Fig. 16. Enthalpy change per cm^2 in Llyn Cwellyn, June 1, 1966. Solid line is calculated from temperature profiles; dashed line based on computed surface flux.

hour 21. The large enthalpy change of -1.1×10^{-2} cal cm^{-2} sec^{-1} from hour 18 to hour 21 cannot be explained in terms of the surface heat flux alone. The difference between the observed enthalpy change and estimated surface heat loss is 8×10^{-3} cal $cm^{-2} sec^{-1}$ and probably represents an advective flux. A progression of observed and predicted temperature profiles at three hour intervals beginning at hour 6 is shown in Fig. 17. Correlation of observed and predicted temperature changes from the initial (6 a.m.) profile is given in Table 5. The

Table 5. Statistics on Llyn Cwellyn Verification Run

Hour	root mean square deviation (°C)	correlation of temperature changes
9	.1	.54
12	.3	.56
15	.4	.74
18	.3	.94
21	.8	.17
24	1.0	-.18

agreement is good prior to the large advective heat loss around hour 21.

The demonstrated simulation of observed temperature changes in a large and small lake is evidence of the

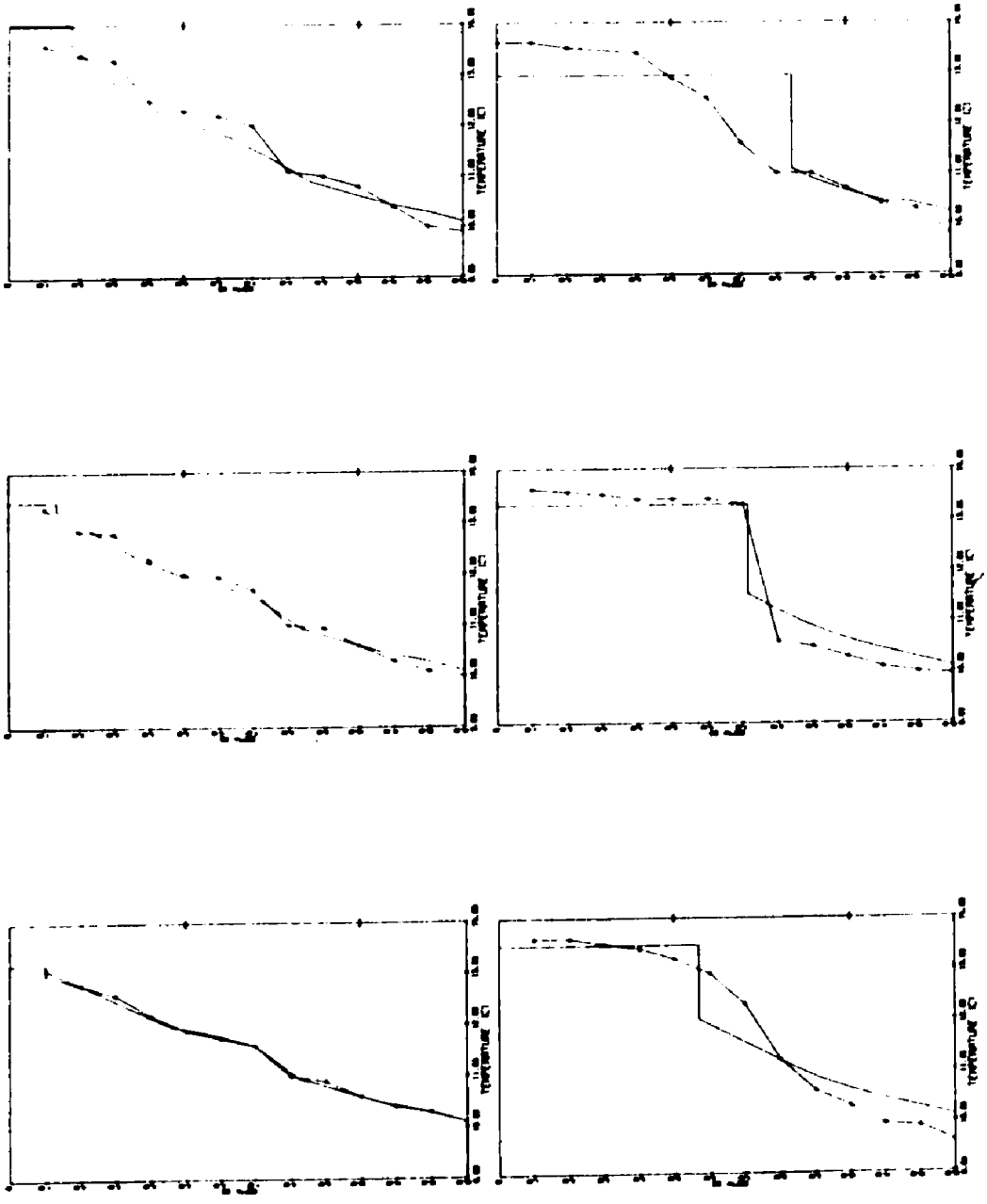


Fig. 17. Llyn Cwellyn temperature profiles, June 1, 1966. Line with symbols at 1 m intervals is as observed by Edwards and Colclough (1973); other line is model predicted. Upper left is hr 6, subsequent graphs at 3 hr intervals. Abscissa is T from 9 to 14 °C. ordinate is z from -13 to 0 m.

utility of the model. Basic model parameters were identical for the three simulations reported in this chapter.

CHAPTER VII

MODEL SENSITIVITY STUDIES

A complementary experiment to the verification results presented in Chapter 6 is one in which the sensitivity of the thermocline model to variations in environmental conditions and basic model parameters is investigated. The model parameter values have been estimated from independent observations with varying degrees of precision. The sensitivity study should indicate a range of parameter values for which the model may adequately simulate the vertical temperature distribution of lakes.

The numerical experiments consist of four day simulations of the formation of a wind-mixed layer from an initially linear profile. All environmental conditions are held constant throughout the period of integration, except for solar radiation which varies over its typical diurnal cycle. A number of simulations are presented, each having the same conditions as a basic reference simulation, but with one variable altered. The surface heat loss is not computed by bulk transfer formulae, but is specified and constant. Thus, a change in wind speed or surface temperature will not alter the surface heat flux. With this constraint, the perturbed cases are more readily compared with the reference.

The reference simulation, for which all model parameter values are identical to the version verified in Chapter 6, will be described in detail. Then the simulations in which one variable is perturbed will be compared with the reference.

For the reference simulation, and all others described in this chapter, the initial temperature distribution is

$T = 15°C,\ z > -1m$

$T = (.1(z+d)+4.)°C,\ -d < z < -1$

where d, the mean depth, is 101 m and z is given in meters.

The profile is linear below 1 m, with a 1° jump at z=-1 m, T_s=15°C, T_h=14°C, h=1 m. A perfectly linear profile is not possible since the model requires that a mixed layer exist, and the 1° jump at z=-1 m allows a convenient initial time step. This initial profile exhibits a Brunt-Vaisala frequency, $N \simeq 10^{-2} sec^{-1}$.

The reference lake has a circular shoreline and a surface area of $10^2 km^2$. The latitude of the lake is 40°N, and the starting date is July 13.

The constant surface heat loss is chosen such that, over the period of simulation, t_{end},

$$\int_o^{t_{end}} B dt = -\frac{1}{2}\int_o^{t_{end}} s dt \ .$$

Consequently the lake is gaining heat. Given the latitude, date, and atmospheric transmission coefficient, P=.80, this condition is met if $B^*=.00455$ cal/cm^{2}sec.

The solar attenuation coefficient, β, for the reference simulation is .01 cm^{-1}. The ratio of wave mixed layer depth to the significant wave height is, as in the results presented in Chapter 6, a=2. The constants relating dissipation rate to velocity and length scales are as given in Chapter 4, as is the ratio $\frac{\tau_w}{\tau_o}=.8$. The constant wind speed at 3 m is 10 m/sec.

The relatively large wind speed, the short time scale of the integration, and the relatively large initial temperature gradient makes the experiment roughly analogous to laboratory experiments of the deepening of a mixed layer in a stratified fluid stirred from above, as, e.g., the experiments of Linden (1975). One might expect that changes in the mechanical energy budget will dominate over variations in the thermal energy balance. Changes in the surface heat flux should have a more pronounced effect over a longer period of integration. Also, it is expected, because of the large value of N, that buoyancy, not rotation, will limit turbulent length scales.

The final profile of the four day integration for the reference state yields a surface temperature of 12.6°C,

and a mixed layer depth of about 35 m. The complete profile is shown as the solid line in Figs. 18-24.

In the first experiment to be discussed, Fig. 18, the perturbed parameter is β, the attenuation coefficient for solar radiation. The perturbed values of β are .001 cm^{-1} and .05 cm^{-1} compared with β=.01 cm^{-1} in the reference state. This range in β is roughly the maximum range observed in lakes. The difference in the final profiles for β=.05 cm^{-1} and .01 cm^{-1} is nearly imperceptible. Independence of β in this range is reasonable since 99% of the surface radiation flux is absorbed in the upper 4.6 m for β=.01 cm^{-1}, in the upper .9 m for β=.05 cm^{-1}. Solar heating is restricted to the upper part of the mixed layer for either of these cases. For β=.001 cm^{-1}, the final surface temperature is .25°C cooler that the reference, and the final mixed layer depth is 3.5 m deeper than the reference. For β=.001 cm^{-1}, the radiant intensity is 3% of the surface intensity at a depth of 35 m. Consequently a small, but significant fraction of the surface solar flux penetrates the mixed layer. Less kinetic energy is required to mix the absorbed heat throughout the mixed layer because of its more uniform distribution. Nonetheless, the effects of variations in the optical characteristics of lakes is not pronounced on the storm event time scale. Over a long term integration, especially from an isothermal distribution, the

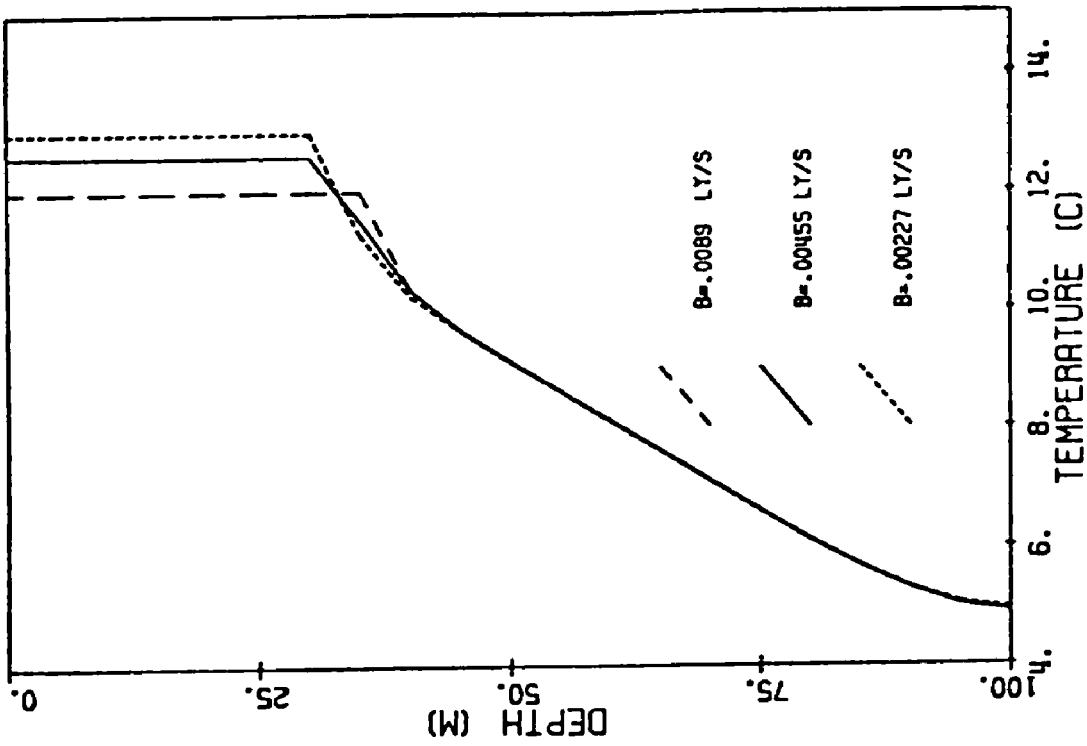


Fig. 19. Model sensitivity to perturbation of B. Final profiles after 4 day simulation.

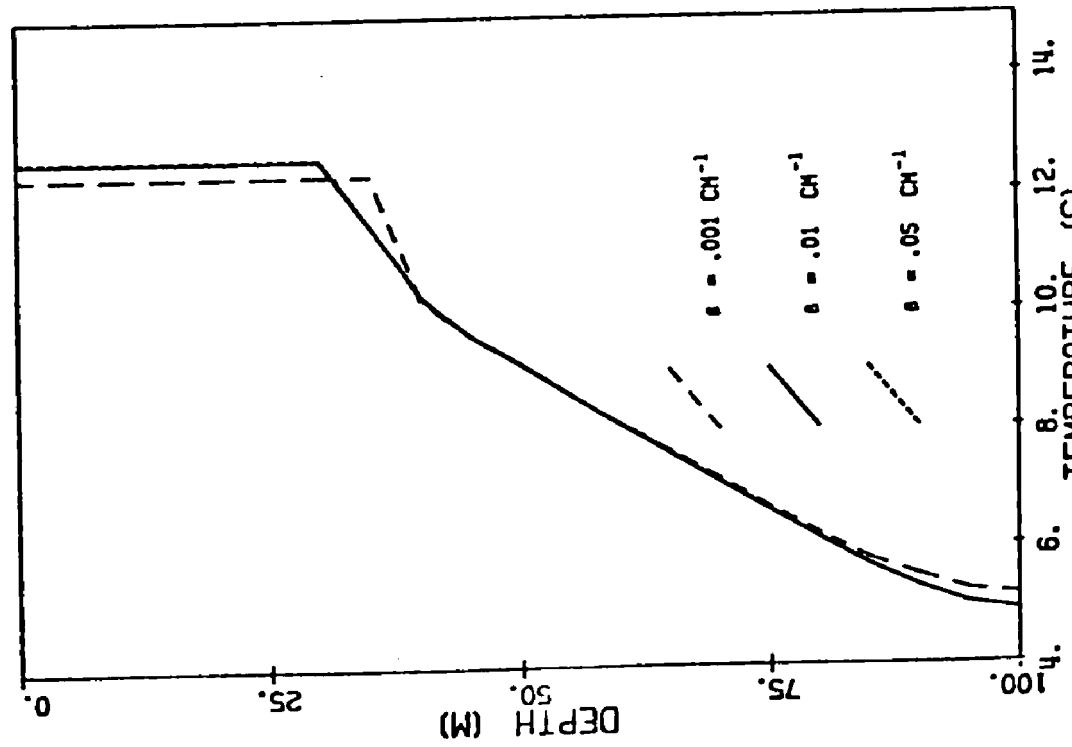


Fig. 18. Model sensitivity to perturbation of β. Final profiles after 4 day simulation.

effects may be more pronounced. The low sensitivity to perturbations of β on this time scale justifies the assumption, $\beta=.01$ cm^{-1}, used for the Llyn Cwellyn simulation presented in Chapter 6, for which no observations of β were available.

The second experiment, for which the final profiles are shown in Fig. 19, considers the response to variations in the surface heat loss, B*. The three profiles presented are for B*=.00227, .00445, .0089 (cal/cm^2 sec). For the first case the four day solar heat input is approximately four times the surface heat loss, and for the third case the heat flux integrals have the same magnitude, implying no net heating. The final profiles exhibit similar mixed layer depths, with a difference of only 3 m between the two extremes. Surface temperature variation is more pronounced, resulting primarily from the different heat inputs to the mixed layer. The relatively constant mixed layer depths indicate that, on the storm event time scale, variations in the surface heat loss, and consequently errors in the bulk transfer formulae, have negligible effects on the mixing characteristics of a lake, and should affect only the surface temperature. The excellent predictions of surface temperature argue for the accuracy of the bulk transfer formulae used to compute B*.

The model dependence on latitude, as it affects the Coriolis parameter, was investigated by moving the lake to 60°N and 20°N. To eliminate solar radiation variations, the starting date was changed to June 21 and July 25, respectively. For the run at 60°N, the atmospheric transmission coefficient was increased from .8 to .86. Under these transformations the four day totals of solar radiation input closely approximated the reference simulation. The results of this experiment are not shown, because the final profiles are virtually identical to the final reference profile. Under the conditions considered here the response is independent of latitude. This probably will not hold in all situations. The interaction of turbulence with stratification, and the influence of the earth's rotation on turbulence can be conceptualized as processes by which the length scales of turbulent eddies are limited to some maximum, ℓ_b, by buoyancy, and ℓ_r, by rotation. The independence of these results on latitude indicates that $\ell_b < \ell_r$, and the buoyancy alone limits turbulence scales. If the stratification were less pronounced ($N << 10^{-2}$), or if the mixed layer deepened even further (such that $h \gtrsim \delta_e$), the limiting effects of the Coriolis acceleration might become apparent.

The sensitivity to changes in lake surface area is exhibited in Fig. 20, showing the final profiles generated for lake surface areas of 1, 10^2, 10^4 (km^2).

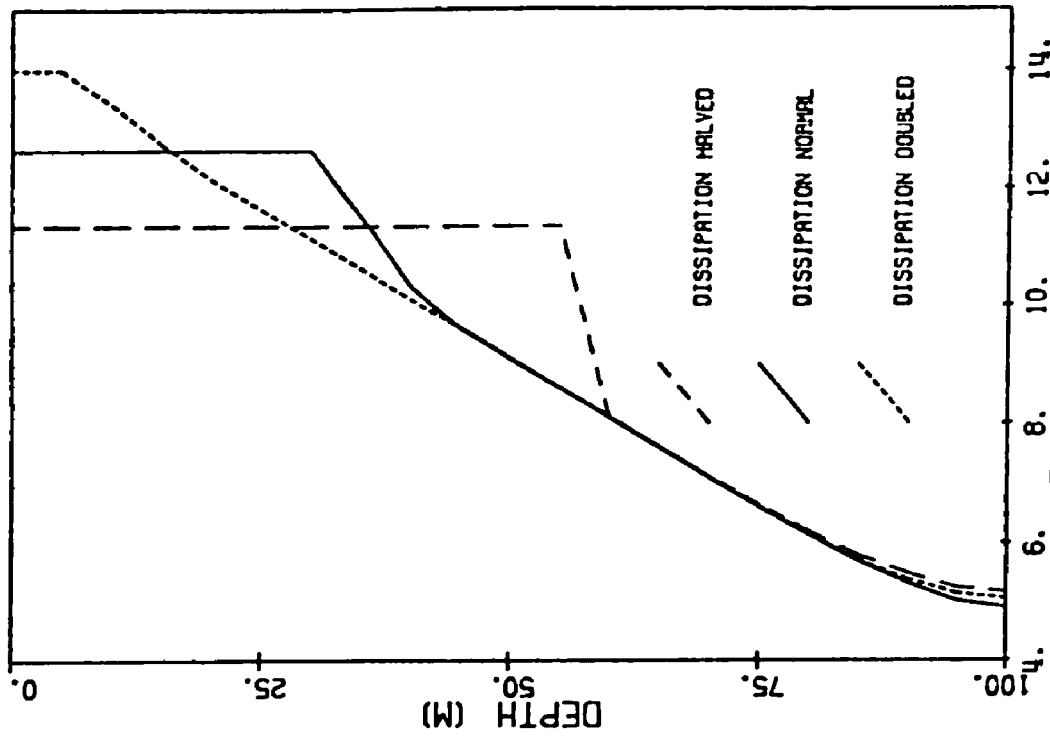


Fig. 21. Model sensitivity to perturbation of the dissipation rate. Final profiles after 4 day simulation.

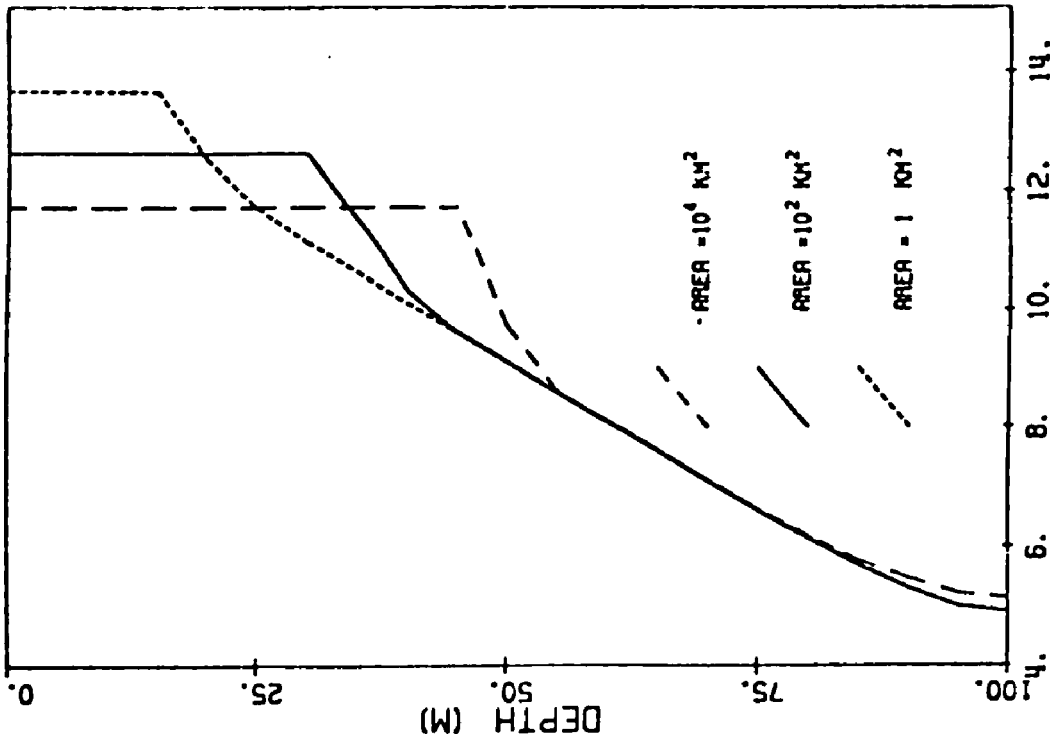


Fig. 20. Model sensitivity to changes in lake surface area. Final profiles after 4 day simulation.

The surface area of Llyn Cwellyn is 1 km^2 while Lake Ontario's surface area is $1.8x10^4 km^2$. Deviations from observed profiles for the verification experiments of Chapter 6 are much smaller than the differences shown in Fig. 20. This indicates that turbulent mixing in lakes is significantly dependent on the surface area, and that the lake thermocline model simulates the magnitude of this dependence correctly. This is a strong indication that turbulence caused by breaking waves is substantially responsible for this fetch dependence. The detailed mechanism presented herein, i.e., restriction of wave action to the wave mixed layer, is not necessarily verified. An alternate mechanism may involve feeding of wave energy to the mean flow, thus promoting shear instability at the bottom of the mixed layer. This alternate mechanism cannot be investigated within the context of this model.

Fig. 21 shows the response of the model to changes in the dissipation terms, D^*_s and D^*_c. For the reference simulation these are computed as outlined in Chapter 4. Two other simulations were also made in which the dissipation was doubled and halved, respectively. The differences are quite pronounced, indicating that alternate dissipation assumptions would not allow adequate simulation of lake conditions.

The two least well known model parameters are the ratio, a, of wave mixed layer depth to significant wave

height and the ratio, $\frac{\tau_w}{\tau_o}$, of momentum flux to waves and the total surface stress. "a" is defined only in the context of the model and has not been directly observed. However, upper and lower bounds of "a" have been observed, $1<a<4$. Estimates of $\frac{\tau_w}{\tau_o}$ have been made by various investigators, notably Dobson ($\frac{\tau_w}{\tau_o}=.9$; 1971) and Hasselmann ($0.5\leq\frac{\tau_w}{\tau_o}\leq 1.0$; 1974), but these studies are not conclusive. The values $a=2$, $\frac{\tau_w}{\tau_o}=.8$ have been used in the verification experiments of Chapter 6 and for the reference simulation. Figs. 22-23 show the final profiles for

$$\frac{\tau_w}{\tau_o} = .8 \qquad a = \begin{cases} 1. \\ 2. \\ 3. \end{cases} \qquad \text{(Fig. 22)}$$

and for

$$a = 2. \qquad \frac{\tau_w}{\tau_o} = \begin{cases} .4 \\ .6 \\ .8 \\ .9 \end{cases} \qquad \text{(Fig. 23)}$$

If the momentum flux to waves is larger than $.8\tau_o$, the energy flux to the waves, $\tau_w c$ is also increased. Then the loss of energy to turbulence by the waves, modeled here by the parameter, a, must be greater in order that the growth of wave energy is similar to that observed. The importance of wave mixing vis-a-vis shear flow turbulence should increase with $\frac{\tau_w}{\tau_o}$. This physical dependence provides a consistent scenario by which the model can accomodate expected improvements in our knowledge of $\frac{\tau_w}{\tau_o}$.

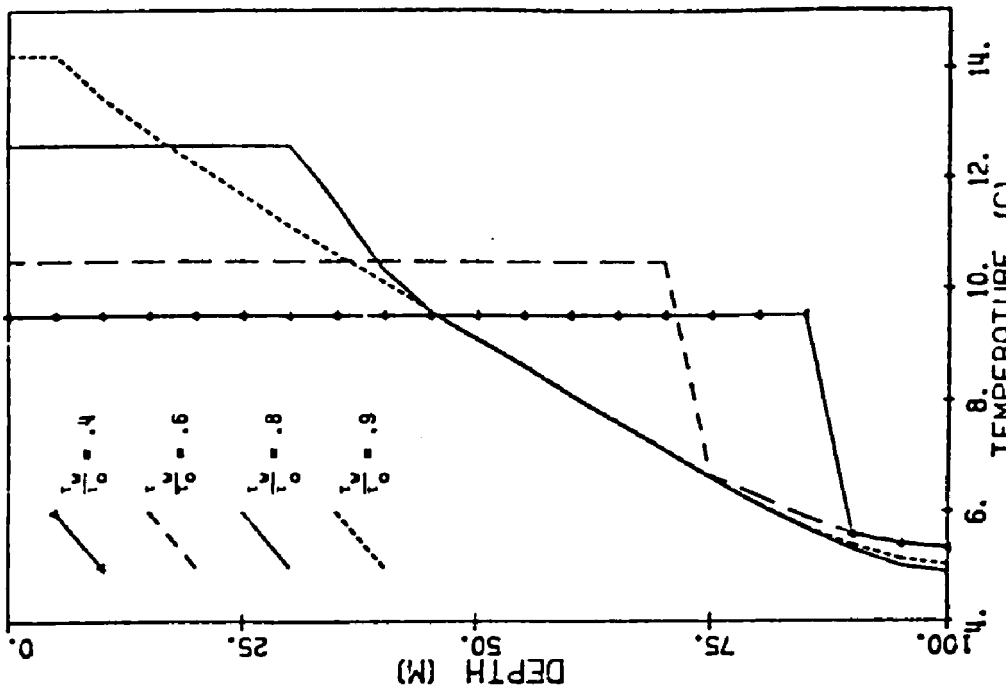


Fig. 22. Model sensitivity to perturbation of the ratio of wave mixed layer depth to significant wave height, a. Final profiles after 4 day simulation.

Fig. 23. Model sensitivity to perturbation of τ_w/τ_o. Final profiles after 4 day simulation.

"a" may be considered a dependent variable of $\frac{\tau_w}{\tau_o}$, such that for any value of $\frac{\tau_w}{\tau_o}$, $0<\frac{\tau_w}{\tau_o}<1$, a value of "a" can be found which allows adequate simulation of observed conditions. The known bounds of "a", $1<a<4$, provide bounds on $\frac{\tau_w}{\tau_o}$ which are acceptable to the model and physically realizable. One day simulations (not shown) indicate these limits are $.7\leq\frac{\tau_w}{\tau_o}\leq.9$. This is the range of $\frac{\tau_w}{\tau_o}$ for which values of "a", $1<a<4$, may be found which force the mixed layer to the same depth as the reference simulation. Whether these limits have a physical significance is unclear and depends on the correspondence of the model to the physical system. It is the author's opinion that this is a realistic model of the physical system. Evidence of verification, as presented in Chapter 6, is often suspect as evidence of model realism if (1) the model is insensitive to significant variations in parameters known to have some influence, or (2) parameter values must be chosen which are not consistent with independent estimates of the parameters. The extreme sensitivity to perturbations of $\frac{\tau_w}{\tau_o}$, and D* belies the notion that just any reasonable model, or set of parameter values, affords adequate simulation of lake temperature changes. In this case, only physically sensible values, either observed or within observed limits, produce correct results.

Fig. 24 demonstrates the dependence of the model response on wind speed. The speed was constant over the four day simulation for each case, and U_3=5, 10, 15 (m/sec) respectively. Note that increased hypolimnion diffusion for U_3= 15 m/sec pumps a considerable amount of heat into the hypolimnion.

Variations of $\frac{\tau_w}{\tau_o}$, a, D* and fetch within reasonable limits are seen to have similar effects to a change in U_3 of 10 m/sec. The pronounced differences in response, coupled with the evidence of verification presented in Chapter 6, indicate that the chosen values of these parameters are either correct or have errors causing offsetting responses of similar magnitude. If only one parameter was in error by an amount comparable to the variations considered here, the model would fail to simulate observed conditions.

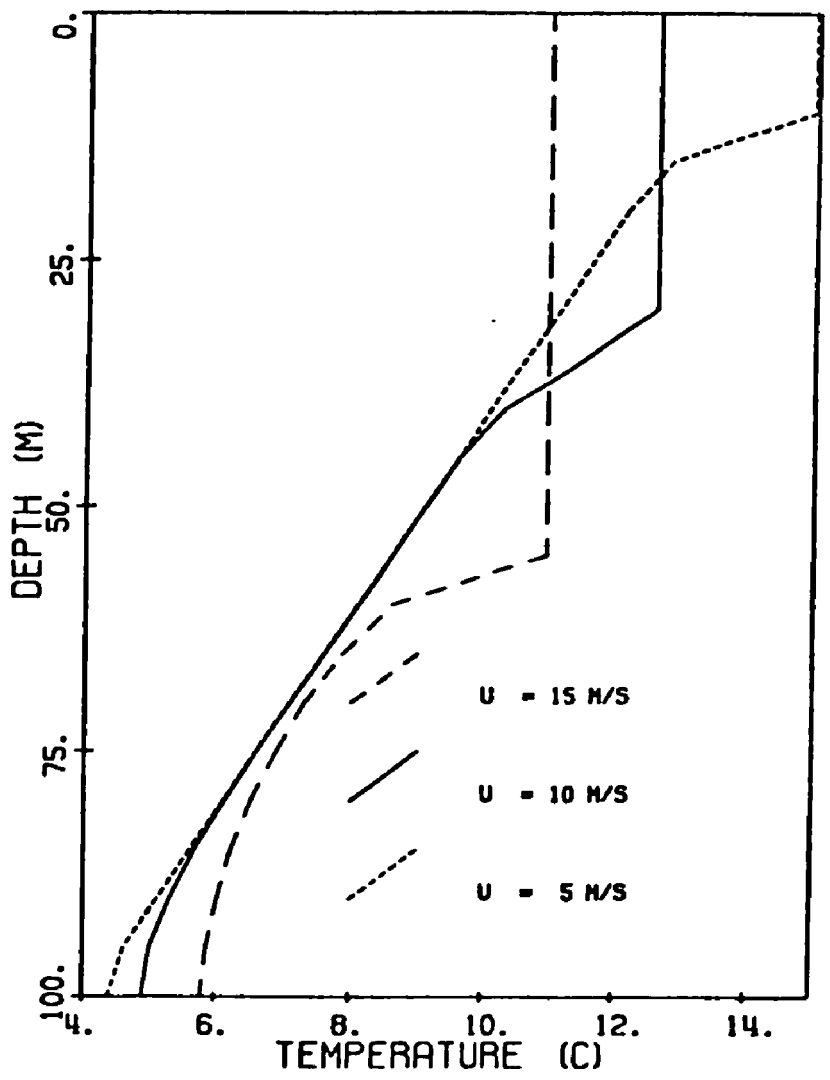


Fig. 24. Model sensitivity to changes in the wind speed at 3 m. Final profiles after 4 day simulation.

CHAPTER VIII

APPLICATIONS

The most likely potential use of the model is as the temperature predicting component of an ecological model. Ecological models of lakes are currently limited to one-dimensional or two-layer "box" models and as such require no more information of the temperature field than that supplied by this model. Indeed, the modelling of diffusive processes controlling various chemical and biological species can be built upon the principles of this work by specifying a homogeneous surface layer, communication between epilimnion and hypolimnion by entrainment, and turbulent diffusion below the epilimnion as specified in Chapter 4. To illustrate the procedure for building such a model, a simple procedure for predicting the vertical distribution of dissolved oxygen, O_2, in Lake Ontario will be presented.

The concentration of O_2 in the epilimnion is assumed to be the saturation concentration for pure water in equilibrium with a standard atmosphere. A quadratic polynomial for $O_2(T_s)$ has been constructed from a table of saturation concentration vs. T_s given by Hutchinson (1957). The O_2 concentration $(\frac{mg}{l})$ is assumed to be continuous at z=-h. Below z=-h, the concentration is assumed to obey

$$\frac{\partial O_2}{\partial t} = K_z \frac{\partial^2 O_2}{\partial z^2} - R;\ O_2 = O_2(T_s),\ z=-h;\ \frac{\partial O_2}{\partial z} = \frac{F_s}{K_z},\ z=-d$$

where R is the rate of oxygen consumption in the free water, and F_s is the flux of oxygen to the sediments. In this study R and F_s are assumed to be constants. For a complete ecological model, complex functions of biochemical oxygen demand could be substituted.

The model of O_2 has been used to simulate the changes of the vertical distribution of O_2 in Lake Ontario in July and August in conjunction with the simulation of the lake temperature structure for the same period. Fig. 25 shows the initial profile of July 1 and the observed and predicted profiles of Aug. 31. Considering the simplicity of the dissolved oxygen model, the correspondence is gratifying.

The implications of the turbulent entrainment process for ecological models may be quite significant. During the summer stratification period, vertical profiles of nutrients generally show a strong negative gradient near z=-h. At the onset of strong winds, entrainment of this nutrient rich water into the epilimnion causes a rapid increase in epilimnetic nutrient concentrations and subsequent increases in phytoplankton production.

As shown in Chapter 6, the surface temperatures predicted by this model are in excellent agreement with

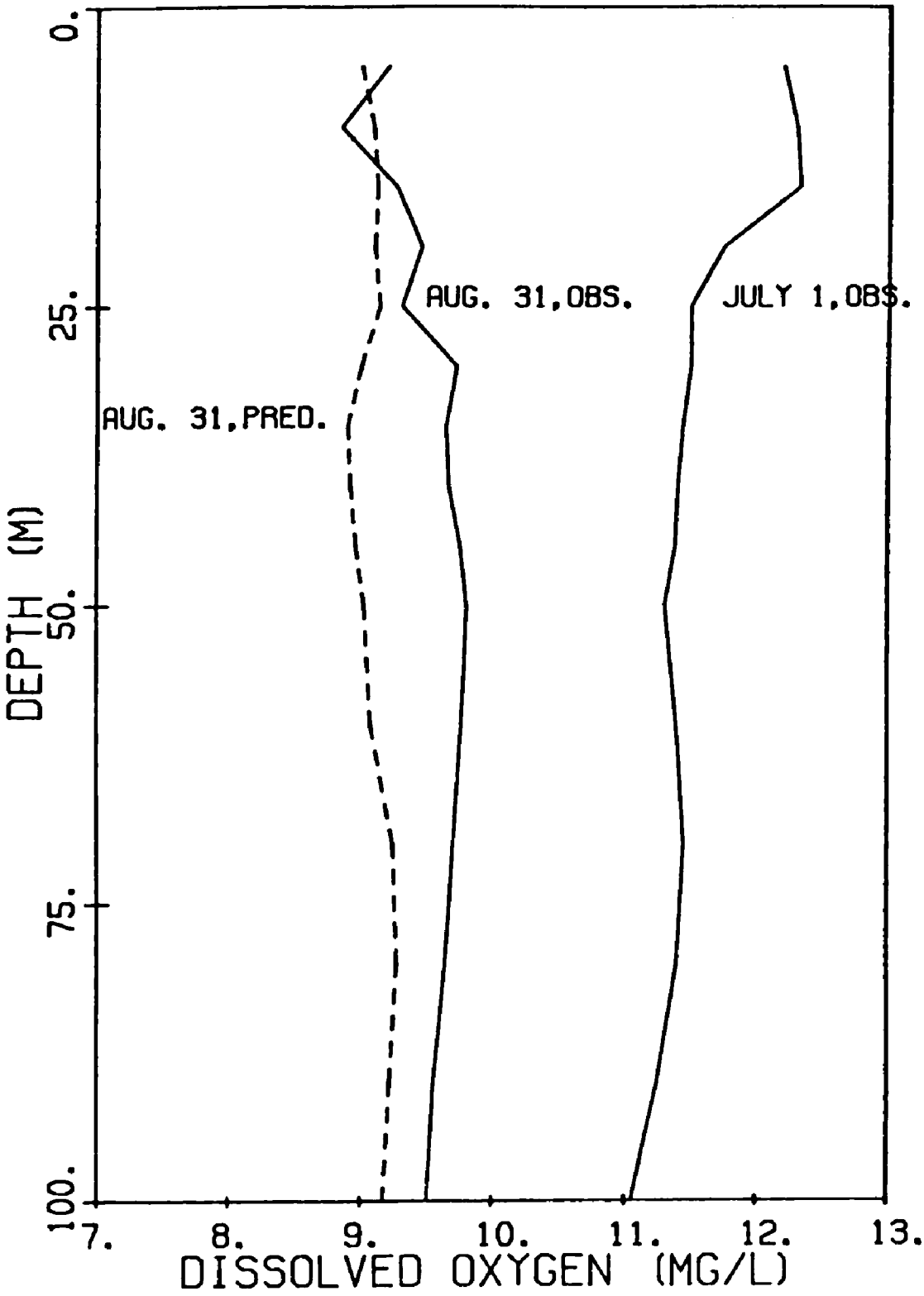


Fig. 25. Lake Ontario, July-Aug., 1972, results of simulation of dissolved oxygen depletion.

observations. Consequently, a model of this type could be used for synoptic scale atmospheric models to provide a lower boundary temperature for lake surfaces. Mesoscale atmospheric phenomena, e.g., lake-land breezes, would require information concerning the horizontal variations of surface temperature not provided by this model.

An avenue for further research lies in the possible coupling of a turbulent entrainment model of this type with a numerical model of lake dynamics. The extent of the coupling possible depends primarily on the complexity of the dynamical model. Consider, e.g., a two layer dynamical model which ignores air-sea heat exchange but requires information about the mean depth of the interface, $\bar{h}$, and the density difference between the two layers, $\Delta\rho$. The model presented herein could be used to update these two parameters at intervals of $t' > \Delta t$, where Δt is the time step of the dynamical model. This may be considered an improvement over the usual assumption that $\bar{h}$ and $\Delta\rho$ are constant in situations where the surface heat flux and entrainment at -h have a significant influence on the dynamics.

For a multi-layer model which includes thermodynamics, e.g. Simons (1973), the coupling would be more direct. In this case though, little of the structure of the present model could be retained. The entrainment model would have

to be applied locally, not on a lake average. However the introduction of the turbulent energy equation as a constraint on the deepening of this layer could prove a valuable addition to the dynamical model. Simon's (1973) model calls for parameterization of the vertical turbulent heat flux at interfaces of the layered model by the eddy diffusion approximation. This term could be readily computed in the manner prescribed in Chapter 4, with

$$-\overline{w\theta}\Big|_{-h} = \Lambda(T_s - T_h)\frac{dh}{dt} + K_z \frac{\partial T}{\partial z}\Big|_{-h}$$

$$\overline{w\theta} = -K_z \frac{\partial T}{\partial z}, \quad z<-h \quad .$$

If the uppermost layer of the model were allowed a moving impermeable ($\frac{dz_i}{dt}=w$, where z_i is the position of the boundary) boundary, (1) would be complete specification of vertical turbulent heat flux required by Simon's model.

If the interfaces between layers were stationary, $\overline{w\theta}$ for $z>-h$ could be obtained by integration of the heat conservation equation,

$$\frac{\partial T}{\partial t} = -\frac{\partial}{\partial z}(\overline{w\theta}) + \beta S^* e^{\beta z}$$

$$\frac{\partial}{\partial z}\frac{\partial T}{\partial t} = 0 \rightarrow \frac{\partial T}{\partial t} = C(t), \quad z>-h$$

$$-\int_{-h}^{z} \frac{\partial}{\partial z}(\overline{w\theta})dz = \int_{-h}^{z}[C(t) - \beta S^* e^{\beta z}]dz$$

$$-\overline{w\theta}\Big|_z = -\overline{w\theta}\Big|_{-h} + (z+h)C(t) - S^* e^{\beta z} + S^* e^{-\beta h} \quad .$$

In addition, velocities computed by the dynamical model might allow more accurate computation of $\frac{\partial U}{\partial z}$ for determination of the vertical diffusivity than the approximation employed in Chapter 4. With the vertical resolution of present dynamical models, few other improvements are possible.

Coupling of boundary layer models to synoptic and mesoscale models of the atmosphere has been a vigorous field of research for only a few years. Analogous oceanic models have not been attempted to date. One significant difference between the two cases is that most of the kinetic energy of lakes and oceans is in the boundary layer. Most atmospheric kinetic energy is associated with processes outside the boundary layer, which may be parameterized as a layer of frictional resistance. Perhaps a model like Niiler (1975) which also treats mixed layer currents is more consistent for use in coupling with numerical dynamical models of oceans and lakes.

CHAPTER IX

CONCLUSIONS

A mixed-layer model satisfying heat and turbulent kinetic energy conservation equations has been presented and shown to be capable of simulating changes in the vertical temperature distribution of fresh water lakes. The model has been verified in two lakes of greatly different morphometry. The dependence of mixing regime on lake size is parameterized in terms of the fetch dependent wave field and the relative importance of convection, wave breaking, and the wind generated shear flow. The characteristics of the turbulence associated with these different turbulent energy sources is formulated in terms of the length scales of the large turbulent eddies generated by these processes. No previous mixed layer model has considered these processes in comparable detail.

The validity of the conceptual picture of turbulent energy sources and sinks presented herein has not been demonstrated unequivocally. In particular, the restriction of the effects of wave produced turbulence to the relatively shallow wave mixed layer has been suggested, but not undeniably verified, by observations. Nonetheless, the modeling assumptions yield forcing functions which vary as expected in direction and magnitude with environmental conditions. In particular, variation of

measured values of the coefficient, m, relating surface kinetic energy input to the rate of increase of potential energy of the water column, have been roughly approximated on the basis of this model. Kraus and Turner (1967) and all subsequent variants of that work have assumed "m" is a constant.

The sensitivity of the model to variation in certain environmental conditions and model parameter values indicates that over a four day period with an initial uniform stratification, $N=10^{-2}s^{-1}$, the model is most sensitive to changes in wind speed, wave mixed layer depth, fetch, $\frac{\tau_w}{\tau_o}$, and dissipation. The sensitivity to changes in attenuation coefficient, surface heat flux, and latitude is slight in these circumstances.

During the fall overturn of Lake Ontario, October 1972, the horizontal non-uniformity of the lake, coupled with a biased sampling of the temperature distribution, prohibits simulation of observed profiles. However if the model temperature distribution is forced to attain an analogous horizontal non-uniformity and is sampled in an identical biased fashion, the resultant horizontal averages compare favorably with the observed averages.

Finally, potential uses of the model have been identified, especially with regard to other modelling efforts. The excellent simulation of lake surface temperature

provided by this relatively economical model suggests its use in prediction of the lower boundary temperature over lakes for models of synoptic scale atmospheric dynamics. Simulation of vertical diffusion processes in one-dimensional lake ecology models can be built upon the principles presented herein. An example of this type of application is shown in the simulation of changes in dissolved oxygen in Lake Ontario in July-August, 1972. It is also suggested that coupling with a model of lake dynamics is possible. However, little research has been conducted along this line of endeavor.

This work demonstrates that a mixed layer model with the constraints of turbulent kinetic energy conservation, originally proposed by Kraus and Turner (1967), may be extended past the overly simplistic energy arguments adopted by those authors and in all subsequent adaptations of their work (Turner, 1969; Denman, 1973; Edwards and Darbyshire, 1973; Niiler, 1975). Their argument, that "m" is constant, has been often criticized and justly so. However there has been a tendency to throw the baby out with the bath water: to ignore the basic simplicity and correctness of the turbulent energy balance approach. This work represents a second step in modelling the turbulent energy balance of the mixed layer or epilimnion of lakes.

REFERENCES

Arajs, A. A. and R. Farooqui. 1974. Nearshore currents and water temperatures along the north shore of Lake Ontario between Pickering and Cobourg. Proc. 17th Conf. Great Lakes Res., Internat. Assoc. Great Lakes Res., pp. 348-357.

Benilov, A. Y. 1973. Generation of ocean turbulence by surface waves. Izv. Akad. Nauk., SSSR, Atmos. and Oceanic Phys., 9, pp. 160-164 (Engl. trans.)

Blackadar, A. K. 1962. The vertical distribution of wind and turbulent exchange in a neutral atmosphere. J. Geophys. Res., 67, pp. 3095-3102.

Blanton, J. O. 1973. Vertical entrainment into the epilimnia of stratified lakes. Limnol. and Oceanog., 18, pp. 697-703.

Bowden, K. F., M. R. Howe and R. I. Tait. 1970. A study of the heat budget over a seven day period at an oceanic station. Deep-Sea Res., 17, pp. 401-411.

Bretschneider, C. L. 1966. Wave generation by wind, deep and shallow water. In: Estuary and Coastline Hydrodynamics (ed. A. T. Ippen). McGraw Hill, pp. 133-196.

Budyko, M. L. 1956. The heat balance of the earth's surface. Clearinghouse for Federal Scientific and Technical Information, Document No. PB 131692, 232pp.

Businger, J. A., J. C. Wyngaard, Y. Izumi, and E. F. Bradley. 1971. Flux-profile relationships in the atmospheric surface layer. J. Atmos. Sci., 28, pp. 181-189.

Darbyshire, J. and M. Colclough. 1972. Measurements of thermal conductivities in a fresh water lake. Pure and Applied Geophys., 93, pp. 151-158.

Darbyshire, J. and A. Edwards. 1972. Seasonal formation and movement of the thermocline in lakes. Pure and Applied Geophys., 93, pp. 141-150.

Deacon, E. L. and J. Stevenson. 1968. Radiation and associated observations made on Indian Ocean cruise. C.S.I.R.O., Div. of Met. Phys. Tech. Pap. #16.

Deacon, E. L. and E. K. Webb. 1962. Small-scale interactions. In: The Sea, v. 1, (ed. M. N. Hill). Interscience.

Deardorff, J. W. 1968. Dependence of air-sea transfer coefficients on bulk stability. J. Geophys. Res., 73, pp. 2549-2558.

Deardorff, J. W. 1970. Convective velocity and temperature scales for the unstable planetary boundary layer and for Rayleigh convection. J. Atmos. Sci., 27, pp. 1211-1213.

Deardorff, J. W. and G. E. Willis. 1967. Investigation of turbulent thermal convection between horizontal plates. J. Fluid Mech., 28, pp. 675-704.

Deardorff, J. W., G. E. Willis and D. K. Lilly. 1969. Laboratory investigation of non-steady penetrative convection. J. Fluid Mech., 35, pp. 7-31.

Degtyarev, G. M., A. A. Sorokin and Y. A. Menshov. 1964. Radiation reflected from the surface of the open sea. Izv., Akad. Nauk., SSSR, Geophys. Ser., no. 10, pp. 1578-1583.

Denman, K. L. 1973. A time dependent model of the upper ocean. J. Phys. Oceanog., 3, pp. 173-184.

Denman, K. L. and M. Miyake. 1973. Upper layer modification at ocean station Papa: Observations and simulation. J. Phys. Oceanog., 3, pp. 185-196.

Dobroklonskiy, S. V. and N. V. Kontoboytseva. 1973. Experiments to determine the thickness of the turbulent layer in monochromatic waves. Izv., Akad. Nauk., SSSR, Atmos. and Oceanic Phys., 9, pp. 117-119.

Dobson, F. W. 1971. Measurements of atmospheric pressure on wind-generated sea waves. J. Fluid Mech., 48, pp. 91-127.

Dutton, J. A. and R. A. Bryson. 1962. Heat flux in Lake Mendota. Limnol. and Oceanog., 7, pp. 80-97.

Edwards, A. and J. Darbyshire. 1973. Models of a lacustrine thermocline. Mem. Societe Royale des Sciences de Liege, Ser. 6e, v. 4, pp. 81-101.

Ertel, H. 1954. Theorie der thermischen Sprungschicht in Seen. Acta Hydrophys., 1, pp. 151-171.

Foster, T. D. 1971. A convective model for the diurnal cycle in the upper ocean. J. Geophys. Res., 76, pp. 666-675.

Geisler, J. E. and E. B. Kraus. 1969. The well-mixed Ekman boundary layer. Deep-Sea Res., supp. to v. 16, pp. 73-84.

Grant, H. L., A. Moilliet and W. M. Vogel. 1968. Some observations of the occurrence of turbulence in and above the thermocline. J. Fluid Mech., 34, pp. 443-448.

Halpern, D. 1974. Observations of the deepening of the wind-mixed layer in the Northeast Pacific Ocean. J. Phys. Oceanog., 4, pp. 454-466.

Hasselmann, K. 1974. On the spectral dissipation of ocean waves due to white capping. Boundary Layer Met., 6, pp. 107-127.

Hasselmann, K., T. P. Barnett, E. Bouws, H. Carlson, D. E. Cartwright, K. Enke, J. A. Ewing, H. Gienapp, D. E. Hasselmann, P. Kruseman, A. Meerburg, P. Muller, D. J. Olbers, K. Richter, W. Sell, and H. Walden. 1973. Measurements of wind wave growth and swell decay during the Joint North Sea Wave Project (JONSWAP). Supp. to Deutsche Hydrographischen Zeitschrift, Ser. A., #12.

Hutchinson, G. E. 1957. A Treatise on Limnology, v. 1, Wiley and Sons, Inc. New York.

Jacobs, C. A. and P. S. Brown. 1974. Three dimensional model results. Final Report, v. IV. Center for the Environment and Man, Inc., 4131-509d.

Jacobs, C. A. and J. P. Pandolfo. 1974a. A description of a general three-dimensional numerical simulation model of a coupled air-water and/or air-land boundary layer. Final Report, v. I. Center for the Environment and Man, Inc., 4131-509a.

Jacobs, C. A. and J. P. Pandolfo. 1974b. One dimensional model results. Final Report, v. III. Center for the Environment and Man, Inc. 4131-509c.

Kalatskiy, V. I. 1973. A two layer model for computing the thickness of an isothermic layer in the ocean. Meteor. and Hydrol., no. 11, pp. 82-93. (Engl. trans.)

Kato, H. and O. M. Phillips. 1969. On the penetration of a turbulent layer into stratified fluid. J. Fluid Mech., 37, pp. 643-655.

Kaye, G. T. 1974. Observations of short period internal waves generated by shear flow instability. Ph.D. Thesis, University of Michigan.

Kitaigorodskiy, S. A. 1960. On the computation of the thickness of the wind-mixing layer in the ocean. Izv., Akad. Nauk., SSSR, Geophys. Ser., pp. 284-287. (Engl. trans.).

Kitaigorodskiy, S. A. and Y. A. Miropolskiy. 1970. On the theory of the open ocean active layer. Izv., Akad. Nauk., SSSR, Atmos. and Oceanic Phys., no. 2, pp. 97-102 (Engl. trans.).

Kraus, E. B. 1972. Atmosphere-Ocean Interaction. Clarendon Press, Oxford.

Kraus, E. B. and C. Rooth. 1961. Temperature and the steady state vertical heat flux in the ocean surface layers. Tellus, 13, pp. 231-238.

Kraus, E. B. and J. S. Turner. 1967. A one-dimensional model of the seasonal thermocline, p. 2. Tellus, 19, pp. 98-106.

Kullenberg, G. 1971. Vertical diffusion in shallow waters. Tellus, 23, pp. 129-135.

Kullenberg, G., C. R. Murthy and H. Westerberg. 1973. An experimental study of diffusion characteristics in the thermocline and hypolimnion region of Lake Ontario. Proc. 16th Conf. Great Lakes Res., Internat. Assoc. Great Lakes Res., pp. 774-790.

Lemmin, U., J. T. Scott and U. H. Czapski. 1974. The development from two-dimensional to three-dimensional turbulence generated by breaking waves. J. Geophys. Res., 79, pp. 3442-3448.

Linden, P. F. 1975. The deepening of a mixed layer in a stratified fluid. J. Fluid Mech., 71, pp. 385-405.

Lumley, J. L. 1964. The spectrum of nearly inertial turbulence in a stably stratified fluid. J. Atmos. Sci., 21, pp. 99-102.

Mellor, G. L. and P. A. Durbin. 1975. The structure and dynamics of the ocean surface mixed layer. J. Phys. Oceanog., 5, pp. 718-728.

Mortimer, C. H. 1961. Motion in thermoclines. Verhand. Internat. Verein. Limnol., 14, pp. 79-83.

Munk, W. H. and E. R. Anderson. 1948. Notes on a theory of the thermocline. J. Mar. Res., 7, pp. 276-295.

Nihoul, J. C. J. 1973. The effect of wind blowing on turbulent mixing and entrainment in the upper layer of the ocean. Mem. Societe Royale des Sciences de Liege, Ser. 6e, v. 4, pp. 115-124.

Niiler, P. P. 1975. Deepening of the wind mixed layer. J. Mar. Res., 33, pp. 405-422.

Ostapoff, F. and S. Worthem. 1974. The intradiurnal temperature variation in the upper ocean layer. J. Phys. Oceanog., 4, pp. 601-612.

Pandolfo, J. P. 1969. Motions with inertial and diurnal period in a numerical model of the navifacial boundary layer. J. Mar. Res., 27, pp. 301-317.

Paulson, C. A. 1967. The mathematical representation of wind speed and temperature profiles in the unstable atmospheric surface layer. J. Appl. Meteor., 9, pp. 857-861.

Phillips, D. W. 1974. IFYGL Weather Highlights. Proc. 17th Conf. Great Lakes Res., Internat. Assoc. Great Lakes Res., pp. 296-320.

Phillips, D. W. and J. A. W. McCulloch. 1972. The Climate of the Great Lakes Basin. Env. Canada Climatological.

Phillips, O. M. 1957. On the generation of waves by turbulent wind. J. Fluid Mech., 2, pp. 417-445.

Phillips, O. M. 1969. The Dynamics of the Upper Ocean. Cambridge Univ. Press, Cambridge.

Phillips, O. M. and M. L. Banner. 1974. Wave breaking in the presence of wind drift and swell. J. Fluid Mech., 66, pp. 625-640.

Pivovarov, A. A., E. P. Anisimova and A. N. Erikova. 1965. Diurnal course of the albedo and of solar radiation penetrating the sea. Izv., Akad. Nauk., SSSR, Atmos. and Oceanic Phys., 1, pp. 713-715. (Engl. trans.)

Pollard, R. T., P. B. Rhines and R. O. R. Y. Thompson. 1973. The deepening of the wind mixed layer. Geophys. Fluid Dyn., 3, pp. 381-404.

Scott, J. T., G. E. Myer, R. Stewart and E. G. Walter. 1969. On the mechanism of Langmuir circulations and their role in epilimnion mixing. Limnol. and Oceanog., 14, pp. 493-503.

Simons, T. J. 1973. Development of three-dimensional numerical models of the Great Lakes. Env. Canada, Scientific Ser. no. 12.

Sivkov, S. I. 1971. Computation of Solar Radiation Characteristics, Gidrometeorologischeskoe Isdatel'stov, Leningrad, trans. by Israel Program for Sci. Trans., Jerusalem.

Snyder, R. L. 1974. A field study of wave induced pressure fluctuations above surface gravity waves. J. Mar. Res., 32, pp. 497-531.

Stewart, R. W. 1961. The wave drag of wind over water. J. Fluid Mech., 10, pp. 89-94.

Stewart, R. W. and H. L. Grant. 1962. Determination of the rate of dissipation of turbulent energy near the sea surface in the presence of waves. J. Geophys. Res., 67, pp. 3177-3180.

Stommel, H., K. Saunders, W. Simmons and J. Cooper. 1969. Observations of the diurnal thermocline. Deep-Sea Res., supp. to v. 16, pp. 269-284.

Sundaram, T. R. 1973. A theoretical model for the seasonal thermal cycle of deep temperate lakes. Proc. 16th Conf. Great Lakes Res., Internat. Assoc. Great Lakes Res., pp. 1009-1025.

Sundaram, T. R. and R. G. Rehm. 1971. Formation and maintenance of thermoclines in temperate lakes. AIAA Journal, 9, pp. 1322-1329.

Sundaram, T. R. and R. G. Rehm. 1972. Effects of thermal discharge on the stratification cycle of lakes. AIAA Journal, 10, pp. 204-210.

Sundaram, T. R. and R. G. Rehm. 1973. The seasonal thermal structure of deep temperate lakes. Tellus, 25, pp. 157-167.

Tennekes, H. and J. L. Lumley. 1972. A First Course in Turbulence. MIT Press, Cambridge, Mass.

Thompson, K. P. B., J. Jerome and W. R. McNeil. 1974. Optical Properties of the Great Lakes. IFYGL Report, Canada Centre for Inland Waters.

Townsend, A. A. 1965. Excitation of internal waves by a turbulent boundary layer. J. Fluid Mech., 22, pp. 241-252.

Turner, J. S. 1968. The influence of molecular diffusivity on turbulent entrainment across a density interface. J. Fluid Mech., 33, pp. 639-656.

Turner, J. S. 1969. A note on wind mixing at the seasonal thermocline. Deep-Sea Res., supp. to v. 16, pp. 297-300.

Turner, J. S. 1973. Buoyancy Effects in Fluids. Cambridge Univ. Press, Cambridge.

Walmsley, J. L. 1973. Numerical experiments with an air-water boundary layer model. J. of the Met. Soc. of Japan, 51, pp. 388-399.

Woods, J. D. 1968. An investigation of some physical processes associated with the vertical flow of heat through the upper ocean. The Meteor. Mag., 97, pp. 65-72.

Wu, J. 1969. Wind stress and surface roughness at air-sea interface. J. Geophys. Res., 74, pp. 444-456.

Yeh, G. T. 1974. Interaction between the atmospheric and oceanic boundary layers. Boundary Layer Meteor., 7, pp. 21-37.